

Fiscal Year 2018: First Quarter

Progress Report **Advanced Battery Materials Research (BMR) Program**

Released March 2018
for the period of October – December 2017

Approved by

Tien Q. Duong, Advanced Battery Materials Research Program Manager
Vehicle Technologies Office, Energy Efficiency and Renewable Energy

TABLE OF CONTENTS

A Message from the Advanced Battery Materials Research Program Manager.....	
Task 1 – Liquid/Polymer Solid-State Electrolytes	1
Task 1.1 – Advanced Lithium-Ion Battery Technology: High-Voltage Electrolyte (Joe Sunstrom, Ron Hendershot, and Alec Falzone, Daikin)	3
Task 1.2 – Multi-Functional, Self-Healing Polyelectrolyte Gels for Long-Cycle-Life, High-Capacity Sulfur Cathodes in Lithium-Sulfur Batteries (Alex Jen and Jihui Yang, University of Washington)	5
Task 1.3 – Development of Ion-Conducting Inorganic Nanofibers and Polymers (Nianqiang (Nick) Wu, West Virginia University; Xiangwu Zhang, North Carolina State University)	9
Task 1.4 – High Conductivity and Flexible Hybrid Solid-State Electrolyte (Eric Wachsman, Liangbing Hu, and Yifei Mo, University of Maryland)	12
Task 1.5 – Self-Forming Thin Interphases and Electrodes Enabling 3D Structured High-Energy-Density Batteries (Glenn Amatucci, Rutgers University)	15
Task 1.6 – Dual Function Solid-State Battery with Self-Forming, Self-Healing Electrolyte and Separator (Esther Takeuchi, Stony Brook University)	17
Task 2 – Diagnostics	19
Task 2.1 – Model System Diagnostics for High-Energy Cathode Development (Guoying Chen, Lawrence Berkeley National Laboratory)	20
Task 2.2 – Interfacial Processes – Diagnostics (Robert Kostecki, Lawrence Berkeley National Laboratory)	23
Task 2.3 – Advanced <i>In Situ</i> Diagnostic Techniques for Battery Materials (Xiao-Qing Yang and Seongmin Bak, Brookhaven National Laboratory)	26
Task 2.4 – Nuclear Magnetic Resonance and Magnetic Resonance Imaging Studies of Solid Electrolyte Interphase, Dendrites, and Electrode Structures (Clare Grey, University of Cambridge)	29
Task 2.5 – Advanced Microscopy and Spectroscopy for Probing and Optimizing Electrode-Electrolyte Interphases in High-Energy Lithium Batteries (Shirley Meng, University of California at San Diego)	32
Task 2.6 – <i>In Situ</i> Diagnostics of Coupled Electrochemical-Mechanical Properties of Solid Electrolyte Interphases on Lithium-Metal Rechargeable Batteries (Xingcheng Xiao, General Motors; Brian W. Sheldon, Brown University; Yue Qi, Michigan State University; and Y. T. Cheng, University of Kentucky)	36
Task 2.7 – Microscopy Investigation on the Fading Mechanism of Electrode Materials (Chongmin Wang, Pacific Northwest National Laboratory)	40

Task 3 – Modeling	43
Task 3.1 – Density of High-Energy, High-Voltage Lithium Batteries through First-Principles Modeling (Kristin Persson, Lawrence Berkeley National Laboratory)	44
Task 3.2 – Addressing Heterogeneity in Electrode Fabrication Processes (Dean Wheeler and Brian Mazzeo, Brigham Young University)	46
Task 3.3 – Understanding and Strategies for Controlled Interfacial Phenomena in Lithium-Ion Batteries and Beyond (Perla Balbuena, Jorge Seminario, and Partha Mukherjee, Texas A&M University)	49
Task 3.4 – Electrode Materials Design and Failure Prediction (Venkat Srinivasan, Argonne National Laboratory)	52
Task 3.5 – First Principles Calculations of Existing and Novel Electrode Materials (Gerbrand Ceder, Lawrence Berkeley National Laboratory)	54
Task 3.6 – Dendrite Growth Morphology Modeling in Liquid and Solid Electrolytes (Yue Qi, Michigan State University)	56
Task 3.7 – First Principles Modeling and Design of Solid-State Interfaces for the Protection and Use of Li-Metal Anodes (Gerbrand Ceder, University of California at Berkeley)	59
Task 3.8 – Large-Scale <i>Ab Initio</i> Molecular Dynamics Simulations of Liquid and Solid Electrolytes (Lin-Wang Wang, LBNL)	61
Task 3.9 – <i>In Operando</i> Thermal Diagnostics of Electrochemical Cells (Ravi Prasher, LBNL)	64
Task 4 – Metallic Lithium	66
Task 4.1 – Lithium Dendrite Prevention for Lithium Batteries (Wu Xu and Ji-Guang Zhang, Pacific Northwest National Laboratory)	68
Task 4.2 – Self-Assembling and Self-Healing Rechargeable Lithium Batteries (Yet-Ming Chiang, Massachusetts Institute of Technology; Venkat Viswanathan, Carnegie Mellon University)	71
Task 4.3 – Engineering Approaches to Dendrite-Free Lithium Anodes (Prashant Kumta, University of Pittsburgh)	73
Task 4.4 – Nanoscale Interfacial Engineering for Stable Lithium-Metal Anodes (Yi Cui, Stanford University)	76
Task 4.5 – Composite Electrolytes to Stabilize Metallic Lithium Anodes (Nancy Dudney and X. Chelsea Chen, Oak Ridge National Laboratory)	79
Task 4.6 – Lithium Batteries with Higher Capacity and Voltage (John B. Goodenough, University of Texas at Austin)	82
Task 4.7 – Advancing Solid State Interfaces in Lithium-Ion Batteries (Nenad Markovic and Larry A. Curtiss, Argonne National Laboratory)	84
Task 4.8 – Mechanical and Defect Properties at the Protected Lithium Interface (Nancy Dudney, Oak Ridge National Laboratory; Erik Herbert, Michigan Technological University; Jeff Sakamoto, University of Michigan)	87

Task 5 –Sulfur Electrodes.....	90
Task 5.1 – Novel Chemistry: Lithium Selenium and Selenium Sulfur Couple (Khalil Amine, Argonne National Laboratory)	92
Task 5.2 – Development of High-Energy Lithium–Sulfur Batteries (Jun Liu and Dongping Lu, Pacific Northwest National Laboratory)	95
Task 5.3 – Nanostructured Design of Sulfur Cathodes for High-Energy Lithium–Sulfur Batteries (Yi Cui, Stanford University).....	98
Task 5.4 – Addressing Internal “Shuttle” Effect: Electrolyte Design and Cathode Morphology Evolution in Lithium-Sulfur Batteries (Perla Balbuena, Texas A&M University).....	101
Task 5.5 – Investigation of Sulfur Reaction Mechanisms (Deyang Qu, University of Wisconsin at Milwaukee; Xiao-Qing Yang, Brookhaven National Laboratory).....	104
Task 5.6 – Statically and Dynamically Stable Lithium–Sulfur Batteries (Arumugam Manthiram, University of Texas at Austin)	106
Task 5.7 – Electrochemically Responsive, Self-Formed Lithium-Ion Conductors for High-Performance Lithium-Metal Anodes (Donghai Wang, Pennsylvania State University).....	109
Task 6 –Air Electrodes / Electrolytes	112
Task 6.1 – Rechargeable Lithium–Air Batteries (Ji-Guang Zhang and Wu Xu, Pacific Northwest National Laboratory)	113
Task 6.2 – Lithium–Air Batteries (Khalil Amine and Larry A. Curtiss, Argonne National Laboratory).....	116

TABLE OF FIGURES

Figure 1. Scanning auger results of a 4.5-V LCO cell cycled at 0.7C.	4
Figure 2. Post-sputter maps of cobalt (blue), oxygen (lime), fluorine (red), and carbon (yellow) of a 4.5-V LCO cell cycled at 0.7C.	4
Figure 3. Discharge capacity of cells cycled at 0.7C.	4
Figure 4. Representative electrochemical impedance spectroscopy data for Gel 2, obtained by placing a 7-mm diameter gel sample between two stainless-steel electrodes. The equivalent circuit used for fitting is shown. The value of R_{bulk} was used in conjunction with film area and thickness to obtain a conductivity value.	6
Figure 5. (a) Stress-strain curves of the self-healing composites prior to any mechanical damage. (b) Recovery of maximum tensile strength upon self-healing of composite films. (c) Recovery of Young's modulus upon self-healing of composite films.....	7
Figure 6. ^7Li NMR of S/C composite cathodes mid-discharge (2.1 V) and at end of discharge (1.9 V). Both types of carbon composite show evidence of Li^+ in both free (peak 2) and aggregated (peak 4) polysulfides, as well as solid Li_2S (peak 3). The modified sample shows a larger ratio of aggregated polysulfide to solid Li_2S at 2.1 V than the unmodified sample.....	7
Figure 7. (a) Transporting barriers for lithium atoms along transporting direction in pure, single-Al, double-Al, and single-N decorated $\text{Li}_{0.33}\text{La}_{0.56}\text{TiO}_2$ structure. The transporting trajectory is marked by dash line in inset, (b) electrochemical impedance spectroscopy profiles of PVDF-HFP/LiTFSI/N-LLTO membrane.	10
Figure 8. Reconstructed model of garnet textile flatness uniformity generated by 3D laser scanning.....	13
Figure 9. Atomic force microscopy scanning of the hybrid polymer/garnet textile composite electrolyte.	13
Figure 10. Focus ion beam analysis of the typical fiber bundle structure in garnet textile.	13
Figure 11. Constant voltage charge / constant current discharge profile representative of new, multicomponent structured architecture cells.	16
Figure 12. Conductivity effects of addition of $\text{LiI}(\text{HPN})_2$	18
Figure 13. Comparison of $\text{LiI}(\text{HPN})_2$ containing solid electrolytes at 30°C.	18
Figure 14. (a) Cycling of cells containing $\text{LiI}(\text{HPN})_2$ additive with and without lithium metal added. (b) Coulombic efficiency.....	18

Figure 15. Cyclic voltammograms of $\text{Li}_{1.3}\text{Nb}_{0.3}\text{Mn}_{0.4}\text{O}_2$ half-cells cycled between 1.5 V and various upper cut off voltages of: (a) 4.2 V, (b) 4.4 V, (c) 4.6 V, and (d) 4.8 V. Scan rate: 5 mV/min.....	21
Figure 16. Voltage profiles of $\text{Li}_{1.3}\text{Nb}_{0.3}\text{Mn}_{0.4}\text{O}_2$ half-cells cycled at 10 mA/g between voltages of: (a) 1.5 – 4.2 V and (b) 1.5 – 4.8 V, and (c) specific discharge capacity and average voltage as a function of cycle number.	21
Figure 17. (a) Atomic force microscopy image, (b) X-ray diffraction, and (c) Raman spectrum of NMC thin-film electrode made by pulsed laser deposition.	24
Figure 18. (a) Voltammogram trace of the NMC thin-film electrode. (b) Fourier transform infrared–attenuated total reflectance spectrum of the pristine and 3-cycled NMC thin-film electrode, tetraethylene glycol and ployethylene glycol standard, 1M LiPF_6 EC/DEC=1/2 (v/v) electrolyte and EC/DEC=1/2.39.....	24
Figure 19. The minority phases identified by the project’s data-mining approach. Panels (a) and (c) show the transmission images of the field-of-views covering particles (P37 and P46), which are identified by the method as minority phases. Panel (e) is the transmission image of another typical field-of-view that contains several normal LiCoO_2 particles. Panels (b), (d), and (f) show the clustering results, with the four different clusters color coded to the corresponding inset. The project compares the spectroscopic fingerprints of all the four clusters in panels (g) and (h). It is interesting to note that clusters 1# and 2# are both similar to LiCoO_2 . The radar chart in panel (i) shows the differences in the spectroscopic fingerprints of the 4 clusters are systematically captured by the data attributes extracted in this approach. The scale bar in panel (a) is 10 microns.	27
Figure 20. (a) Comparison of the experimental isotropic region of the ^7Li nuclear magnetic resonance (NMR) spectrum of $\text{LiTi}_{0.2}\text{Mn}_{1.8}\text{O}_4$ (solid black, fit in solid red) and the density functional theory simulated resonance assuming a random distribution of Ti^{4+} and $\text{Mn}^{3+/4+}$ (dashed red) with the peaks fit to the experimental spectrum (purple, green, yellow, magenta, blue, cyan, and gray). (b) Isotropic region of the experimental ^7Li NMR spectrum (solid black) and the simulated spectrum (dashed red) of $\text{Li}_{0.6}\text{Ti}_{0.1}\text{Mn}_{0.3}[\text{Li}_{0.4}\text{Ti}_{1.4}\text{Mn}_{0.2}]\text{O}_4$. For each lithium coordination, the corresponding peak is shown, as calculated with the reverse Monte Carlo method. The corresponding cation ordering in the P4_332 lattice is shown in the top-left inset.....	30
Figure 21. Scanning transmission electron microscopy annular bright-field (STEM/ABF) images of (a) uncoated Li-rich layered oxide (LRLO) and (b) LRLO material coated with 1 wt% LLTO. (c) Electron energy loss spectroscopy (EELS) Ti-L edge spectra at surface regions of LRLO sample coated with LLTO before and after cycling. (d, e) ABF and high angle annular dark field images of LRLO material coated with LLTO after cycling. (f) EELS O-K edge spectra of LRLO sample coated with LLTO after cycling collected at bulk and surface region, respectively.	33

Figure 22. First charging comparison of (a) electrochemical performance and (b) strain generation for Li-rich layered oxide electrode under different rate. (c, d) The strain distribution along the [003] direction inside of the nanoparticle charged at 50 mA/g for two representative states of charge. The scale bar is 100 nm.	34
Figure 23. (a) X-ray diffraction comparison of the commercial Li-metal powder at 300 K and 100 K. Electron energy loss spectra comparison of the reference (commercial lithium ribbon and LiF) to the electrochemically deposited lithium metal in (b) Li-K edge, (c) O-K edge, and (d) F-K edge.....	34
Figure 24. (a-c) Finite element modeling of morphological evolution of solid electrolyte interphase (SEI) on Li-metal anode (a) before 1 st lithium plating half-cycle, (b) after 1 st lithium plating half-cycle, and (c) after 1 st lithium stripping half-cycle. (d) Stress*thickness response of the SEI.....	37
Figure 25. Self-forming nanocomposite has a unique nanostructure where LiF nanocrystals embedded in polymeric matrix (a). The cross-section image shows the coating is dense and has good adhesion to lithium metal.	38
Figure 26. The combination of the protective coating with high-concentration LiFSi in dimethoxyethane enables long cycle stability.	38
Figure 27. High-angle annular dark field scanning transmission electron microscopy (HAADF-STEM) images of cycled $\text{LiNi}_{0.76}\text{Co}_{0.10}\text{Mn}_{0.14}\text{O}_2$ in the regular electrolyte. STEM images of the surface structures at (a) {003} exit surface and (c) the surface parallel to {003} plane, respectively, seen along the [010] zone axis. The white dashed lines outline the boundaries of the rocksalt phase, the red and blue arrows indicate the {003} atomic plane direction and the rocksalt growth direction, respectively. (b/d) The colored maps correspond to (a/c), respectively.	41
Figure 28. Experimentally measured conductivity as a function of salt concentration for LiAsF_6 and LiPF_6 in dimethyl carbonate. The bottom rectangles (left to right) illustrate the neat solvent, an electrolyte with only associated salt (with dipole moments drawn as directed arrows), and finally an electrolyte with both associated (arrows) and dissociated salt (no arrows). ^[1]	45
Figure 29. Free energy of dissociation for LiAsF_6 (black) and LiPF_6 (blue) into their respective free ions as computed from first principles using the polarizable continuum model. ^[1]	45
Figure 30. Large-format Shapeoko CNC stage produced by Carbide 3D, with a custom-made N-line probe attachment.....	47
Figure 31. Measured bulk conductivity and contact resistance values (with 95% confidence intervals) on ANL AC006 cathode film using both large-format (“Big Red”) and high-resolution stages, compared to results from the (old) rigid 4-line probe.	47

Figure 32. Snapshots of the lithiated graphene oxide/copper (221) interface model. Panels (a) and (b) show lithium diffusion in scenarios (i) and (ii), respectively (see text). Purple, orange, grey, and red spheres represent lithium, copper, carbon, and oxygen atoms, respectively.....	50
Figure 33. (a) Demonstration of inhomogeneous solid electrolyte interphase (SEI) resistance, which may have a sharp variation (black line) or a wide drop (red line). (b) Initial lithium electrolyte interface, which is flat. (c) Sharp drop in SEI resistance leads to growth of a thin dendritic protrusion. (d) Wider variation in SEI resistance forms a thick dendritic protrusion.	53
Figure 34. (a) Increase in height of dendritic protrusions with time for sharp and wide drop in solid electrolyte interphase resistance. Growth of dendrites decreases with time because of increase in surface area and surface curvature induced suppression mechanisms. (b) As the surface energy between lithium and electrolyte increases, the width of the dendritic protrusions increases (red circles), and the aspect ratio of the protrusions drops (black squares).	53
Figure 35. LiCoO ₂ -LiF phase diagram.....	55
Figure 36. Local fluorine environments present in Li _{1.125} Mn _{0.875} O _{1.75} F _{0.25} disordered rocksalt phases.	55
Figure 37. Superposition of the low fluorine region of the phase diagrams obtained for the titanium, vanadium, chromium, manganese, iron, cobalt, and nickel LMO systems.	55
Figure 38. The observed lithium (upper left) and magnesium (upper right) plating morphology [Yoo et al., <i>ACS Applied Materials & Interfaces</i> (2015): 7001]. The simulated morphology difference of lithium and magnesium plating (lower panels).	57
Figure 39. Destabilizing transport mechanisms. (a) Higher mobility along defects and grain boundaries. (b) Surface asperity flux concentration.....	60
Figure 40. The different stages of oxidization of the back phosphorene.	62
Figure 41. The formation energy of Li _x POs(1-x) for different POs (s=1,2,3,4) (a); the atomic structure of fully lithiated P ₄ O ₂ (b) and P ₄ O ₄ (c). The project found the system will become unstable if the number of lithium is larger than the number of oxygen.	62
Figure 42. (Top) Heat must flow across all layers of the repeating unit cell to escape the Li-ion battery. (Bottom left) Scanning electron microscopy (SEM) image of a real cathode; too messy to get a controlled thermal transport measurement of the isolated active material. (Bottom right) SEM image of epitaxially grown pristine cathode material ideal for time domain thermoreflectance cross-plane thermal conductivity measurements.....	65

Figure 43. Representative raw time domain thermoreflectance data for one LNMO.....	65
Figure 44. Top view scanning electron microscopy images of the Li-metal anodes in the Li NMC cells after 100 cycles at the same charge and discharge current density of 2.0 mA cm^{-2} after 3 formation cycles at 0.2 mA cm^{-2} at 30°C using the electrolytes of (a) ELY-14, (b) ELY-19, and (c) ELY-13.	69
Figure 45. Temperature dependence of ionic conductivity of salt mixtures of LiTFSI-LiFSI (2:8 by mol) with ionic liquids PY14-TFSI (a) and PY13-TFSI (b) at different compositions.	69
Figure 46. Li-Li asymmetric cell cycling with 1 M LiPF_6 EC-DMC (1:1) and 1 M LiPF_6 + F-containing additive electrolytes. Cycling condition is 0.6 mA/cm^2 current density and 3.0 mAh/cm^2 areal capacity.	72
Figure 47. Coulombic efficiency of multilayer porous foams with graphene coating, without graphene coating, and of unmodified copper foil serving as reference.	74
Figure 48. Nucleation overpotential for copper foil, copper foam, and graphene-Cu foam during the first 50 cycles.....	74
Figure 49. Scanning electron microscopy images of (a) pristine lithium foil and lithium foil imprinted with (b) coarse and (c) fine patterns. Scale Bar = 100 nm.	74
Figure 50. (a) Schematics of selective atomic layer deposition (ALD) LiF deposition on h-BN. (b) Scanning electron microscopy (SEM) characterization of 50 cycles of ALD LiF deposition on continuous h-BN. (C) SEM characterization of 50 cycles of ALD LiF deposition on the edge of h-BN.	77
Figure 51. Coulombic efficiency during long-term cycling.	77
Figure 52. A picture of the spray coater.....	80
Figure 53. Charge/discharge voltage curves of the Li//Li symmetric cells with the Al_2O_3 - and $\text{LiZr}_2(\text{PO}_4)_3$ -filled LiTFSI:PEO membranes at the 10 th cycle and 60°C	83
Figure 54. Charge/discharge cycle performance of the Li//Li symmetric cells with the (a) Al_2O_3 - and (b) $\text{LiZr}_2(\text{PO}_4)_3$ -filled LiTFSI:PEO membranes at 60°C	83
Figure 55. (a) X-ray scattering spectrum of LLZO heated to 473 K and 1073 K, respectively. (b) C 1s and (c) O 1s X-ray photoelectron spectroscopy core level before (blue) and after (red) heating to 773 K to burn off surface contamination species.	85
Figure 56. X-ray photoelectron spectroscopy core level spectra before (blue) and after (red) lithium deposition on clean LLZO surface. Reduction of: (a) Nb in Nb:LLZO; (b) Zr in Nb:LLZO; (c) Zr in Al:LLZO; and (d) Zr in Ta:LLZO.	85

Figure 57. Area specific resistance as a function of the adhesion strength of the Li-LLZO interface. Optical microscope images show the fracture surface of the lithium and LLZO disks at low and high area specific ionic resistance. The red dashed line indicates the measured tensile strength of lithium metal.	88
Figure 58. (a) Cycle performance and (b) charge/discharge voltage profiles of Li/Se-S battery with 45 wt% Se-S loading in 3M LiTFSI/ANL-2 at C/10.	93
Figure 59. Cycle performance of Li/Se-S battery with 45 wt% Se-S loading in (a) 5M LiTFSI/DME+ANL-2, (b) 5M LiTFSI/DOL+DME and (c) 5M LiTFSI/DOL+ANL-2 at C/10.	93
Figure 60. (a) Comparison of Brunauer–Emmett–Teller surface areas of pristine Integrated Ketjen Black / carbon nanofiber (IKB/CNF) carbon materials and after mixed with 10 wt% of different binders and (b) corresponding pore volume. (c) Cyclic voltammetry of IKB/CNF electrodes with polyarylamide and polytetrafluoroethylene (PAA and PTFE) binders (1.5-3.0 V, 0.05 mV/s), and (d) first discharge curves of sulfur electrodes with PAA and PTFE binders (sulfur loading > 6.3 mg/cm ² , E/S=4 μ L /mg, 0.05C).	96
Figure 61. Inductively coupled plasma – atomic emission spectroscopy data of sulfur-to-lithium atoms concentration ratio (a) remaining in supernatant solutions and (b) adsorbed onto candidate materials, after 3-mM Li ₂ S ₆ adsorption test.	99
Figure 62. X-ray photoelectron spectroscopy sulfur 2p spectra of candidate materials surface after Li ₂ S ₆ adsorption test for (a) carbon black, (b) TiO ₂ , and (c) V ₂ O ₅	99
Figure 63. (a) Effects of porosity, sulfur loading, and morphology on cell performance. (b) Evolution of different resistance modes during discharge. As the resistance value goes to 1, the mode becomes dominant.	102
Figure 64. (a) Lithium-sulfur bonding and lithium-carbon interaction at low lithium contents. (b) Electronic charge distribution at low lithium contents. Color code: carbon, grey; sulfur, yellow; and lithium, purple. In part (b) atoms are colored according to their electrostatic charge shown in the color bar.	102
Figure 65. (a) High-performance liquid chromatography/ultraviolet chromatograms for electrolytes with polysulfides after contacted with different current collectors for 180 days and for stock electrolyte with polysulfides after rest for 180 days at room temperature. (b) X-ray photoelectron spectroscopy measurements of sulfur 2p for five current collectors after contacted with electrolyte (containing 25-mM polysulfides) for 180 days. Black dot: raw data; black dash: baseline; red line: fitted data; blue line: different fitting sulfur 2p species.	105
Figure 66. Overpotential of lithium-lithium symmetric cells (a) with and (b) without the KW-stabilization layer at 2 mA cm ⁻²	107

Figure 67. (a) Overpotential of a symmetric cell with composite-coated separator for over 100 hours. (b) Cycling performance of the composite-coated separator in Li-S cells.	107
Figure 68. Possible molecular conformation of aromatic-based lithium organosulfide (a) and lithium organopolysulfide (b) originating from PSD polymer; alkyl amine-based lithium organosulfide (c) and lithium organopolysulfide (d) originating from PST polymer.....	110
Figure 69. The photos of PSD-90-Ely before cycling (a) and after 1 st cycle of lithium plating/stripping: (b) with separator covering on stainless steel, and (c) separator was peeled off.	111
Figure 70. Cycling performance of 2 wt% PSDs containing different sulfur contents as additives.....	111
Figure 71. (a) Voltage profiles of Li Li cells in 1M LiTFSI-DME, 1M LiTFSI-DME with 2% TTMSPi, or 1M LiTFSI-DME with 5% TTMSPi electrolytes, respectively, cycled at 0.2 mA cm ⁻² . (b) Enlarged voltage profiles of (a). (c) Voltage profiles of Li Li cells in 1M LiTFSI-DME with 2% TTMSPi and 1M LiTFSI-DME with 2% LiDFOB electrolytes, respectively, cycled at 0.2 mA cm ⁻²	114
Figure 72. Schematic of platinum modified MOF-derived catalysts. BND-Co@G = biphasic N-doped cobalt@graphene, Pt-SC-BND-Co@G = Pt surface-coating BND-Co@G, and Pt-BD-BND-Co@G = Pt bulk-doping BND-Co@G.	117

TABLE OF TABLES

Table 1. Conductivity of ionogels based on solvate ionic liquid.....	6
Table 2. Stress-strain behavior of self-healing composites.....	7
Table 3. Cells fabricated in Q1 FY 2018. Tests by electrochemical impedance spectroscopy and cycling at 0.1 or 0.01C.	80
Table 4. Prepared sulfur-containing polymers with different sulfur content.	110

A MESSAGE FROM THE ADVANCED BATTERY MATERIALS RESEARCH PROGRAM MANAGER

This document summarizes the BMR investigators' activities performed during the period from October 1, 2017, through December 31, 2017. Selected highlights from this first quarter of FY 2018 are summarized below:

- University of Washington (Jen and Yang's groups) synthesized solvate ionogels containing varying ratios and structures of polymerizable components. All solvate ionogels appeared as thin, transparent, flexible films. Gels containing long-chain (~ 3500 Da) PEGDMA were universally less stiff and more tolerant to handling than those with short-chain (750 Da) PEGDMA. Every formula tested showed an ionic conductivity of greater than 0.7 mS/cm, which is in itself higher than most previously-reported gel electrolytes based on Li⁺-containing ionic liquid of any kind.
- Lawrence Berkeley National Laboratory (Chen's group) investigated the impact of oxygen anionic redox on the performance of a disordered Li-excess oxide cathode and revealed that voltage fade and hysteresis/path dependence begin only after triggering anionic redox, all of which grow progressively with either deeper oxidation of oxygen at higher potential or extended cycling.
- University of California at San Diego (Meng's group) performed single-particle based *operando* Bragg coherent diffraction imaging and demonstrated the correlation between strain network formation and oxygen activity in a layered Li-excess oxide cathode.
- Texas A&M University (Balbuena's Group) demonstrated by a combination of experimental and simulation techniques that 2D films of graphene oxide can mitigate the dendrite growth by favoring a smooth deposition of lithium over the current collector.

The next BMR quarterly report will cover the progress made during January through March 2018 and will be available June 2018. For additional information regarding these efforts, please join us at our Annual Merit Review and Peer Evaluation meeting that will take place on June 18 – 21, 2018, at the Crystal Gateway Marriott hotel in Arlington, Virginia. The agenda for this event is now available online (<https://www.energy.gov/eere/vehicles/annual-merit-review-agenda>). We look forward to seeing you.

Sincerely,

Tien Q. Duong

Tien Q. Duong
Manager, Advanced Battery Materials Research (BMR) Program
Batteries R&D
Vehicle Technologies Office
Energy Efficiency and Renewable Energy
U.S. Department of Energy

TASK 1 – Liquid/Polymer Solid-State Electrolytes

Summary and Highlights

The BMR Program goal is to develop long-life batteries superior to commercial Li-ion systems in terms of cost, vehicle range, and safety. The BMR Program addresses the fundamental problems of electrode chemical and mechanical instabilities that have slowed development of affordable, high performance, automotive batteries. The aim is to identify electrode/electrolyte materials that yield enhanced battery performance and lead to greater acceptance of electric vehicles (EVs). Currently, the U. S. Department of Energy (DOE) Vehicle Technologies Office (VTO) supports six projects in the BMR Program under this Electrolytes Task. These projects can be categorized into three general topics:

- **Liquid.** The projects for liquid electrolyte aim to develop electrolyte formulations, based on fluoro-chemistries, to achieve significantly improved operating voltage, increased durability, and increased energy density of Li-ion batteries at a reasonable cost.
- **Polymer.** The target of polymer electrolyte projects is mainly for use in Li-S batteries. Inorganic/polymer and polymer/gel hybrid electrolytes that have flexibility, mechanical strength, thermal stability, high ionic conductivity, stable interfaces against lithium metal, and polysulfide-trapping capability will be developed to enable energy densities twice that of start-of-the-art Li-ion batteries, with comparable cycle life.
- **Self-Forming & Self-Healing.** The self-forming & self-healing electrolyte projects are focused on developing and implementing Li-metal-based metal fluorite and metal iodide batteries, capable of energy densities > 400-500 Wh/kg and 1000 Wh/L.

Highlights

At the Daikin group, in addition to expanding new surface analysis capabilities using X-ray photoelectron spectroscopy (XPS) and atomic emission spectroscopy (AES), cells with NMC (111, 532) cathodes were tested as a function of voltage and fluorinated ethylene carbonate (FEC) concentration. For discharge capacity of cells cycled at 4.6 V at 0.7C, they found that an increase in nickel content (50% in NMC-532 and 33% in NMC-111) and FEC concentration leads to improved performance of cells at high voltage. These results are consistent with reported findings from the fourth quarter of FY 2017 on LCO and NMC-622 cells cycled at 4.6 V.

The University of Maryland (UMD) group has successfully characterized microstructures of the hybrid solid-state electrolyte (SSE) with focused ion beam – scanning electron microscopy (FIB/SEM), atomic force microscopy (AFM), and profilometer.

At University of Washington (UW), the group has synthesized solvate ionogels containing varying ratios and structures of polymerizable components. All solvate ionogels appeared as thin, transparent, flexible films. Gels containing long-chain (~ 3500Da) poly(ethylene glycol) dimethacrylate (PEGDMA) were universally less stiff and more tolerant to handling than those with short-chain (750 Da) PEGDMA. Every formula tested showed an ionic conductivity of greater than 0.7 mS/cm, which is in itself higher than most previously reported gel electrolytes based on Li⁺-containing ionic liquid of any kind. In addition, extensive mechanical testing was carried out on series of self-healing polymer composites with varying self-healing temperatures termed PP-1, PP-Py, and PP-dbNDI to demonstrate their tensile properties and ability to recover following self-healing. Furthermore, to better understand the effect of thiol surface modification on S/C cathode performance, a series of ⁷Li nuclear magnetic resonance (NMR) experiments was performed.

The West Virginia University (WVU) group made progress in the following areas: synthesizing the inorganic nanofiber-polymer composite electrolytes by *in situ* polymerization of polymer on the surface of inorganic nanofibers; characterizing the microstructure of composite electrolytes, and studying the nanofiber-polymer interface; and measuring the temperature-dependent ionic conductivity of composite electrolytes, the transference number, and the electrochemical stability window.

At Stony Brook University (SBU), State University of New York (SUNY), three sets of solid electrolytes with variable LiI:AgI₂Al₂O₃ ratios were tested, each with three different amounts of LiI(HPN)₂ additive. These LiI(HPN)₂ containing samples were compared to solid electrolytes of the same composition without LiI(HPN)₂ additive. An increase in conductivity of up to 2 orders of magnitude was observed. To obtain higher ionic conductivities, while maintaining most of the mass of the electrolyte as LiI, three compositions, including 70% and 80% LiI in the solid electrolyte, were selected for development of cell construction next quarter. Preliminary cycling data were collected using a solid electrolyte containing LiI(HPN)₂ additive. All cells could be charged and functioned effectively, but efficiency was found to be higher for the Li-metal containing cells. Furthermore, investigations on modifications of the interface at the cathode side, including incorporation of poly-2-vinylpyrrolidine additive (P2VP), have been initiated.

At Rutgers University, the group refocused on continued development of the reactive positive current collector compositions and microstructure to further improve the utilization or degree of conversion into the initial amount of active metal fluoride during *in situ* formation. The group has developed a unique vapor deposition technique to enable rapid fabrication of unique multicomponent structured architectures with feature scales that can be easily adjusted from 1 nm to > 100 nm. With this scalable approach allowing increased F⁻ ion transport, the group has increased the positive reactive current collector utilization from approximately 30% to 63%. In addition, areal capacities increased over a factor of two, leading to full electrode capacities in excess of 1000 mAh/cc with an areal capacity approaching 0.4 mAh/cm². Furthermore, this technique has allowed for improved cycling stability.

Task 1.1 – Advanced Lithium-Ion Battery Technology: High-Voltage Electrolyte (Joe Sunstrom, Ron Hendershot, and Alec Falzone, Daikin)

Project Objective. The overall project objective is to identify electrolyte formulations, based on fluoro-chemistries, that will allow significantly improved operating voltage, increased durability, and increased energy density of Li-ion batteries at a reasonable cost. The project objective is to understand the conditions under which the electrolyte degrades, the effect on battery performance, and solutions that can overcome current limitations of the electrolyte. Gassing in Li-ion batteries is one of the most common failure mechanisms and poses the greatest safety risk in consumer devices. This project aims to investigate the gas composition as a function of cathode material, electrolyte formulation, and operating voltage, and proposes optimal cell compositions at decomposition voltages.

Project Impact. Developing an understanding of the operating conditions in which gasses form in Li-ion batteries enables the project to propose optimized cell compositions, which operate at higher voltages for a longer period. Different fluorinated electrolyte components and additives may suppress and/or eliminate gas generation at or above hypothesized decomposition voltages. To investigate these topics, it is imperative that the project utilize multiple approaches, including, but not limited to: cathode material, electrolyte composition, operating voltage, and cycle number.

Approach. The evolving composition of the electrolyte in the battery will be examined by various analytical instruments to study volatiles [gas chromatography – mass spectrometry (GC-MS)/thermal conductivity detector (TCD)], liquid [liquid chromatography MS (LC-MS)], and solid [time-of-flight secondary ion mass spectrometry (TOF-SIMS), thermogravimetric analysis MS (TGA-MS), XPS, and AES] electrolyte decomposition products during battery operation. In the first year, the team addressed the gas composition and kinetics for both hydrocarbon and fluorocarbon as a function of several charge/discharge conditions. In the second year, the project will transition into analysis of the solid-state electrolyte decomposition components of its tested batteries to obtain valuable information about solid electrolyte interphase (SEI) layer formation and how it manifests change in both the anode (graphite) and cathode (LCO and NMC).

Out-Year Goals. Work will progress toward understanding how electrolyte formulation, cathode chemistry, and cell operation affect SEI layer formation/properties. Specifically, measurements of thickness and elemental composition as a function of fluorinated electrolyte composition and voltage will be performed. Understanding the SEI layer and other solid-state components of Li-ion batteries will provide valuable information on the required surface properties for increased performance at high voltage.

Collaborations. There are currently no active collaborations.

Milestones

1. Gassing kinetics as a function of FEC concentration under different operating conditions. (Milestone 1.3; Completed)
2. Film thickness versus time/voltage complete. (Milestone 2.1; In Progress)
3. Film composition (elemental) versus time/voltage complete. (Milestone 2.2; In Progress)

Progress Report

An initial Auger survey and depth profile of a 200-mAh cell cycled 200 times at 4.5 V is depicted in Figure 1. This battery contains an electrolyte formulation of FEC:EC:EMC:FE + 1% PS (10:10:60:20 v/v), where FE is a fluorinated ether. Sulfur and phosphorus were absent in the SEI layer using the project's initial method on this cell at 5 keV. During sputtering of the SEI layer, there is a significant decrease in carbon abundance. In addition, the cobalt and oxygen abundance increases as the LCO cathode becomes exposed. The team is working on perfecting its AES and XPS methods to obtain accurate SEI layer properties, in addition to creating a known carbon-based film to serve as a sputter-rate standard.

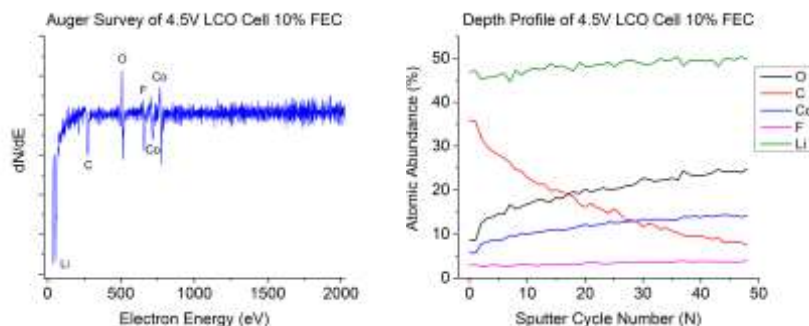


Figure 1. Scanning Auger results of a 4.5-V LCO cell cycled at 0.7C.

Figure 2 depicts the elemental maps (cobalt, fluorine, oxygen, carbon) from stereo-electrochemical deposition images after 50 sputter cycles of the SEI layer, exposing the LCO cathode particles. The regional cobalt (blue) and oxygen (lime) presence is almost identical, which is characteristic of the bulk LCO cathode post-ion sputtering. Fluorine (red) is present throughout the sample, and emanates from multiple sources including the SEI layer, polyvinylidene fluoride (PVDF) binder, and LiPF_6 salt residue in the LCO cathode. The distribution of carbon is limited to the presence of SEI layer, as seen in both Figure 1 and Figure 2. The surface topography of the cathodes and SEI layer is rough, which protects some areas from the ion gun beam. Carbon that is present after 50 sputter cycles is visible in Figure 2 as the positive intensity.

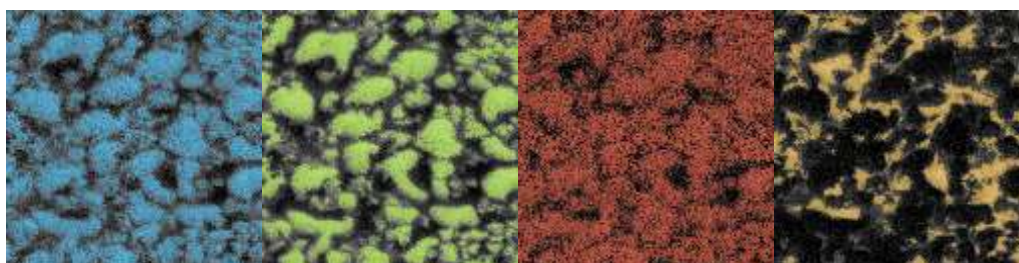


Figure 2. Post-sputter maps of cobalt (blue), oxygen (lime), fluorine (red), and carbon (yellow) of a 4.5-V LCO cell cycled at 0.7C.

In addition to expanding the project's new surface analysis capabilities (XPS and AES) at Daikin, cells with NMC (111, 532) cathodes were tested as a function of voltage and FEC concentration. Figure 3 depicts the discharge capacity of cells cycled at 4.6 V at 0.7C. Both an increase in nickel content (50% in NMC-532 and 33% in NMC-111) and FEC concentration leads to improved performance of cells at high voltage. These results are consistent with reported findings in the fourth quarter of FY 2017 on LCO and NMC-622 cells cycled at 4.6 V.

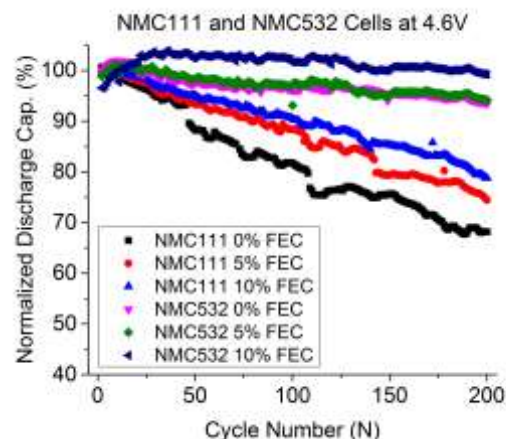


Figure 3. Discharge capacity of cells cycled at 0.7C.

Task 1.2 – Multi-Functional, Self-Healing Polyelectrolyte Gels for Long-Cycle-Life, High-Capacity Sulfur Cathodes in Lithium-Sulfur Batteries

(Alex Jen and Jihui Yang, University of Washington)

Project Objective. The project objective is to develop self-healing and polysulfide-trapping polyelectrolyte gels containing room-temperature ionic liquid (RTIL) for the Li-S battery system. The battery design will be able to achieve gravimetric and volumetric energy densities of ≥ 800 Wh/kg and ≥ 1000 Wh/L, respectively.

Project Impact. The Li-S battery system is currently hampered by poor capacity retention, primarily caused by dissolution of polysulfide reaction intermediates in typical organic electrolytes, as well as poor electrical contact between insulating sulfur and the conductive carbon matrix. This project aims to produce a high-capacity, long-cycle-life Li-S battery system by using rational molecular design strategies to address each capacity loss mechanism directly. A long-cycle-life Li-S battery system with the capability of doubling Li-ion energy density would enable production of lighter, longer range EVs at a cost that is affordable to the average U. S. household.

Approach. The team will develop Li-S coin cells that utilize self-healing, interpenetrated ionomer gel electrolytes in both the cathode and separator. The team will synthesize necessary starting materials and fabricate components of these gels while testing their relevant electrochemical and mechanical properties. All components will be combined into interpenetrating structures, which will be tested both alone and in cell configurations. Device performance data will be collected and used to further optimize designs of both material and cell, culminating in an optimized Li-S battery design capable of doubling the energy density of traditional Li-ion batteries. During the first year, the team is focusing on (1) synthesis of a variety of precursors for gel electrolytes, (2) fabrication and testing of both baseline materials and novel materials made from these precursors, and (3) iterative validation and improvement of design principles through both materials and device testing.

Out-Year Goals. Work will progress toward developing structure-property relationships for the self-healing, interpenetrated gel ionomer electrolyte and its individual components, as well as successful incorporation of such an electrolyte into a working Li-S cell. The team plans to demonstrate significant improvements in both capacity and retention when using the project's novel materials, as compared to state-of-the-art baseline systems.

Collaborations. This project funds work at the UW. Dr. Alex Jen, principal investigator (PI), focuses on design, synthesis, and testing of novel materials, as well as device-based verification of design principles. Dr. Jihui Yang (Co-PI) focuses on optimization of device fabrication and testing, as well as investigation of failure mechanisms in devices using novel materials. Pacific Northwest National Laboratory (PNNL) facilities will be used for detailed study of device operation.

Milestones

1. Select a particular self-healing gel formulation (set of organic starting materials) for continued study based on electrochemical and mechanical properties. (Q2, FY 2018)
2. Provide detailed cell performance data for concept cells containing currently-best materials designs. (Q4, FY 2018)

Progress Report

Multifunctional Ionomer Gels. Using the project's previously developed gel fabrication method, the team screened several solvate ionogel formulas containing varying ratios and structures of polymerizable components. The overall volume percentage of liquid was kept constant at 80%. Hand die cutters were used to punch circular samples from cured gels, which were then used to test properties including bulk ionic conductivity and Li-metal stripping/plating ability. Conductivity was measured at 23°C through electrochemical impedance spectroscopy (EIS), as shown in Figure 4; results are summarized in Table 1. All conductivities listed are the average of several measurements from multiple samples. All solvate ionogels appeared as thin, transparent, flexible films. Gels containing long-chain (~3500 Da) PEGDMA were universally less stiff and more tolerant to handling than those with short-chain (750 Da) PEGDMA.

Table 1. Conductivity of ionogels based on solvate ionic liquid.

Gel #	PEGDMA (750 Da)	PEGDMA (3500 Da)	PyrTFSIMA	TEGMA	Li(G4)TFSI	1,4-diox	σ (10^{-3} S/cm)
1	20%	0%	0%	0%	80%	0%	0.73
2	0%	20%	0%	0%	80%	0%	1.05
3	0%	10%	10%	0%	80%	0%	1.07
4	0%	10%	0%	10%	80%	0%	0.92
5	0%	20%	0%	0%	66.6%	13.3%	2.15

Several interesting conductivity trends are observable. First, every formula tested showed an ionic conductivity of greater than 0.7 mS/cm, which is in itself higher than most previously reported gel electrolytes based on Li^+ -containing ionic liquid of any kind. In fact, the conductivities of formulas 2 and 3 were measured to be slightly above 1 mS/cm, which is unprecedented and approaches that of neat Li(G4)TFSI (1.6 mS/cm at 30°C). Both formulas contain a long-chain PEGDMA synthesized in-house. Because the ratio of methacrylate end caps to PEG becomes smaller with increasing chain length, more PEG is present in long-chain samples when overall volume percentage of PEGDMA is kept constant. This increased PEG content may lead to weakening of electrostatic interactions between ions and to improved mobility, much like the effect of an organic solvent diluent. When an actual diluent (1,4-dioxane) is introduced in a 1:5 ratio with Li(G4)TFSI, a doubling of conductivity to above 2 mS/cm is observed, indicating that solvent addition is a viable strategy for improving conductivity.

The ability of solvate ionogels to reversibly strip and plate lithium metal was tested by fabricating a Li||Li symmetric cell using an ionogel separator (0.23 mm). This was compared to a symmetric cell containing neat Li(G4)TFSI in a porous glass fiber separator (0.125 mm). Both cells were subjected to repeated 3-hour intervals of $\pm 0.1 \text{ mA/cm}^2$ current density (6 hours per cycle). Both samples showed smooth, repeatable overpotential curves, with the gel sample actually displaying lower overpotential after 10 cycles (~40 mV) than neat Li(G4)TFSI (~75 mV), despite larger overall separator thickness. This demonstrates one advantage of using a freestanding gel film as opposed to a porous separator with liquid electrolyte, which decreases effective conductivity.

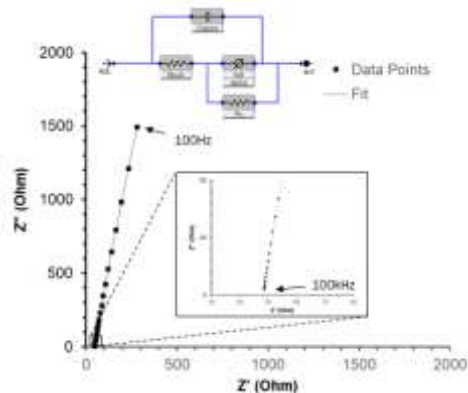


Figure 4. Representative electrochemical impedance spectroscopy data for Gel 2, obtained by placing a 7-mm diameter gel sample between two stainless-steel electrodes. The equivalent circuit used for fitting is shown. The value of R_{bulk} was used in conjunction with film area and thickness to obtain a conductivity value.

Self-Healing Materials. Previously, the team demonstrated a series of self-healing polymer composites with varying self-healing temperatures termed PP-1, PP-Py, and PP-dbNDI. Extensive mechanical testing was carried out on these composites to demonstrate their tensile properties and ability to recover following self-healing. Stress-strain curves (50 mm/min loading rate) for all three composites are displayed in Figure 5a, and data are summarized in Table 2. Notably, all composites exhibit Young's moduli far above the vast majority of self-healing materials in literature (< 10 MPa). The high stiffness of the composite should help it to maintain conductive pathways in a battery cathode environment.

Table 2. Stress-strain behavior of self-healing composites.

Specimen	Maximum Tensile Stress (MPa)	Maximum Tensile Strain (%)	Young's Modulus (MPa)
PP-1	2.84	109%	116.47
PP-Py	2.11	66%	69.97
PP-dbNDI	3.48	87%	219.47

Representative films were sliced in two, contacted under minimal pressure, and healed for 12 hours at 40–60°C, followed by stress-strain testing. Figure 5b–c summarizes the results. All films are able to self-heal to some degree, even at 40°C, as evidenced by recovery of mechanical properties. Due to its weaker binding strength and lower crosslinking density, PP-Py possesses the highest self-healing efficiency.

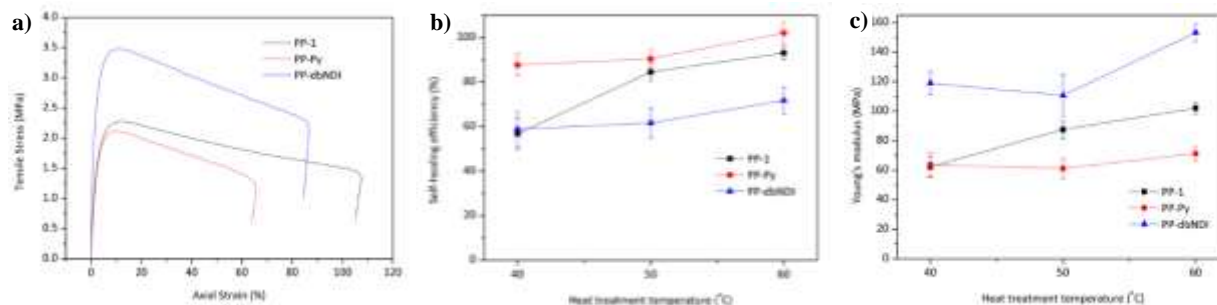


Figure 5. (a) Stress-strain curves of the self-healing composites prior to any mechanical damage. (b) Recovery of maximum tensile strength upon self-healing of composite films. (c) Recovery of Young's modulus upon self-healing of composite films.

Mesoporous Carbon Functionalization. To better understand the effect of thiol surface modification on S/C cathode performance, a series of ^7Li NMR experiments was performed in conjunction with Dr. Ying Chen at PNNL. Both modified and unmodified carbons were exposed to Li_2S_x , generated either chemically (not pictured here) or *in situ* electrochemically in a functioning S/C cathode. The team observed a series of convoluted peaks clustered around 0 ppm, all of which represent solvated Li^+ ions in relatively different chemical environments. Peaks appearing relatively downfield represent Li^+ ions in closer proximity to one another than in solution, that is, aggregated polysulfides. During cell discharge, modified samples exhibit a preference for aggregating Li_2S_x rather than forming solid Li_2S , as shown in pristine samples. This could be interpreted as indirect evidence for the proposed mechanism of polysulfide sequestration by chemically induced aggregation in thiol-modified samples. The team continues to analyze this data.

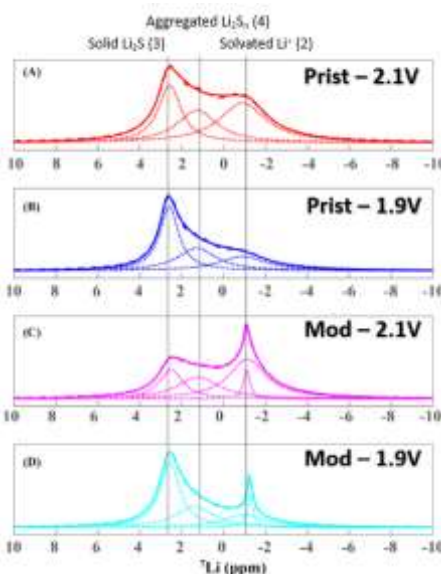


Figure 6. ^7Li NMR of S/C composite cathodes mid-discharge (2.1 V) and at end of discharge (1.9 V). Both types of carbon composite show evidence of Li^+ in both free (peak 2) and aggregated (peak 4) polysulfides, as well as solid Li_2S (peak 3). The modified sample shows a larger ratio of aggregated polysulfide to solid Li_2S at 2.1 V than the unmodified sample.

Patents/Publications/Presentations

Publications

- Qin, J., F. Lin, D. Hubble, Y. Wang, Y. Li, I. Murphy, S.-H. Jang, J. Yang, and A. K.-Y. Jen. “Tuning Self-Healing Properties of Stiff, Ion-Conductive Polymers.” In preparation.
- Hubble, D., J. Qin, F. Lin, Y. Li, I. Murphy, S.-H. Jang, J. Yang, and A. K.-Y. Jen. “Solvate Ionogels with High Conductivity for Use in Lithium Metal Batteries.” In preparation.
- Li, Y., I. Murphy, F. Lin, D. Hubble, J. Qin, S.-H. Jang, A. K.-Y. Jen, and J. Yang. “Improved Li-S Battery Performance Using Thiol-Modified Mesoporous Carbon Hosts.” In preparation.

Task 1.3 – Development of Ion-Conducting Inorganic Nanofibers and Polymers (Nianqiang (Nick) Wu, West Virginia University; Xiangwu Zhang, North Carolina State University)

Project Objective. The project objective is to develop SSEs based on the highly-conductive inorganic nanofibrous network in the polymer matrix for lithium batteries.

Project Impact. The research team will conduct research and development (R&D) on solid-state inorganic nanofiber-polymer composite electrolytes that will not only provide higher ionic conductivity, improved mechanical strength, and better stability than the polyethylene oxide polymer electrolyte, but also exhibit better mechanical integrity, easier incorporation, and better compatibility with the Li-metal anode than the planar ceramic membrane counterparts. The proposed inorganic nanofiber-polymer composite electrolytes will enable practical use of high-energy-density, high-power-density Li-metal batteries, and Li-S batteries.

Approach. Integration of the highly Li^+ -conductive inorganic nanofiber network into the polymer matrix not only provides the continuous Li^+ transport channels, but also kinetically inhibits the crystallization from the amorphous state of polymer electrolyte. The inorganic nanofibers will be fabricated with an electrospinning technique; the ionic conductivity of inorganic nanofibers will be improved by chemical substitution or doping. Highly ionic-conductive polymers will be developed by cross-linking and/or creation of a block-copolymer structure. The composition and microstructure of the composite electrolyte will be designed to suppress the Li-dendrite formation.

Out-Year Goals. Work will progress toward synthesis of the inorganic nanofibers and the polymer matrix. The goal is to find the optimal synthetic route to achieve the desirable conductivity.

Collaborations. This project funds work at WVU and North Carolina State University (NCSU). Dr. Nianqiang (Nick) Wu at WVU serves as PI, and Dr. Xiangwu Zhang at NCSU acts as Co-PI. Sujan Kasani (Ph.D. student at WVU), Hui Yang (Postdoctoral Fellow at WVU), Botong Liu (Ph.D. student at WVU), Chaoyi Yan (Ph.D. student at NCSU), and Mahmut Dirican (Postdoctoral Fellow at NCSU) contributed to the project.

Milestones

1. Synthesize the inorganic nanofiber-polymer composite electrolytes by *in situ* polymerization of polymer on the surface of inorganic nanofibers – Subtask 2.1. (Q1, FY 2018; Completed, 30%)
2. Characterize microstructure of composite electrolytes; study nanofiber-polymer interface – Subtask 2.2. (Q1, FY 2018; Completed, 20%)
3. Measure temperature-dependent ionic conductivity of composite electrolytes, transference number, and electrochemical stability window – Subtask 2.3. (Q1, FY 2018; Completed, 30%)

Progress Report

The theoretical calculation was performed on the nitrogen doping of erovskite-type lithium lanthanum titanate $\text{Li}_{0.33}\text{La}_{0.56}\text{TiO}_3$ (lithium-lanthanum-titanium-oxide, LLTO) nanofibers. The transporting barrier for N-doped structure decreased from 0.365 eV to 0.185 eV. In addition, the cross-linked poly(ethylene oxide) (PEO) polymers (CLP) and lithium poly[(4-styrenesulfonyl) (trifluoromethanesulfonyl)imide-co-polyethylene glycol methacrylate]/PEO cross-linked polymers (Li-c-PGMEA CLP) were synthesized using the photo-initiated polymerization process. The electrochemical performance of the CLP-P4-LLTO composite solid electrolytes was evaluated.

Synthesis and Characterization of Inorganic Nanofibers

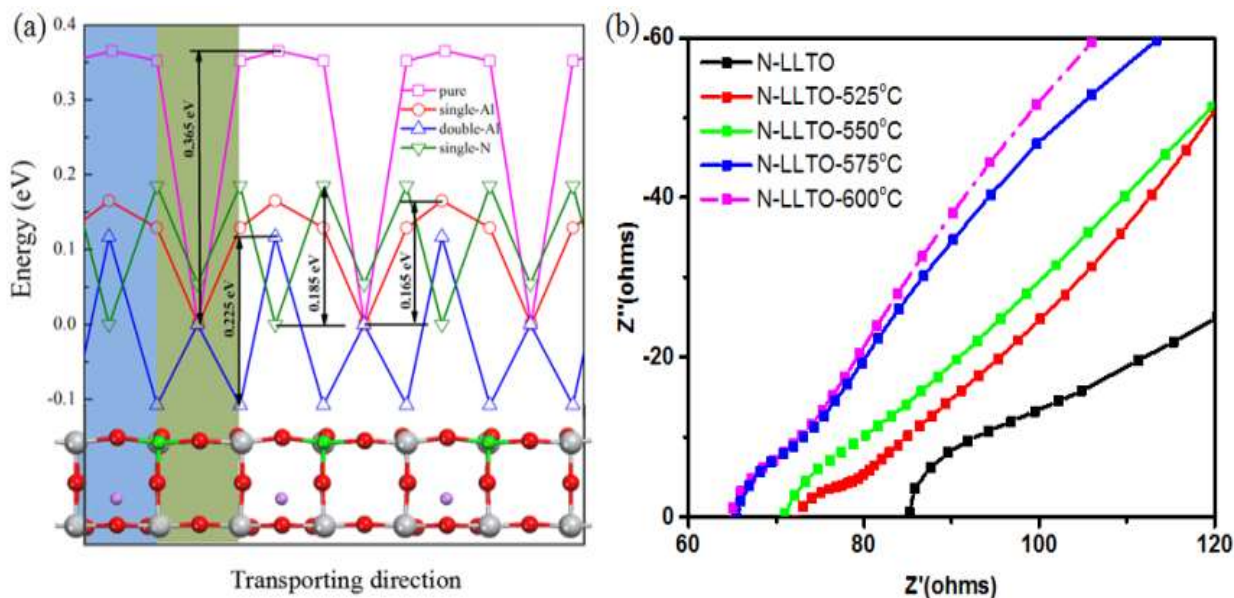


Figure 7. (a) Transporting barriers for lithium atoms along transporting direction in pure, single-Al, double-Al, and single-N decorated $\text{Li}_{0.33}\text{La}_{0.56}\text{TiO}_3$ structure. The transporting trajectory is marked by dash line in inset, (b) electrochemical impedance spectroscopy profiles of PVDF-HFP/LiTFSI/N-LLTO membrane.

Calculation of N-Doped LLTO structures. In LLTO, the oxygen atom sites can be doped by nitrogen atoms. After that single-O atom was doped by a nitrogen atom, the transporting barriers for pure, single-N decorated structure are 0.365 eV and 0.185 eV (Figure 7a), respectively. The distance between lithium and titanium atoms in the door was larger than the distance between lithium and oxygen atoms in the door. The electron changing value for the N-doped LLTO was smaller than that of the Al-doped counterpart. The Coulomb potential for the N-doped LLTO was smaller than that of the Al-doped counterpart. Besides calculation, the project treated the LLTO nanofibers with ammonia under 525~600°C. The ionic conductivity for PVDF-hexafluoropropylene (PVDF-HFP)/LiTFSI/N-LLTO of the pristine LLTO and the N-doped LLTO at 550°C was 0.6×10^{-4} S/cm and 3.8×10^{-4} S/cm, respectively (Figure 7b).

Synthesis of Polymer Matrix

Cross-Linked PEO Polymer with LiTFSI Salt. This quarter, the PEO CLPs were synthesized using a photo-initiated polymerization process. Adding plasticizer in the CLP can greatly improve the ionic conductivity, which was due to a decrease in the glass transition temperature of the CLP. The ionic conductivity for CLP, CLP-P1, CLP-P2, CLP-P3, and CLP-P4 with 10 wt%, 20 wt%, 30 wt%, and 40 wt% plasticizer was 2.96×10^{-5} , 7.62×10^{-5} , 1.05×10^{-4} , 1.25×10^{-4} , and 1.65×10^{-4} S/cm, respectively.

Li[PSTFSI-co-PGMEA]/PEO CLPs. Lithium poly[(4-styrenesulfonyl) (trifluoro-methanesulfonyl)imide-co-polyethylene glycol methacrylate]/PEO CLPs (Li-c-PGMEA CLP) were also synthesized. Instead of LiTFSI lithium salt, lithium (4-styrenesulfonyl) (trifluoromethanesulfonyl)imide (LiSsTFSI) monomer was used. With different molar ratios of ethylene oxide monomer to lithium monomer ($[\text{EO}]/[\text{Li}^+] = 32, 16, 8$), Li-c-PGMEA CLP1 demonstrates the highest ionic conductivity of $7.68 \times 10^{-6} \text{ S cm}^{-1}$ at room temperature, while the corresponding ionic conductivities of Li-c-PGMEA CLP2 and Li-c-PGMEA CLP3 are 3.94×10^{-6} and $1.88 \times 10^{-6} \text{ S/cm}$, respectively.

Development of Inorganic Nanofibers-Polymer Composites

Inorganic nanofiber/cross-linked PEO polymer composite solid electrolytes were fabricated by dispersing $\text{Li}_{0.33}\text{La}_{0.557}\text{TiO}_3$ (LLTO) ceramic nanofibers in a prepolymer solution (PEGDMA, PGMEA, HPCK, and LiTFSI). CLP-P4 was selected as the polymer matrix since it gives the highest ionic conductivity $1.65 \times 10^{-4} \text{ S/cm}$. The CLP-P4-LLTO-3 with 30 wt% LLTO nanofibers showed the highest ionic conductivity of $2.13 \times 10^{-4} \text{ S/cm}$.

Linear sweep voltammetry (LSV) was carried out to test the stability of CLP-P4 polymer electrolyte and CLP-P4-LLTO-3 composite solid electrolyte. Both the solid electrolytes exhibit stable voltage windows between 1 V to 5 V versus Li/Li^+ . The CR2032 coin type cells with LiFePO_4 cathode, Li-metal anode, and the optimal solid composite electrolyte membrane of CLP-P4 with 30 wt% LLTO (CLP-P4-LLTO-3) were assembled in the glovebox. The all-solid-state $\text{LiFePO}_4|\text{CLP-P4-LLTO-3}|\text{lithium}$ cell demonstrates high capacity retention of $\sim 98\%$ and high Coulombic efficiency (CE) of 99% after 100 cycles, indicating that the CLP-P4-LLTO-3 composite solid electrolyte can sustain a stable cycling in Li-ion batteries. Moreover, the all-solid-state cell shows excellent rate capability. Discharge capacities of 158, 154, 147, 138, and 122 mAh g^{-1} can be obtained at varied C rates of 0.05, 0.1, 0.2, 0.5, and 1, respectively. Stable charge and discharge plateaus of all-solid-state cells were consistent with those of conventional liquid cells.

Task 1.4 – High Conductivity and Flexible Hybrid Solid-State Electrolyte (Eric Wachsmann, Liangbing Hu, and Yifei Mo, University of Maryland)

Project Objective. The project objective is to develop flexible hybrid electrolyte with garnet nanofibers to achieve the following: (1) flexible, with greater mechanical strength (~ 10 MPa) and thermal stability than polymer electrolytes; (2) high room-temperature ionic conductivity, ~ 0.5 mS/cm; (3) stable interface with lithium metal and effective blocking of lithium dendrites at current densities up to 3 mA/cm²; and (4) battery performance with Li-S chemistry with an energy density of ≥ 450 Wh/kg (and ≥ 1000 Wh/L) and maintaining $\geq 80\%$ of capacity up to 500 cycles.

Project Impact. Instability and/or high resistance at the interface of lithium metal with various solid electrolytes limit the use of the metallic anode for batteries with high energy density, such as Li-air and Li-S batteries. The critical impact of this endeavor will be focused on developing a new type of SSE that is highly conductive, highly flexible, and electrochemically stable. The new SSE will enable Li-metal anodes with excellent interfacial impedance and blocking of Li-dendrite formation.

Approach. The project will synthesize garnet nanofibers, fill the porous region with polymer electrolyte, and characterize the flexible hybrid membrane properties. The flexible hybrid SSE microstructure will be determined using FIB/SEM and integrated with electrochemical methods to investigate the properties and stability with Li-metal anode.

Out-Year Goals. This project will develop further understanding of electrochemical, mechanical, and thermal properties of produced hybrid electrolytes, and characterize the three-dimensional (3D) structures. It will evaluate electrochemical performance of thin hybrid electrolytes with Li-metal anodes and demonstrate dendrite-free cycling.

Collaborations. This project funds work at UMD, College Park. Dr. Eric D. Wachsmann (PI) will focus on optimizing the garnet network to achieve high ionic conductivity and flexibility using FIB/SEM and EIS characterization. Dr. Liangbing Hu (Co-PI) focuses on synthesis of the hybrid electrolyte and test for Li-metal anode with the hybrid electrolyte. Dr. Yifei Mo (Co-PI) will lead efforts on computational modeling of the garnet nanofiber hybrid electrolytes for fundamental mechanistic understanding.

Milestones

1. Fully characterize microstructures with FIB/SEM, AFM, and profilometer. (Q2, FY 2018; Completed January 2018)
2. Fully characterize electrochemical, mechanical, and thermal properties of hybrid SSE. (Q3, FY 2018)
3. Fabricate hybrid SSE with 20- μ m thickness and understand the Li-hybrid SSE interface through Li-SSE-Li symmetric cells. (Q4, FY 2018)
4. Understand lithium stripping and plating in thin SSE at a current density of 3 mA/cm². (Q1, FY 2019)
5. *Go/No-Go Decision*: No lithium dendrites at 3 mA/cm² for 500 cycles.

Progress Report

The 3D morphology of garnet textile was scanned using a LK-H082 semiconductor laser model with a wavelength of 655 nm (Keyence). The reconstructed digital structure in Figure 8 shows a typical over-one –under-one, plain-weave textile pattern. Height profiles of the topography indicate the distance between the highest position of the cross-yarn junction and the lowest position with ground contact in the pattern. The junction areas were generally around 200- μm in height, while some of the edge areas showed slightly larger values. The upward edge curling can be eliminated by strict process control to ensure proper sintering.

The surface morphology of the composite electrolyte was analyzed by AFM within an area of 10 μm *10 μm (Figure 9). As the polymer material has been infiltrated to fully fill the open pores and cover the surface of the individual fibers within the textile structure, it is able to form flat and continuous surface of the composite electrolyte. By controlling the infiltration procedure, the surface roughness of the composite electrolyte was effectively limited to a value of less than 2 μm .

Epoxy bond was infiltrated into the ceramic fiber mat sample and cured for 3D FIB tomography. The exposed polished cross-section sample was mounted in the Tescan XEIA FIB-SEM sample holder. First, the project used a high ion beam current to mill out the region of interest for 3D sampling. Then, it used a lower ion beam current to remove the redeposited material and polish the sides of the region of interest. Finally, it used an even lower ion beam current to finish polishing. The 3D sampling produced secondary electron images with good contrast between the ceramic fiber mat particles (which appeared bright) and the infiltrated epoxy (which appeared dark), as shown in Figure 10. Two typical images of the fiber-bundle slices during the 3D run are shown in Figure 10; the ceramic fibers run in the plane of the image, so the cross-sections are visible. The continuous ceramic fiber structure will provide structure reinforcement and abundant fast Li-ion conductive pathways within the composite electrolyte.

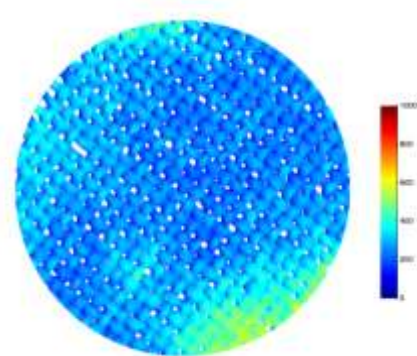


Figure 8. Reconstructed model of garnet textile flatness uniformity generated by 3D laser scanning.

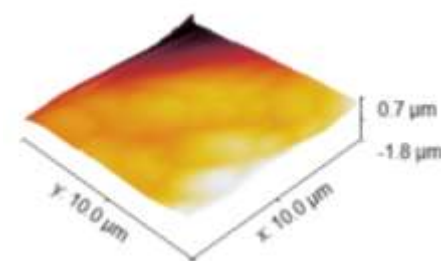


Figure 9. Atomic force microscopy scanning of the hybrid polymer/garnet textile composite electrolyte.

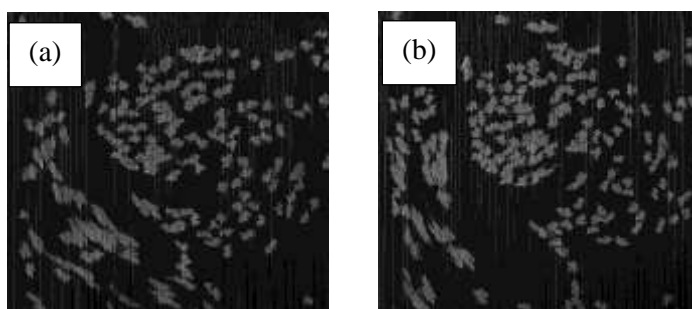


Figure 10. Focus ion beam analysis of the typical fiber bundle structure in garnet textile.

Patents/Publications/Presentations

Publication

- Gong, Y., K. Fu, S. Xu, J. Dai, T. R. Hamann, L. Zhang, G. T. Hitz, Z. Fu, Z. Ma, D. W. McOwen, X. Han, L. Hu, and E. D. Wachsman. “Lithium-Ion Conductive Ceramic Textile: A New Architecture for Flexible Solid-State Lithium Metal Batteries.” *Materials Today*. In press.

Task 1.5 – Self-Forming Thin Interphases and Electrodes Enabling 3D Structured High-Energy-Density Batteries (Glenn Amatucci, Rutgers University)

Project Objective. The project objective is to develop and implement a novel *in situ* formed Li-metal-based metal fluoride battery that will enable packaged 10-mAh batteries of energy densities > 1000 Wh/L and > 400 Wh/kg at 12 V.

Approach. The project is divided into two main tasks that focus on the advance of the self-forming chemistry concurrent to the cell design and fabrication. The self-forming chemistry task is comprised of three subtasks encompassing the negative and positive reactive current collectors, and the bi-ion glass conductor. The cell design and fabrication target the development and integration of the bipolar configuration to achieve the 12-V single cell goal.

Impact. Successful realization of 3D batteries formed *in situ* with a practical approach to large-scale fabrication would address some of the DOE EV performance goals, including: (1) areal capacity increase, (2) improved rates, and (3) designs to enable high-voltage unit cells.

Out-Year Goals. Work will continue toward improving reactive current collectors and cell design to optimize electrochemical performance of the cell stack in terms of energy density both gravimetric and volumetric as well as capacity retention upon cycling. A secondary focus will be implementation of bipolar design within the cell structure.

Collaborations. All project tasks will be performed at Rutgers University.

Milestones

1. Establish negative reactive current collector compositions that enable high efficiency of lithium plating and stripping in excess of 90% during the *in situ* formation step and > 95% during subsequent cycles. (Q2, FY 2018; In progress)
2. Establish optimal type and composition of bi-ion conductors that achieve ionic conductivities in excess of 1×10^{-4} S/cm after *in situ* formation. (Q3, FY 2018; Concluded in Q1, FY 2017).
3. Establish cell-stack design with 75% utilization of the positive reactive current collector and 12 V. (Q1, FY 2018; In progress)
4. *Go/No-Go Decision:* Achieve self-formed cell-stack of at least 1000 Wh/L and 300 Wh/kg at a rate of C/10, output voltage of 12 V, and > 80% capacity retention after 100 cycles.

Progress Report

Consistent progress has been realized in FY 2017 through advancements in chemistry, cell architecture, and hybridization of transport pathways. One main accomplishment consisted in achieving the end-goal of 500-Wh/L energy density with cells reaching 570 Wh/L. This quarter, the project refocused on the continued development of the reactive positive current collector compositions and microstructure to further improve the utilization or degree of conversion into the initial amount of active metal fluoride during *in situ* formation. Although the team had been able to achieve constant advance throughout the past year by improving the reactive positive current collector utilization up 30%, much work is still needed to attain satisfying levels for practical use.

As such, the team concluded it was prudent to establish a pathway to understand the limitations and optimize the positive and negative electrode reactions separately. It isolated the positive electrode formation reaction and evaluated all the cell components in a more traditional stacked arrangement. Initial studies replicated the electrode areal capacities and >30% utilization of the positive electrode achieved in the full planar *in situ* formed architecture. The team then embarked on evaluating the transport limited processes involved within the *in situ* formed positive electrode. It identified severe transport limitations that precluded achievement of higher utilizations. In response, the team developed a unique vapor deposition technique to enable the rapid fabrication of unique multicomponent structured architectures with feature scales that can be easily adjusted from 1 nm to > 100 nm. With this scalable approach allowing increased F^- ion transport, the project has increased the positive reactive current collector utilization from approximately 30% to 63%. In addition, areal capacities increased over a factor of two, leading to full electrode capacities in excess of 1000 mAh/cc with an areal capacity approaching 0.4 mAh/cm². Furthermore, this technique has allowed for improved cycling stability as shown in Figure 11.

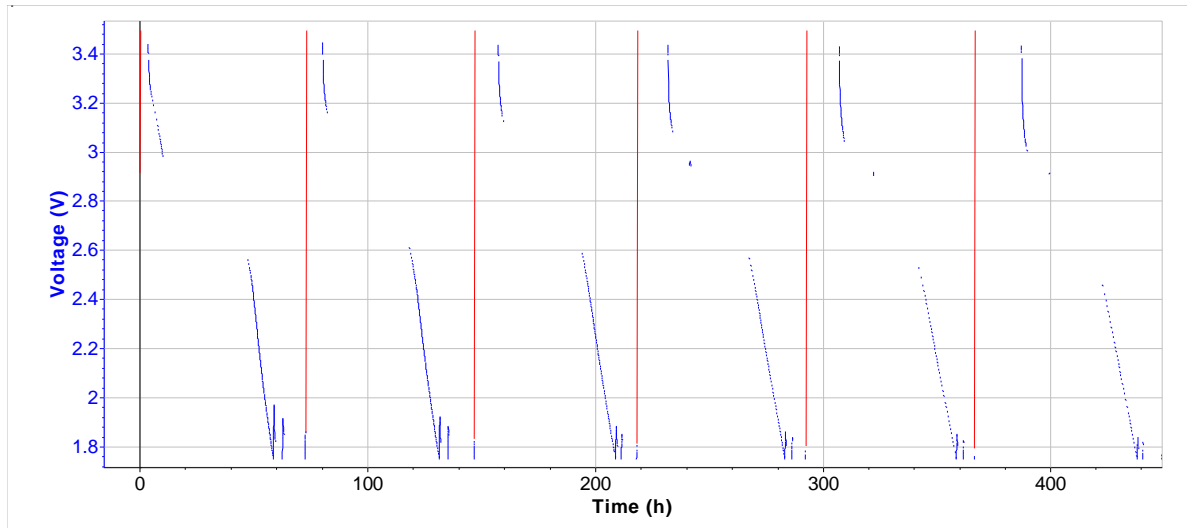


Figure 11. Constant voltage charge / constant current discharge profile representative of new, multicomponent structured architecture cells.

The next step is to characterize and remediate changes in electronic conductivity of the positive electrode, followed by a distinct focus on the kinetics and reactivity of the deposited lithium metal at the negative electrode. All rates continue to be in the C/2-C/20 range, which represents a two-order magnitude of rate increase from one year ago.

Task 1.6 – Dual Function Solid-State Battery with Self-Forming, Self-Healing Electrolyte and Separator (Esther Takeuchi, Stony Brook University)

Project Objective. The project objective is to demonstrate a solid-state rechargeable battery based on a Li-metal anode and iodine cathode with a self-forming, self-healing electrolyte and separator with high gravimetric and volumetric energy density.

Project Impact. This program will enable demonstration of the proposed rechargeable battery with improved power capability, high energy density, and a self-forming, self-healing SSE/separator. Technical insight will be gained regarding improved conductivity of the solid lithium iodide (LiI) based electrolyte, power capability of the proposed system, the self-healing nature of the LiI layer, the nature of the electrode-electrolyte interfaces, and feasibility of the system to reach the DOE targets.

Approach. The proposed concept is a dual function rechargeable solid-state battery utilizing LiI combined with silver iodide (AgI) as the electrolyte, with lithium metal (and small quantities of silver metal) as the anode and iodine as the cathode with a self-forming, self-healing separator/electrolyte. The battery will be assembled in the discharged state where the anode and cathode will be created during the first formation (charge) step. Initially, silver ion (Ag^+) will diffuse toward the negative electrode and be reduced to silver metal (Ag^0), and iodine ion (I^-) will be oxidized to elemental iodine (I_2) at the cathode side. As the formation of the battery continues, lithium ion (Li^+) will form a Li-metal layer at the anode, with generation of iodine at the cathode. LiI will remain and serve as both the separator and electrolyte.

Out-Year Goals. This is a multiyear program where the effort is divided into three major tasks.

- Year 1 involves electrolyte preparation and characterization including preparation of SSEs and conductivity measurements.
- Year 2 will focus on cell construction and testing including both *in situ* and *ex situ* analysis.
- Year 3 will focus on cell characterization. Under the program, cycle life, efficiency, energy density, and the functional capacity of cells will be determined.

Collaborations. This project collaborates with Amy Marschlok and Kenneth Takeuchi of SBU.

Milestones

1. Identify the 3 most conductive silver containing LiI solid electrolytes with or without $\text{LiI}(\text{HPN})_2$. (Q1, FY 2018; Completed)
2. Develop cell construction A (current collectors, tab configuration, etc.) for Li/I_2 batteries with or without P2VP. (Q2, FY 2018; Initiated)
3. Prepare construction A cells with the 3 most conductive electrolytes from Subtask 2.1.0. (Q3, FY 2018; Initiated)
4. *Go/No-Go Decision*: Formation of Li^0 , Ag^0 at anode and iodine at cathode with charging. (Q4, FY 2018; Initiated)

Progress Report

Ag Containing LiI Solid Electrolytes with or without Polymer Additive. The milestone this quarter was identification of the three most conductive silver containing LiI solid electrolytes with or without polymer 3-hydroxypropionitrile additive. This additive was initially combined with solid LiI to form LiI(HPN)_2 , which was incorporated into solid LiI and Ag containing electrolytes in varying ratios. The addition of LiI(HPN)_2 was evaluated for improvements in ionic conductivity as measured and quantified by AC impedance and equivalent circuit modeling. LiI(HPN)_2 additive was systematically studied in solid electrolytes with a fixed ratio of $\text{AgI:Al}_2\text{O}_3$. Three sets of variable $\text{LiI:AgI:Al}_2\text{O}_3$ ratios were tested, each with three different amounts of LiI(HPN)_2 additive. These LiI(HPN)_2 containing samples were compared to solid electrolytes of the same composition without LiI(HPN)_2 additive. A select number of samples with LiI(HPN)_2 additive across the temperature range from 42–28°C are shown in Figure 12, where an increase in conductivity of up to 2 orders of magnitude is observed.

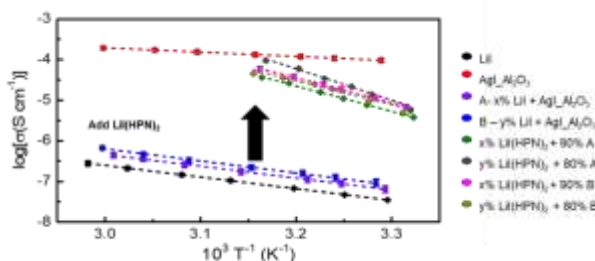


Figure 12. Conductivity effects of addition of LiI(HPN)_2 .

Figure 13 shows a comparison of ionic conductivities of prepared LiI(HPN)_2 containing solid electrolytes at 30°C. To obtain higher ionic conductivities, while maintaining most of the mass of the electrolyte as LiI, three compositions, including 70% and 80% LiI in the solid electrolyte, were selected for development of cell construction A (Q2 milestone).

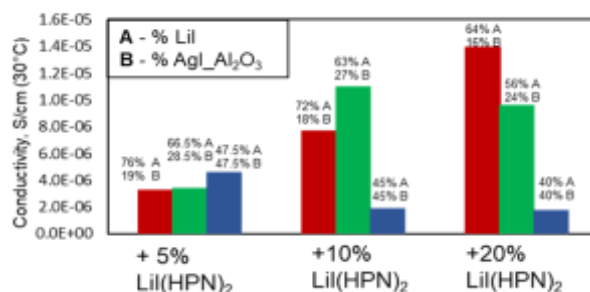


Figure 13. Comparison of LiI(HPN)_2 containing solid electrolytes at 30°C.

Preliminary Electrochemical Data. Preliminary cycling data were collected using a solid electrolyte containing LiI(HPN)_2 additive. Cells were constructed with and without an additional lithium source and were cycled to test feasibility (Figure 14a) as well as to evaluate the CE compared to cycle number (Figure 14b). Both sets of cells could be charged and functioned effectively, but the efficiency was higher for the Li-metal containing cells.

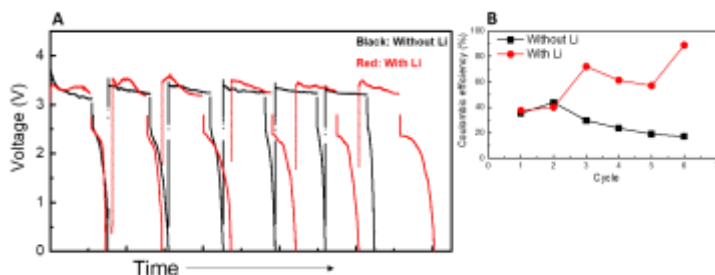


Figure 14. (a) Cycling of cells containing LiI(HPN)_2 additive with and without lithium metal added. (b) Coulombic efficiency.

Polymer Additives at the Cathode Interface. Investigations on modifications of the interface at the cathode side, including the incorporation of P2VP, have been initiated; the modifications will be studied in solid electrolytes containing LiI(HPN)_2 additive.

TASK 2 – DIAGNOSTICS

Summary and Highlights

To meet the goals of the VTO Multi-Year Program Plan and develop lower-cost, abuse-tolerant batteries with higher energy density, higher power, better low-temperature operation, and longer lifetimes suitable for the next-generation of EVs, hybrid EVs (HEVs), and plug-in hybrid EVs (PHEVs), there is a strong need to identify and understand structure-property-electrochemical performance relationships in materials, life-limiting and performance-limiting processes, and various failure modes to guide battery development activities and scale-up efforts. In pursuit of batteries with high energy density, both high cell operating voltages and demanding cycling requirements lead to unprecedented chemical and mechanical instabilities in cell components. Successful implementation of newer materials such as silicon anode and high-voltage cathodes also requires better understanding of fundamental processes, especially those at the solid/electrolyte interface of both anode and cathode.

This Task takes on these challenges by combining model system, *ex situ*, *in situ*, and *operando* approaches with an array of state-of-the-art analytical and computational tools. Four subtasks are tackling the chemical processes and reactions at the electrode/electrolyte interface. Researchers at Lawrence Berkeley National Laboratory (LBNL) use *in situ* and *ex situ* vibrational spectroscopy, far- and near-field scanning probe spectroscopy and laser-induced breakdown spectroscopy (LIBS) to understand the composition, structure, and formation/degradation mechanisms of the SEI at silicon anode and high-voltage cathodes. The University of California at San Diego (UCSD) combines scanning transmission electron microscopy – electron energy loss spectroscopy (STEM/EELS), XPS, and *ab initio* computation for surface and interface characterization and identification of instability causes at both electrodes. At the University of Cambridge, NMR is being used to identify major SEI components, their spatial proximity, and how they change with cycling. Subtasks at Brookhaven National Laboratory (BNL) and PNNL focus on the understanding of fading mechanisms in electrode materials, with the help of synchrotron-based X-ray techniques (diffraction and hard/soft X-ray absorption) at BNL and high-resolution transmission electron microscopy (HRTEM) and spectroscopy techniques at PNNL. At LBNL, model systems of electrode materials with well-defined physical attributes are being developed and used for advanced diagnostic and mechanistic studies at both bulk and single-crystal levels. These controlled studies remove the ambiguity in correlating a material's physical properties and reaction mechanisms to performance and stability, which is critical for further optimization. The final subtask takes advantage of the user facilities at Argonne National Laboratory (ANL) that bring together X-ray and neutron diffraction, X-ray absorption, emission and scattering, HRTEM, Raman spectroscopy, and theory to investigate the structural, electrochemical, and chemical mechanisms in the complex electrode/electrolyte systems. The diagnostics team not only produces a wealth of knowledge key to developing next-generation batteries, it also advances analytical techniques and instrumentation that have a far-reaching effect on material and device development in various fields.

The highlights for this quarter are as follows:

- Lawrence Berkeley National Laboratory (Chen's group) investigated the impact of oxygen anionic redox on the performance of a disordered Li-excess oxide cathode and revealed that voltage fade and hysteresis/path dependence begin only after triggering anionic redox, all of which grow progressively with either deeper oxidation of oxygen at higher potential or extended cycling.
- UC San Diego (Meng's group) performed single-particle based *operando* Bragg coherent diffraction imaging and demonstrated the correlation between strain network formation and oxygen activity in a layered Li-excess oxide cathode.

Task 2.1 – Model System Diagnostics for High-Energy Cathode Development (Guoying Chen, Lawrence Berkeley National Laboratory)

Project Objective. This project will use a rational, non-empirical approach to design and synthesize next-generation high-energy, high-voltage cathode materials. Combining a suite of advanced diagnostic techniques with model cathode materials and model electrode/electrolyte interfaces, the project will perform systematic studies to achieve the following goals: (1) obtain new insights into solid-state chemistry, particularly cationic and/or anionic redox activities during charge and discharge of high-capacity lithium transition metal (TM) oxides, (2) gain fundamental understanding on cathode/electrolyte interfacial chemistry and charge transfer process as a function of operating voltage, (3) reveal performance- and stability-limiting properties and processes in high-energy, high-voltage cathodes, and (4) develop strategies to mitigate the structural and interfacial instabilities.

Project Impact. The project will improve the commercial viability of next-generation high-energy cathode materials. The findings will enable more stable high-voltage cycling of existing Li-TM oxides as well as development of novel high-capacity cathode materials for advanced Li-ion batteries.

Approach. The project will prepare crystal samples of Li-stoichiometric and Li-excess TM oxides with well-defined physical attributes. It will perform advanced diagnostic and mechanistic studies at both bulk and single-crystal levels. Global properties and performance of the samples will be established from the bulk analyses, while the single-crystal-based studies will utilize time- and spatial-resolved analytical techniques to probe the material redox transformation process and failure mechanisms under battery operating conditions.

Out-Year Goals. In the out-years, the project will obtain fundamental knowledge on performance-limiting physical properties, phase transition mechanisms, parasitic reactions, and transport processes that prevent cathode materials from delivering higher capacities and achieving more stable cycling at high voltages. It will develop approaches to mitigate cathode structural and interfacial instabilities during high-voltage operation. Further, it will design and synthesize optimized Li-TM oxide cathodes as well as novel high-energy electrode materials.

Collaborations. This project collaborates with the following: G. Ceder, K. Persson, M. Doeff, B. McCloskey, and P. Ross (LBNL); V. Srinivasan (ANL); D. Nordlund and Y. Liu (Stanford Synchrotron Radiation Lightsource, SSRL); C. Wang (PNNL); C. Grey (Cambridge); and A. Huq and J. Nanda (Oak Ridge National Laboratory, ORNL).

Milestones

1. Characterize oxygen activities during charge/discharge and extended cycling of Li-TM oxides and understand effect on cathode structural and electrochemical reversibility. (December 2017; Completed)
2. Investigate analytical techniques to determine the kinetics of anion redox process, and evaluate factors influencing rate capability of Li-TM oxide cathodes. (March 2018; On schedule)
3. Apply advanced diagnostic techniques to investigate the reactivities of model oxide surfaces and understand their impact on oxide performance and safety. (June 2018; On schedule)
4. *Go/No-Go Decision:* Reveal the impact of oxide chemistry and particle morphology on the extent of reversible oxygen redox versus lattice oxygen loss, and understand how to fine tune oxygen activities at high voltages. *No-Go:* if the processes of reversible oxygen redox and lattice oxygen loss cannot be decoupled with diagnostic studies. (September 2018; On schedule)

Progress Report

Layered LMR cathode materials have met significant challenges in commercialization due to performance deterioration associated with structural changes. Recent interest has turned to alternative high-capacity oxides with a disordered structure. This quarter, the impact of oxygen redox activities on electrochemical performance of Li-excess disordered oxide cathodes was investigated on a model rock-salt $\text{Li}_{1.3}\text{Nb}_{0.3}\text{Mn}_{0.4}\text{O}_2$ sample. Previous studies revealed a two-step redox process with dominating $\text{Mn}^{3+}/\text{Mn}^{4+}$ redox at low state of charge and oxygen activities at voltages above 4.3 V. To systematically adjust the extent of oxygen redox participation, cyclic voltammetry (CV) scans between 1.5 V and various upper cut off voltages of 4.2, 4.4, 4.6, and 4.8 V were performed on $\text{Li}_{1.3}\text{Nb}_{0.3}\text{Mn}_{0.4}\text{O}_2$ cathode. As shown in Figure 15a, stable cycling with an anodic peak centered at ~ 3.2 V and a cathodic peak at ~ 3.0 V was observed when the voltage limit was set to 4.2 V, suggesting full reversibility of the cation redox. Increasing the limit to 4.4 V triggered a new anodic peak at the cut-off voltage that signals the activation of oxygen redox (Figure 15b). Although stability mostly maintains, slight upper voltage shift of the anodic peak and current reduction of the cathodic peak were observed with cycling. Further increasing the voltage limit to 4.6 and 4.8 V largely increases the participation of oxygen redox, as evidenced by the much larger anodic peak centered at ~ 4.5 V (Figure 15c-d). With cycling, the intensity of this peak decreased quickly, suggesting that the oxygen redox is largely irreversible. Furthermore, the anodic peak centered at ~ 3.2 V continued to shift towards high voltage, while the cathodic peak at ~ 3.0 V was gradually replaced by a weak reduction peak at ~ 2.2 V. After 25 cycles, the CV profiles were dominated by a pair of redox peaks separated by more than 2 V. The results demonstrate a clear correlation between oxygen anionic redox participation, voltage fade, and hysteresis/path dependence. Voltage fade and hysteresis begin only after triggering anionic redox, which grows progressively with either deeper oxidation of oxygen at higher potential or extended cycling. This is remarkably similar to what was observed on the layered LMR materials, suggesting that the negative impact of oxygen redox is not limited to the layered structure.

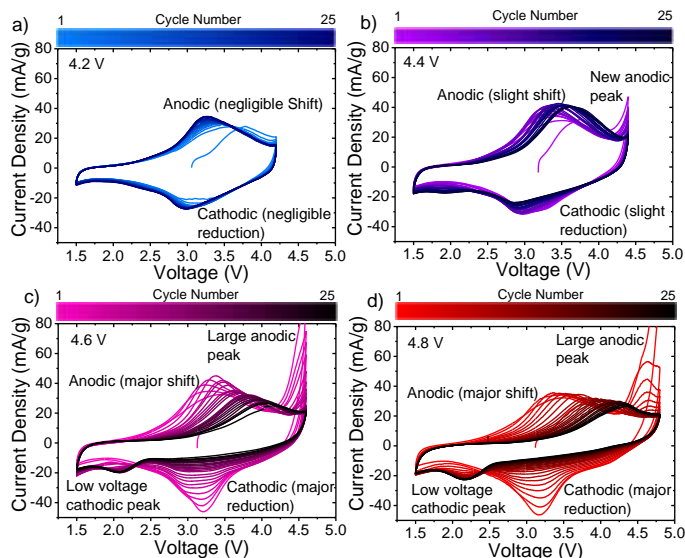


Figure 15. Cyclic voltammograms of $\text{Li}_{1.3}\text{Nb}_{0.3}\text{Mn}_{0.4}\text{O}_2$ half-cells cycled between 1.5 V and various upper cut off voltages of: (a) 4.2 V, (b) 4.4 V, (c) 4.6 V, and (d) 4.8 V. Scan rate: 5 mV/min.

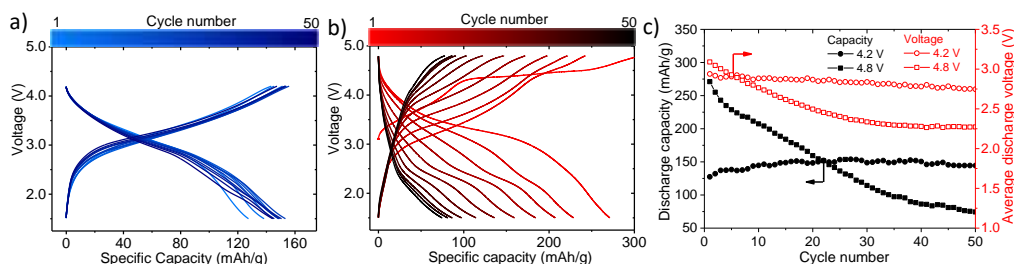


Figure 16. Voltage profiles of $\text{Li}_{1.3}\text{Nb}_{0.3}\text{Mn}_{0.4}\text{O}_2$ half-cells cycled at 10 mA/g between voltages of: (a) 1.5 – 4.2 V and (b) 1.5 – 4.8 V, and (c) specific discharge capacity and average voltage as a function of cycle number.

The correlation between upper limit voltage and performance deterioration was further evidenced in charge/discharge cycling of $\text{Li}_{1.3}\text{Nb}_{0.3}\text{Mn}_{0.4}\text{O}_2$ half-cells. Figure 16a-b shows voltage profiles of cells cycled to 4.2 and 4.8 V, respectively. While stable cycling was achieved at the 4.2 V cutoff voltage, significant capacity fade and voltage decay were observed in the cell cycled to 4.8 V. Involvement of oxygen redox leads to a high initial discharge capacity of ~ 275 mAh/g, but only ~ 70 mAh/g remains after 50 cycles, as shown in Figure 16c.

Patents/Publications/Presentations

Publication

- Kan, W. H., D. Chen, J. K. Papp, A. K. Shukla, A. Huq, C. M. Brown, B. McCloskey, and G. Chen. “Unravelling Solid-State Redox Chemistry in $\text{Li}_{1.3}\text{Nb}_{0.3}\text{Mn}_{0.4}\text{O}_2$ Single-Crystal Cathode Material.” Submitted to *Chemistry of Materials* (2018).

Presentations

- 232nd Electrochemical Society (ECS) Meeting, National Harbor, Maryland (October 2017): “Strategies for Developing High-Energy Lithium-Ion Battery Cathodes”; D. Chen, J. Zhu, and G. Chen.
- 2017 Bay Area Battery Summit, Livermore, California (November 2017): “Advanced High-Energy Cathode Materials for Lithium-Ion Batteries”; J. Zhu and G. Chen.

Task 2.2 – Interfacial Processes – Diagnostics (Robert Kostecki, Lawrence Berkeley National Laboratory)

Project Objective. This collaborative project will develop and apply advanced experimental methodologies to study and understand the mechanism of operation and degradation of high-capacity materials for rechargeable cells for PHEV and EV applications. The objective is to develop and apply *in situ* and *ex situ* far- and near-field optical multi-functional probes to obtain detailed insight into the active material structure and physicochemical phenomena at electrode/electrolyte interfaces at a spatial resolution corresponding to the size of basic chemical or structural building blocks. The goal is to design new diagnostic techniques and experimental methodologies capable of unveiling the structure and reactivity at hidden or buried interfaces and interphases that determine material, composite electrode, and full-cell electrochemical performance and failure modes.

Project Impact. Instability and/or high resistance at the interface of battery electrodes limits electrochemical performance of high-energy density batteries. A better understanding of the underlying principles that govern these phenomena is inextricably linked with successful implementation of high-energy-density materials in Li-ion and Li-based cells for PHEVs and EVs. The proposed work constitutes an integral part of the concerted effort within the BMR and supports development of new electrode materials for high-energy rechargeable cells.

Approach. The pristine and cycled composite electrode and model thin-film electrodes will be probed using various surface- and bulk-sensitive techniques, including Fourier transform infrared (FTIR), attenuated total reflectance (ATR)–FTIR, near-field infrared (IR) and Raman spectroscopy and microscopy and scanning probe microscopy to identify and characterize changes in materials structure and composition. Novel *in situ/ex situ* far- and near-field optical multifunctional probes in combination with standard electrochemical and analytical techniques are developed to unveil the structure and reactivity at interfaces and interphases that determine materials electrochemical performance and failure modes.

Out-Year Goals. In the out-years, the project aims to: (1) determine the degradation mechanism(s) of high-voltage cathodes; and (2) propose and test effective remedies to intrinsic interfacial instability of these materials and composite electrodes.

Collaborations. Electrode materials and composite electrodes tested under different cycling regimes by M. Doeff (LBNL) and C. Ban (National Renewable Energy Laboratory, NREL) will be studied. The diagnostic studies will be carried out in sync with differential electrochemical mass spectrometry (DEMS) analysis by B. McCloskey (LBNL) and other diagnosticians in the BMR program. He will also work closely with V. Battaglia (LBNL) to obtain samples from full-cell cycling experiments.

Milestones

1. Controlled growth of model thin-film electrodes by pulsed laser deposition (PLD) as model system for fundamental electrochemical studies. *Go/No-Go Decision*: Stoichiometric thin films produced with sub-nanometer roughness. (December 2017; Completed)
2. Characterize bulk and surface structure of model PLD thin films and the relation to electrochemical properties. *Go/No-Go Decision*: Electrochemical performance of model system in line with that of bulk materials. (Q2, FY 2018; On schedule)
3. Characterize chemistry of electrolyte decomposition at model PLD thin-film electrodes with near-field technique. (Q3, FY 2018; On schedule)
4. Determine electrochemical impedance contribution from interface between organic electrolyte and electrode active material. *Go/No-Go Decision*: Development of model electrodes with high electrochemical stability and low impedance. (Q4, FY 2018; On schedule)

Progress Report

This quarter, the project deposited NMC thin films on aluminum substrate by PLD and demonstrated that it is a suitable approach for studying electrode/electrolyte interfaces in rechargeable batteries. The surface morphology of the electrode was analyzed by AFM (Figure 17a). The film consists of densely packed 100-nm grains with surface roughness ca. 10.9 nm (root mean square, RMS). The X-ray diffraction (XRD) (Figure 17b) and Raman (Figure 17c) analysis both confirmed the NMC layered structure with a pronounced preferred crystal orientation along $\langle 003 \rangle$ direction. The chemical analysis of the thin film, performed by inductively coupled plasma (ICP) resulted in Ni: Mn: Co ratio equal to 50.1: 29.2: 20.7 (wt%), which confirmed the same composition as the pristine NMC-532 powder used for target in the PLD system.

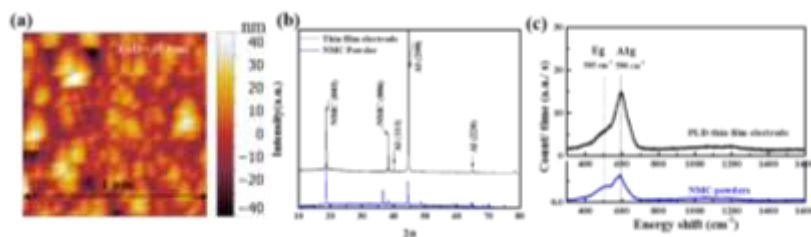


Figure 17. (a) Atomic force microscopy image, (b) X-ray diffraction, and (c) Raman spectrum of NMC thin-film electrode made by pulsed laser deposition.

Electrochemical tests of the thin-film electrodes were performed in a Swagelok cell. Lithium foil was used as counter electrode, and 1M LiPF₆ in EC/DEC=1/1 (v/v) as electrolyte. The cyclic voltammogram (Figure 18a) exhibits a main reduction and oxidation peak at 3.7 V and 4 V respectively, similar to those typically observed for NMC composite electrodes.

The binder and carbon additive free PLD thin-film electrodes allow selective and specific chemical analysis of electrode/electrolyte interfaces without interference from other active and passive components. The FTIR-ATR spectrum of the pristine- and the cycled- electrode are shown in Figure 18b. Each adsorption peak was indexed with certain vibration modes

characteristic for specific functional groups. The pristine thin-film electrode shows small amount of Li₂CO₃, which is a common impurity at NMC surface. After 3 cycles, many adsorption peaks emerged, and most of them can match well with spectral features of glycols (blue band), $\nu(\text{P-F})$ (purple band), and $\nu(\text{C=O})$ (orange band). The formation of glycol species has also been previously reported for LiMn₂O₄^[1]; however, here, it is reported for the first time in NMC electrode by IR analysis. It is known that polyethylene glycol species exhibit Li⁺ conductivity. Indeed, they have also been employed as components for gel-based electrolytes in Li-ion batteries^[2]. Thus, glycol species in the surface film may not be responsible for the observed impedance rise due to ion diffusion limitations. However, their poor electronic conductivity may contribute to the rise of the contact resistance between particles in the composite electrodes, resulting in electrode and cell performance degradation. This completes the first quarter FY 2018 milestone.

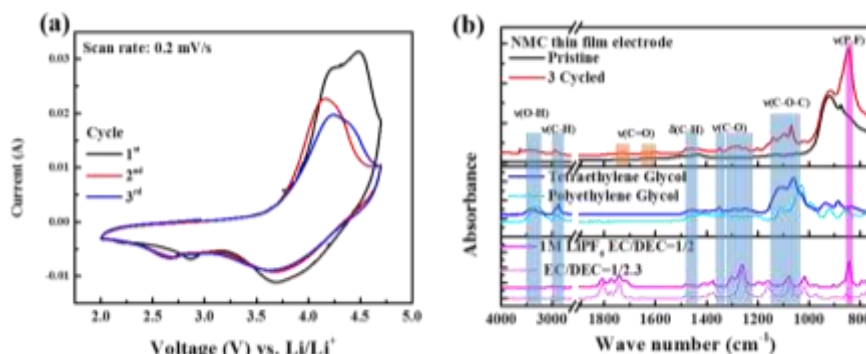


Figure 18. (a) Voltammogram trace of the NMC thin-film electrode. (b) Fourier transform infrared-attenuated total reflectance spectrum of the pristine and 3-cycled NMC thin-film electrode, tetraethylene glycol and polyethylene glycol standard, 1M LiPF₆ EC/DEC=1/2 (v/v) electrolyte and EC/DEC=1/2.39.

[1] Liu, Y. M., B. G. Nicolau, J. L. Esbenshade, and A. A. Gewirth. *Analytical Chemistry* 88 (2016): 7171–7177.

[2] Meyer, W. H. *Advanced Materials* 10 (1998): 439.

Patents/Publications/Presentations

Presentations

- 232nd ECS Meeting, National Harbor, Maryland (October 3, 2017): “The Mechanism of Impedance Increase in Nickel-Rich NMC Cathodes”; Rung-Chuan Lee, Chixia Tian, Marca Doeff, and Robert Kostecki.
- 2017 Bay Area Battery Summit, Livermore, California (November 14, 2017): “Study the Degradation Mechanism of NMC Cathodes in Li-ion Batteries”; Rung-Chuan Lee and Robert Kostecki.

Task 2.3 – Advanced *In Situ* Diagnostic Techniques for Battery Materials (Xiao-Qing Yang and Seongmin Bak, Brookhaven National Laboratory)

Project Objective. The primary project objective is to develop new advanced *in situ* material characterization techniques and to apply these techniques to support development of new cathode and anode materials for the next generation of Li-ion batteries for PHEVs. To meet the challenges of powering the PHEV, Li-ion batteries with high energy and power density, low cost, good abuse tolerance, and long calendar and cycle life must be developed.

Project Impact. The VTO Multi-Year Program Plan describes the goals for battery: “Specifically, lower-cost, abuse-tolerant batteries with higher energy density, higher power, better low-temperature operation, and longer lifetimes are needed for development of the next-generation of HEVs, PHEVs, and EVs.” The knowledge gained from diagnostic studies through this project will help U. S. industries develop new materials and processes for new generation Li-ion batteries in the effort to reach these VTO goals.

Approach. This project will use the combined synchrotron-based *in situ* X-ray techniques (XRD; hard and soft X-ray absorption spectroscopy, XAS) with other imaging and spectroscopic tools such as HRTEM and MS to study the mechanisms governing the performance of electrode materials.

Out-Year Goals. In the out-years, the project will complete development of diagnostic techniques using X-ray pair distribution function (x-PDF), XRD, and XAS combined with neutron diffraction and neutron PDF (n-PDF), as well as STEM imaging and transmission X-ray microscopy (TXM) for cathode materials studies. It will then apply these techniques to study the structural changes of various new cathode materials.

Collaborations. The BNL team will work closely with material synthesis groups at ANL (Drs. Shin and Amine) for the high-energy composite; and at PNNL for the Si-based anode materials. The project will also collaborate with industrial partners at GM and Johnson Controls, as well as with international collaborators.

Milestones

1. Complete the *in situ* TXM studies of LiCoO₂ cathode materials during charge-discharge cycling to evaluate the inhomogeneity of the charged (discharged) states among large number of material particles and using data mining technique to detect the under (over) reacted minority regions (particles). (Q1, December 2017; Completed)
2. Complete the neutron diffraction studies of LiCoO₂ as high-energy-density cathode material at high-voltage charge in comparison with the pristine state. (Q2, March 2018; In progress)
3. Complete the PDF studies of LiCoO₂ using both x-PDF and n-PDF probes to study the mechanism of anionic redox reaction (ARR) in such widely used commercial cathode materials for Li-ion batteries and explore the potential of using this material for high-energy-density cell applications. (Q3, June 2018; In progress)
4. Complete the experimental design, data collection and analysis of 3D STEM tomography studies of high-energy-density Li_{1.2}Ni_{0.15}Co_{0.1}Mn_{0.55}O₂ cathode materials at pristine state and after multiple cycling. (Q4, September 2018; In progress)

Progress Report

This quarter, the first milestone for FY 2018 was completed, and progress toward other milestones was made. BNL focused on designing and developing an *in situ* TXM imaging technique for battery material research. The team designed and constructed a special pouch-cell setup for TXM study and used this setup to study the inhomogeneity of the charged states of LiCoO_2 cathode material among a large number of particles using a data mining technique to detect the under (over) reacted minority regions. Among all the particles scanned in the experiment, the clustering algorithm identified four clusters of pixels (cluster maps are shown in Figure 19b/d/f; corresponding spectra are shown in Figure 19g-h). The first two clusters are anticipated, and they cover more than 98% of the data, but cluster analysis identified two spectrally distinct particles (clusters 3# and 4# in P37 and P46, respectively). The team would emphasize that it is not possible to identify P37 and P46 as distinct from the rest of the particles solely by analysis of each of the data attributes individually, or by examination of the transmission images (see Figure 19a/c/e for transmission images collected at 7850 eV). In Figure 19a/c/e, the team notices the highest contrast in P37, P46, and P14, which actually contain all four different clusters. It again echoes the discussion regarding importance of data attribute weighting for emphasizing chemical heterogeneity rather than density. As shown in the radar chart in Figure 19i, the differences in the spectroscopic signatures of the unanticipated species are fully captured only by combining several of the extracted data attributes, which also highlights the effectiveness of the project's data mining analysis approach.

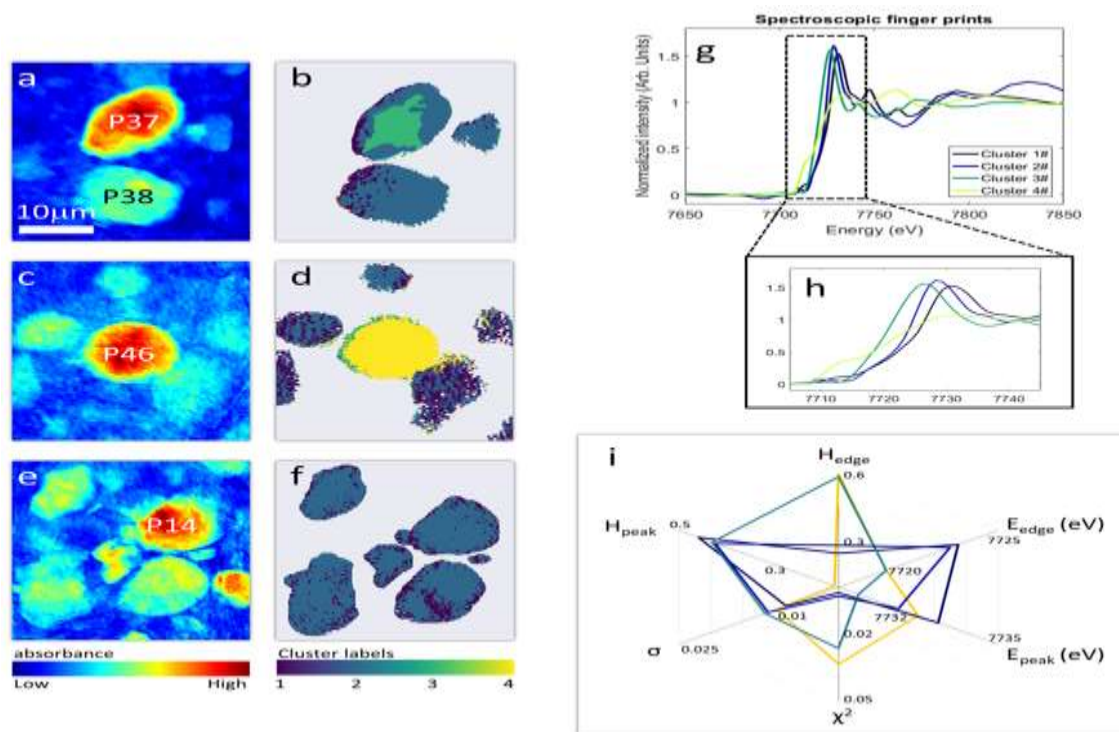


Figure 19. The minority phases identified by the project's data-mining approach. Panels (a) and (c) show the transmission images of the field-of-views covering particles (P37 and P46), which are identified by the method as minority phases. Panel (e) is the transmission image of another typical field-of-view that contains several normal LiCoO_2 particles. Panels (b), (d), and (f) show the clustering results, with the four different clusters color coded to the corresponding inset. The project compares the spectroscopic fingerprints of all four clusters in panels (g) and (h). It is interesting to note that clusters 1# and 2# are both similar to LiCoO_2 . The radar chart in panel (i) shows that the differences in the spectroscopic fingerprints of the 4 clusters are systematically captured by the data attributes extracted in this approach. The scale bar in panel (a) is 10 microns.

Patents/Publications/Presentations

Publications

- Lyu, Yingchun, Enyuan Hu, Dongdong Xiao, Yi Wang, Xiqian Yu, Guiliang Xu, Steven N. Ehrlich, Khalil Amine, Lin Gu, Xiao-Qing Yang, and Hong Li. “Correlations between Transition Metal Chemistry, Local Structure and Global Structure in $\text{Li}_2\text{Ru}_{0.5}\text{Mn}_{0.5}\text{O}_3$ Investigated in a Wide Voltage Window.” *Chemistry of Materials*. Web publication Date: October 20, 2017. doi: 10.1021/acs.chemmater.7b02299.
- Zhang, Kai, Fang Ren, Xuelong Wang, Enyuan Hu, Yahong Xu, Xiao-Qing Yang, Hong Li, Liquan Chen, Piero Pianetta, Apurva Mehta, Xiqian Yu, and Yijin Liu. “Finding a Needle in the Haystack: Identification of Functionally Important Minority Phases in an Operating Battery.” *Nano Letters* 17, no. 12 (2017): 7782–7788. Web publication date: November 8, 2017. doi: 10.1021/acs.nanolett.7b03985.

Presentation

- 1st International Conference on Energy Storage Materials (ICEnSM), Shenzhen, China (November 18 – 21, 2017): “Using Synchrotron Based X-ray Scattering and Absorption Spectroscopy and TXM imaging Techniques to Study the New Cathode Materials for Next Generation of Batteries”; Seongmin Bak, Enyuan Hu, Xiao-Qing Yang, Hung-Sui Lee, Mingyuan Ge, Yong Chu, Xiqian Yu, Hong Li, Yuguo Guo, and Yijin Liu. Invited.

Task 2.4 – Nuclear Magnetic Resonance and Magnetic Resonance Imaging Studies of Solid Electrolyte Interphase, Dendrites, and Electrode Structure (Clare Grey, University of Cambridge)

Project Objective. The growth of a stable SEI on most electrode materials is key to long-term capacity retention of a working Li-ion battery. On anodes such as silicon, this is particularly critical because the continual expansion and contraction of this intermetallic upon alloying with lithium exposes fresh, reactive surfaces that result in further electrolyte decomposition and SEI growth. This project will perform a detailed multinuclear NMR study of the SEI that forms on silicon, where thick SEIs typically grow and where SEI stability is a key aspect hindering commercialization. The focus will be to determine how additives (for example, FEC) and charging parameters (for example, voltage) influence SEI composition and stability. Fundamental studies of SEI structure *in operando* will be complemented by a synthetic program aimed at preparing new silicon coatings based on phosphazene (P-N) elastomeric polymers to increase CE. Further, the nature of SEI is one factor that appears to control the type of lithium microstructures that form on lithium metal during cycling. To test this hypothesis, the project will use magnetic resonance imaging (MRI) to investigate lithium dendrite versus moss formation in different electrolytes as a function of salt concentration and with different additives. Finally, it will compare lithium and sodium metal anode chemistries to determine composition, morphology, and stability of local structures that form on sodiating anodes such as tin and hard carbons.

Project Impact. The first impact of this project will be a molecular-level understanding of how factors such as applied voltage and electrolyte additives modify the SEI that forms on silicon anodes. The insight gained from these studies will guide the design of new P-N coatings for silicon. A rationally designed surface coating has the potential to improve SEI stability, and thus increase CE for silicon and beyond. A description of how SEI composition influences lithium microstructures will provide the foundation to mitigate dendrite formation during cycling that currently limits the safety of many promising electrode materials. These approaches will be extended to study Na-ion battery electrodes to provide an understanding of how to chemically manipulate both electrodes as well as the electrolyte to avoid adverse failure mechanisms in next-generation batteries.

Out-Year Goals. The project goals are as follows: (a) determine the effect of voltage and additives (for example, FEC) on the composition of the silicon SEI; (b) synthesize and test new inorganic coatings to increase the CE seen on cycling silicon; (c) identify correlations between SEI structure and thickness and Li-metal dendrite formation; and (d) determine the local and long-range structures formed on cycling sodium anode materials and compare with lithium. To facilitate these goals, the project will prepare ^{13}C -enriched FEC for ^{13}C NMR multinuclear studies to investigate the SEI that forms on silicon during cycling. It will synthesize new P-N polymers for coating silicon nanoparticles and probe changes in performance in the presence of these coatings. In addition, the project will use MRI to correlate lithium dendrite formation with the nature of the SEI. Finally, it will apply the methods developed to study lithium chemistries to investigate sodium electrodes.

Collaborations. This project collaborates with B. Lucht (University of Rhode Island); Y. Shirley Meng (UCSD), S. Whittingham (SUNY – Binghamton); P. Bruce (St. Andrews); S. Hoffman and A. Morris (Cambridge); and P. Shearing (University College London).

Milestones

1. Synthesize ^{13}C FEC. (Q1, FY 2018; Completed)
2. Prepare P-N coatings on silicon; complete. Develop *in situ* ^{19}F NMR studies of FEC; ongoing. (Q2, FY 2018)
3. Prepare multinuclear NMR studies of SEI coatings on silicon with FEC. (Q3, FY 2018; Completed, with first manuscript published and second manuscript in preparation)
4. Test P-N coatings. (Q4, FY 2018; Ongoing – MRI/dendrite studies of 2 ionic liquids; focus on additives)

Progress Report

The team has developed a comprehensive approach to determining cation and charge ordering in spinel electrode materials and is applying it to study potential Li-ion battery cathode materials $\text{LiTi}_x\text{Mn}_{2-x}\text{O}_4$, $0.2 \leq x \leq 1.5$, since the ordering and distribution of Li/Ti/Mn in the structure and the cation oxidation states, both central to the resulting electrochemical performance of the material, are not fully understood. Here, the team uses a combination of ^7Li magic-angle spinning (MAS) NMR spectroscopy and *ab initio* density functional theory (DFT) calculations to understand the structural changes of the Mn-oxide spinel framework as a function of titanium doping. Analysis of NMR results involved *ab initio* calculation of magnetic and hyperfine parameters, allowing the team to parse various contributions to the experimental ^7Li NMR shift.

The ^7Li NMR shifts of $\text{LiTi}_x\text{Mn}_{2-x}\text{O}_4$, $0.2 \leq x \leq 1.5$ are first calculated for various lithium configurations with different numbers and arrangements of manganese ions in the first metal coordination shell and then decomposed into Li–O–Mn bond pathway contributions to the shift. These Li–O–Mn bond pathways are then used to simulate and assign the experimental NMR spectra of different configurations and stoichiometries beyond those in the initial subset of configurations via a random distribution model and a reverse Monte Carlo approach. This approach enables a detailed understanding of the experimental ^7Li NMR spectra, allowing the variations in the local ordering of the ions in the structure to be identified. For low titanium content ($x = 0.2$), a random distribution of $\text{Ti}^{4+}\text{Mn}^{3+/4+}$ sites in the $Fd\bar{3}m$ structure was determined (Figure 20a). At higher titanium concentrations ($x = 0.4$), this structure evolves into an inhomogeneous lattice of Mn^{3+} -rich/ Mn^{4+} -rich phases for $x = 0.4$ and a single-phase solid solution for $x = 0.6$ and 0.8 . In the $1.1 \leq x \leq 1.5$ structures, the results showed the preferential formation of coexisting disordered Mn^{3+} -rich ($Fd\bar{3}m$) and ordered Mn^{2+} -rich (partially inverse $P4_332$) phases. Additionally, for $\text{LiTi}_{1.5}\text{Mn}_{0.5}\text{O}_4$, a specific cation ordering within the partially inverse spinel framework of $P4_332$ symmetry was determined, that is, $(\text{Li}_{0.6}\text{Ti}_{0.1}\text{Mn}_{0.3})_8\text{c}[(\text{Li}_{0.1}\text{Ti}_{1.4})_{12}\text{d}(\text{Li}_{0.3}\text{Mn}_{0.2})_4\text{b}]\text{O}_4$ (Figure 20b), which transforms into a two-phase network of disordered Mn^{3+} -rich and ordered Mn^{2+} -rich domains for $x = 1.1$ – 1.4 .

The combination of first-principles shift calculations, random solution/Monte Carlo model, and experimental NMR enabled the team to acquire a detailed understanding of the complex trend of cation ordering in the mixed $\text{LiTi}_x\text{Mn}_{2-x}\text{O}_4$ series. The high degree of cation disorder found at intermediate $0.2 \leq x < 1$ values of the series may hinder a cooperative Jahn–Teller distortion in the bulk and facilitate the mechanical stability during electrochemical cycling. On the other hand, the observed increasing ratio of $\text{Li}(\text{Oh})/\text{Mn}^{2+}(\text{Td})$ mixing with increasing x may hinder the extraction of Li^+ from the structure, effectively resulting in a lower capacity. In general, the combination of the calculated NMR shifts with the random distribution and reverse Monte Carlo methods represents a robust approach that can be extended to include additional energetic/configurational constraints to analyze other complex systems of interest to the battery field such as $\text{LiZn}_x\text{Mn}_{2-x}\text{O}_4$, $\text{LiNi}_x\text{Mn}_{2-x}\text{O}_4$, Li-excess $\text{Li}_{1+\alpha}\text{Mn}_{2-\alpha}\text{O}_4$ materials, and layered phases.

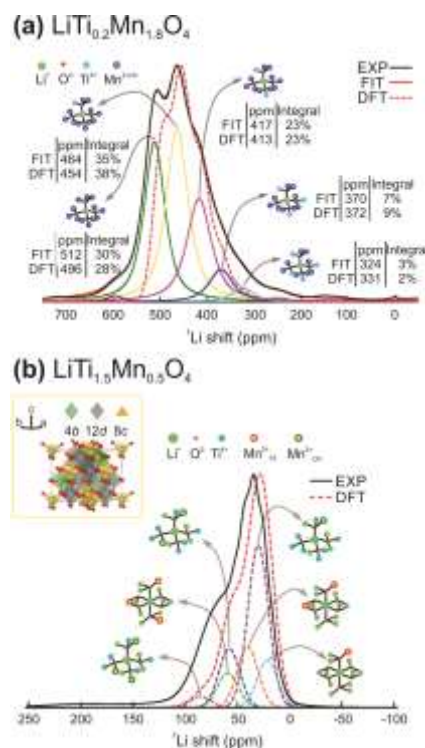


Figure 20. (a) Comparison of the experimental isotropic region of the ^7Li nuclear magnetic resonance (NMR) spectrum of $\text{LiTi}_{0.2}\text{Mn}_{1.8}\text{O}_4$ (solid black, fit in solid red) and the density functional theory simulated resonance assuming a random distribution of Ti^{4+} and $\text{Mn}^{3+/4+}$ (dashed red) with the peaks fit to the experimental spectrum (purple, green, yellow, magenta, blue, cyan, and gray). (b) Isotropic region of the experimental ^7Li NMR spectrum (solid black) and the simulated spectrum (dashed red) of $\text{Li}_{0.6}\text{Ti}_{0.1}\text{Mn}_{0.3}[\text{Li}_{0.4}\text{Ti}_{1.4}\text{Mn}_{0.2}]\text{O}_4$. For each lithium coordination, the corresponding peak is shown, as calculated with the reverse Monte Carlo method. The corresponding cation ordering in the $P4_332$ lattice is shown in the top-left inset.

Patents/Publications/Presentations**Publication**

- Pigliapochi, R., I. D. Seymour, C. Merlet, A. J. Pell, D. T. Murphy, S. Schmid, and C. P. Grey. “Structural Characterization of the Li-ion Battery Cathode Materials $\text{LiTi}_x\text{Mn}_{2-x}\text{O}_4$ ($0.2 \leq x \leq 1.5$): A Combined Experimental ^7Li NMR and First-Principles Study.” *Chemistry of Materials* (2018). Accepted. doi: 10.1021/acs.chemmater.7b04314.

Presentations

- 232nd ECS Meeting, National Harbor, Maryland (October 2017).
- Inorganic Chemistry Laboratory, Oxford, England (November 2017).

Task 2.5 – Advanced Microscopy and Spectroscopy for Probing and Optimizing Electrode-Electrolyte Interphases in High-Energy Lithium Batteries (Shirley Meng, University of California – San Diego)

Project Objective. The proposed research aims to develop advanced microscopy and spectroscopy tools to probe, understand, and optimize the anion activities that govern the performance limitations such as capacity and voltage stabilities in high-energy Li-excess TM (such as nickel, cobalt, manganese) oxides cathode materials. The approach uniquely combines atomic resolution STEM, EELS, *operando* Bragg Coherent Diffraction Imaging (BCDI), and first-principles computation to probe anion redox and oxygen evolutions in Li-excess NMC materials. Furthermore, the project will track the lithium and oxygen dynamics under electrochemical testing via *operando* neutron diffraction, which will enhance understanding of the overall structural changes due to anion activities. Ultimately, this will hone in on the synthesis efforts to produce the modified materials with optimum bulk compositions and surface characteristics at large scale for consistently good performance. The above-mentioned characterization tools will be extended to diagnose various anode types, such as Li-metal anode.

Project Impact. If successful, this research will enable *operando* imaging at the single-particle level by advanced microscopy imaging and high-energy-resolution oxygen K-edge EELS. This work will provide an in-depth understanding of anion activities in high-voltage electrode materials, which can lead to significant improvement in stabilizing operation voltage and electrode-electrolyte interface for future generation high-energy-density electrodes.

Approach. This unique approach combines STEM/EELS, *operando* BCDI, and *ab initio* computation as diagnostic tools for probing anion redox and oxygen evolutions in Li-excess NMC materials. This allows for pinning down the atomistic/molecular mechanism of anion oxidation and determining the speciation compositions and surface characteristics for enabling high rate and long life in the proposed materials. Neutron enables the characterization of bulk material properties to enhance and further optimize high-energy electrode materials.

Out-Year Goals. The goal is to probe and control defects generation due to oxygen activity in the high-energy composite cathodes and to characterize electrode/electrolyte interface in lithium anodes so that their cycle life and efficiency can be significantly enhanced.

Collaborations. This work funds collaborations on EELS (Miaofang Chi, ORNL); neutron diffraction (Ken An, ORNL); and soft XAS (Marca Doeff, LBNL). It supports collaborative work with Zhaoping Liu and Yonggao Xia at Ningbo Institute of Materials Technology and Engineering in China. It also supports collaboration with the Battery500 consortium.

Milestones

1. BCDI characterization on single particle of Li-rich layered oxide during electrochemical cycling. (Q1, December 2017; Completed)
2. Chemical composition and structure of electrochemically deposited lithium metal at nano scale. (Q1, December 2017; Completed)
3. Benchmark electrode performance of bulk and surface *modified* Li-excess NMC. (Q2, March 2018; On track)

Progress Report

Investigation of Nanoscale LLTO Surface Coating Effect on Li-Rich Layered Oxide (LRLO).

Experimentally, coating LRLO material ($\text{Li}_{1.13}\text{Ni}_{0.3}\text{Mn}_{0.567}\text{O}_2$) with LLTO could significantly improve cycling CE and capacity retention. As shown previously, the uncoated LRLO shows only 74.2% capacity retention after 200 cycles, while the

LLTO coating improves the capacity retention to 82.3%. Understanding the effect of LLTO coating is of extreme importance to eventually solving the cycling issues in this material. Annular bright-field STEM (ABF/STEM) images were applied to the uncoated LRLO and to the LRLO material coated with 1 wt% LLTO to confirm the uniformity of the coating. As shown in Figure 21a-b, the uncoated particles have a clean surface with lithium and TM layers extending to the outermost surface. After LLTO coating, there is a uniform nanoscale layer (around 1 nm in thickness) found on the particle surface. There is a clear Ti-L edge peak in the spectra obtained on the surface region of the coated sample, where Ti-L_3 and Ti-L_2 were induced by the electron transitions from $2p^{3/2}$ and $2p^{1/2}$, respectively, to unoccupied 3d orbitals. Surprisingly, the coating layer on LRLO particles is still conformal, even after 200 cycles at a current density of 25 mA/g. After cycling, the positions of Ti-L edges shift to a lower energy

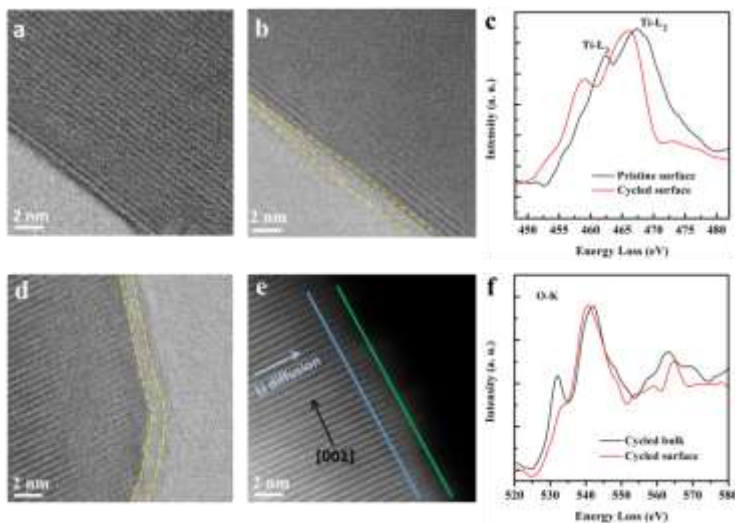


Figure 21. Scanning transmission electron microscopy annular bright-field (STEM/ABF) images of (a) uncoated Li-rich layered oxide (LRLO) and (b) LRLO material coated with 1 wt% LLTO. (c) Electron energy loss spectroscopy (EELS) Ti-L edge spectra at surface regions of LRLO sample coated with LLTO before and after cycling. (d, e) ABF and high angle annular dark field images of LRLO material coated with LLTO after cycling. (f) EELS O-K edge spectra of LRLO sample coated with LLTO after cycling collected at bulk and surface region, respectively.

region, indicating the reduction of titanium ions. A thin amorphous cathode SEI layer was also observed for the cycled sample (to the right of the yellow dashed line in Figure 21d). More importantly, TM-ions migration into the lithium layer was only found within the 2-nm region from the surface (see Figure 21e). There is a clear O-K edge pre-peak in the spectrum obtained in bulk of the particles after cycling. However, the pre-peak decreases when it comes to the reconstruction region, which is due to oxygen vacancy formation. In other words, the coating layer effectively prevents oxygen vacancy generation as well as cation rearrangement during cycling, which ultimately improves the structure integrity and cycling stability.

BCDI Characterization on Single Particle of LRLO during Electrochemical Cycling. To investigate strain network generation dynamics in LRLO material, *operando* BCDI was carried on single particle when the battery was charged at different rate. No obvious difference was found in the voltage curve until ~ 4.35 V (see Figure 21a). However, only 20% of total lithium is deintercalated from the structure after 4.4 V at higher rate, which is substantially smaller than that of material charged at lower rate. It well illustrates the sluggish charging process during the plateau region, which is dominated by the oxygen activity. Figure 21b shows that the average strain grows dramatically after 4.3 V for the sample under lower charging rate only. Note that the percentage strain for both charging rates is normalized to the pristine state. The strain field distribution further confirms that no obvious strain is built in the bulk of the particles during the higher rate charging process, which manifests that the strain network formation is highly correlated to the oxygen activity. The more oxygen redox participates, the larger bulk strain grows.

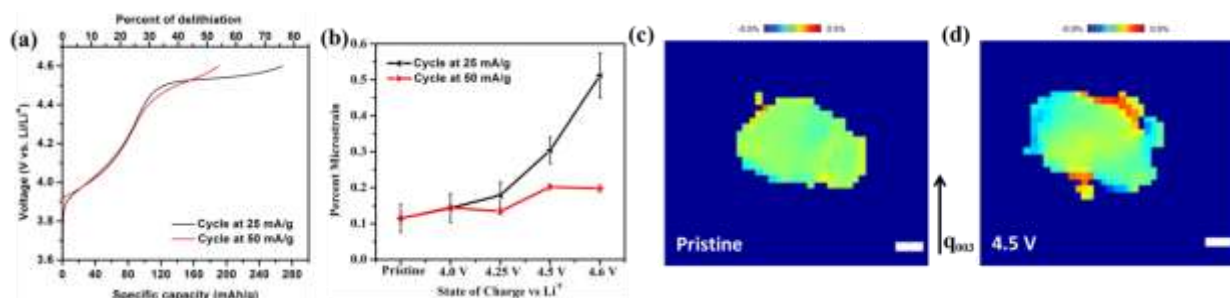


Figure 22. First charging comparison of (a) electrochemical performance and (b) strain generation for Li-rich layered oxide electrode under different rate. (c, d) The strain distribution along the [003] direction inside of the nanoparticle charged at 50 mA/g for two representative states of charge. The scale bar is 100 nm.

Structure and Chemical Composition of Electrochemically Deposited Lithium Metal at Nano Scale. The last report demonstrated that electrochemically deposited lithium metal (EDLi) for five minutes at 0.5 mA/cm is amorphous with an unevenly distributed SEI that consists of amorphous organic species and crystalline LiF. To investigate the influence of low temperature on the Li-metal crystallinity, cryo-XRD was performed on commercial lithium powders. As shown in Figure 23a, two XRD patterns recorded at 300 K and 100 K are quite similar. The slight peak shift to high angles demonstrates a tiny volume shrinkage due to the cooled-down atomic thermal motion when the temperature dropped from 300 K to 100 K.

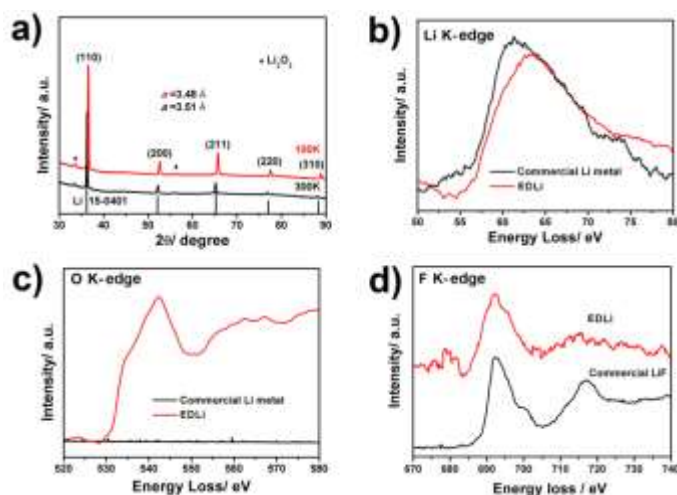


Figure 23. (a) X-ray diffraction comparison of the commercial Li-metal powder at 300 K and 100 K. Electron energy loss spectra comparison of the reference (commercial lithium ribbon and LiF) to the electrochemically deposited lithium metal in (b) Li-K edge, (c) O-K edge, and (d) F-K edge.

Therefore, the cryo-XRD results suggest a negligible effect of low temperature on the Li-metal structure. The results from the cryo-TEM are the true reflection of the EDLi dominated by the electrochemical process. EELS was used to elucidate the chemical information on the EDLi. The absence of a peak in the O-K edge EELS spectrum of the commercial lithium metal (Figure 23c) confirms no significant Li-metal oxidation, indicating that the transfer process avoids air exposure. The Li-K edge spectrum of the EDLi (pre-peak at 56 eV and a major broad peak at 63 eV) is similar to the reference spectrum (Figure 23b), which implies that the EDLi is indeed metallic. The presence of the SEI on the EDLi is validated by the O-K (Figure 23c) and F-K (Figure 23d) edge spectra.

Patents/Publications/Presentations

Publications

- Singer, A., M. Zhang, Y. S. Meng, et al. “Nucleation of Dislocations and Their Dynamics in Layered Oxides Cathode Materials during Battery Charging.” *Nature Energy*. Under review.
- Wang, X., M. Zhang, J. Alvarado, S. Wang, M. Sina, B. Lu, J. Bouwer, W. Xu, J. Xiao, J.-G. Zhang, J. Liu, and Y. S. Meng. “New Insights on the Structure of Electrochemically Deposited Lithium Metal and Its Solid Electrolyte Interphases via Cryogenic TEM.” *Nano Letters* 17, no. 12 (2017): 7606.

Task 2.6 – *In Situ* Diagnostics of Coupled Electrochemical-Mechanical Properties of Solid Electrolyte Interphases on Lithium Metal Rechargeable Batteries

(Xingcheng Xiao, General Motors; Brian W. Sheldon, Brown University; Yue Qi, Michigan State University; and Y. T. Cheng, University of Kentucky)

Project Objective. The project objective is to develop a comprehensive set of *in situ* diagnostic techniques combined with atomic/continuum modeling schemes to investigate and understand the coupled mechanical/chemical degradation of the SEI layer/lithium system during lithium cycling. The goal of this understanding is to develop a new coating design strategy to achieve high cycle efficiency/dendrite free and extend the cycle life of high-energy-density batteries with lithium as the anode for EV application.

Project Impact. The fundamental understanding of the coupled mechanical/chemical degradation of the SEI layer during lithium cycling will enable the project to identify the desirable mechanical properties on SEI/lithium as a system and the specific transport properties that enable the homogenous lithium stripping/plating while avoiding the mossy structure. Furthermore, it will allow the project to develop a highly impactful strategy to protect lithium metal and achieve dendrite-free high cycle efficiency, which can dramatically increase the energy density of lithium batteries for EV applications.

Approach. Different *in situ* techniques, including AFM, nano-indentor, dilatometer, and stress-sensor, will be developed to investigate the mechanical compatibility between SEI and soft lithium and the relationship between surface morphology and current density distribution that results in an inhomogeneous lithium plating/stripping process. Multiple strategies will be developed to tailor the mechanical and transport properties of SEI and to properly engineer the protective coating/lithium interface.

Out-Year Goals. The out-year goals involve using *in situ* electrochemical tools to reveal failure mechanisms of SEI/lithium as whole electrode system, including correlating mechanical failure mechanisms of SEI/lithium, morphology evolution, cycle efficiency, and transport properties of SEI. Then, the project will develop continuum framework to establish the failure modes of SEI layer on lithium metal and provide the governing mechanical/material properties of SEI responsible for the critical failure mode based on the experimental results and atomic scale simulation.

Collaborations. Prof. Huajian Gao (Brown University) and Dr. Qinglin Zhang (GM) will be the key researchers involved in continuum simulation and postmortem analysis. Dr. Chongmin Wang (PNNL), Dr. Wangli Yang (LBNL), and Dr. Jie Xiao will be collaborators on advanced *in situ* analysis and electrolyte additives.

Milestones

1. A continuum model of SEI growth, which can predict potential SEI failure modes and incorporate them into the continuum model. (Q1, December 2017; Completed)
2. The impact of lithium deposition induced stress on lithium morphology and cycle efficiency. (Q2, March 2018; On schedule)
3. The mechanical properties of SEIs measured by nanoindentation and the SEI composition measured by XPS. (Q3, June 2018; On schedule)
4. Interface adhesion energy calculations; and predication of where interface delamination will occur. Lithium plating kinetics at a lithium/single-component SEI/electrolyte interface predicted by molecular dynamics (MD) simulation. (Q4, September 2018; On schedule)

Progress Report

A Potential SEI Wrinkling Mechanism during Lithium Plating. The recent multibeam optical stress sensor (MOSS) measurements on lithium plating/stripping revealed that the magnitude of stress*thickness of the deposited lithium film increases at the beginning of lithium plating, followed by an abnormal small drop, and then increased again until the end of lithium plating. As an attempt to understand this stress*thickness drop, an SEI wrinkling mechanism was considered, in which a finite element model of an SEI layer on a lithium thin film was built to simulate the cycling of lithium plating/stripping (Figure 24). In this model, the SEI was assumed to have a compressive stress of 2 GPa before lithium plating, based on the observed compressive stress of ~1 GPa in the SEI layer on carbon electrodes during SEI formation; lithium was assumed to be elastic and perfectly plastic experiencing isotropic volume expansion/shrinkage during lithium plating/stripping. The Young's modulus and yield stress of lithium metal were taken to be 3.5 GPa and 100 MPa, respectively. The SEI modulus was assumed to be 10 GPa. The bottom of the lithium film was fixed, and periodic boundary conditions were imposed on both sides of the simulation box. SEI remained flat at the beginning of the first lithium plating half-cycle (Figure 24a), but wrinkled as extensive plastic deformation occurred in the growing lithium (Figure 24b). Subsequently, during the first lithium stripping half-cycle, SEI became wrinkled as the lithium thickness shrank (Figure 24c). The stress*thickness response of the SEI/Li film calculated in the simulation was plotted in Figure 24d. The drop in the magnitude of the stress*thickness during the first lithium plating half-cycle due to SEI wrinkling was similar to what was observed in MOSS measurements. However, the stress*thickness drop did not appear in subsequent cycles. Direct evidence of SEI wrinkling on lithium metal is required to support this proposed mechanism.

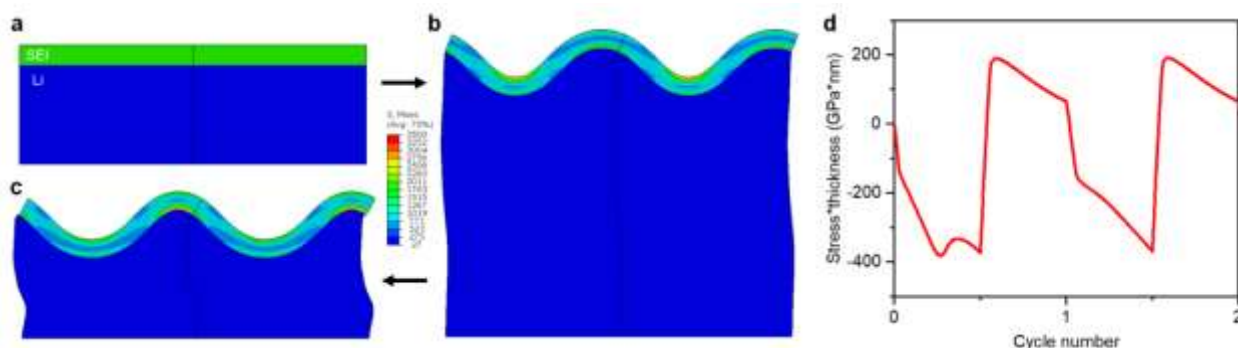


Figure 24. (a-c) Finite element modeling of morphological evolution of solid electrolyte interphase (SEI) on Li-metal anode (a) before 1st lithium plating half-cycle, (b) after 1st lithium plating half-cycle, and (c) after 1st lithium stripping half-cycle. (d) Stress*thickness response of the SEI.

Developed Fluorine-Based Polymer Coating to Protect Li-Metal Electrode. It has been found that adding FEC into the electrolyte can significantly improve the cycle stability by forming LiF and polymeric matrix in SEI. However, FEC is gradually consumed during the long-term cycling process. In addition, the gas generation from the reaction between FEC and lithium metal could be a potential issue related with the abuse tolerance. The project has developed a simplified process to coat Li-metal electrode with fluorine-based coatings. The defluorination will occur once C-F species from the plasma contact with lithium, forming LiF nano-sized and carbonaceous polymer matrix immediately. The self-forming nanocomposite coating is conformal and dense, and effectively isolates lithium metal from electrolyte. The flexibility of the coating can accommodate the volume changes of the electrode. The high conductivity can make the current distribution uniform to ensure homogenous lithium plating and stripping. The protected Li-metal electrodes, combined with high-concentration salt electrolyte developed at PNNL, show significantly improved cycle stability in symmetrical cells under harsh testing conditions. Further validation will be carried out in a large pouch cell paired with high-energy NMC or sulfur positive electrodes.

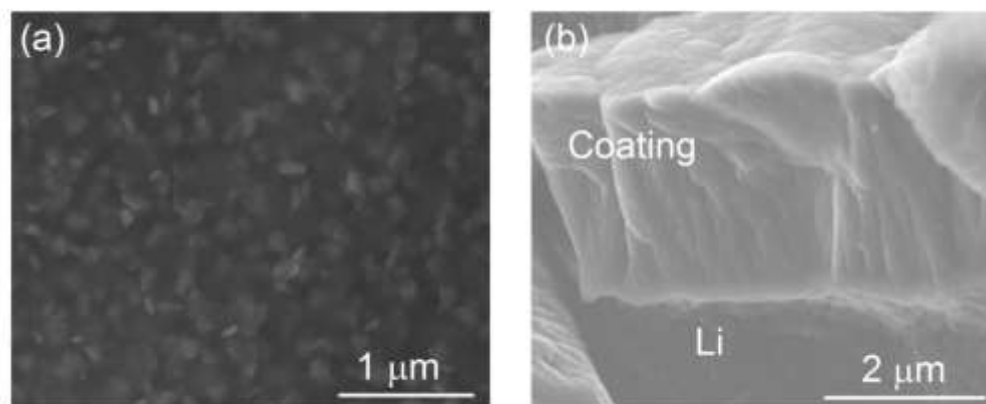


Figure 25. Self-forming nanocomposite has a unique nanostructure where LiF nanocrystals embedded in polymeric matrix (a). The cross-section image shows the coating is dense and has good adhesion to lithium metal.

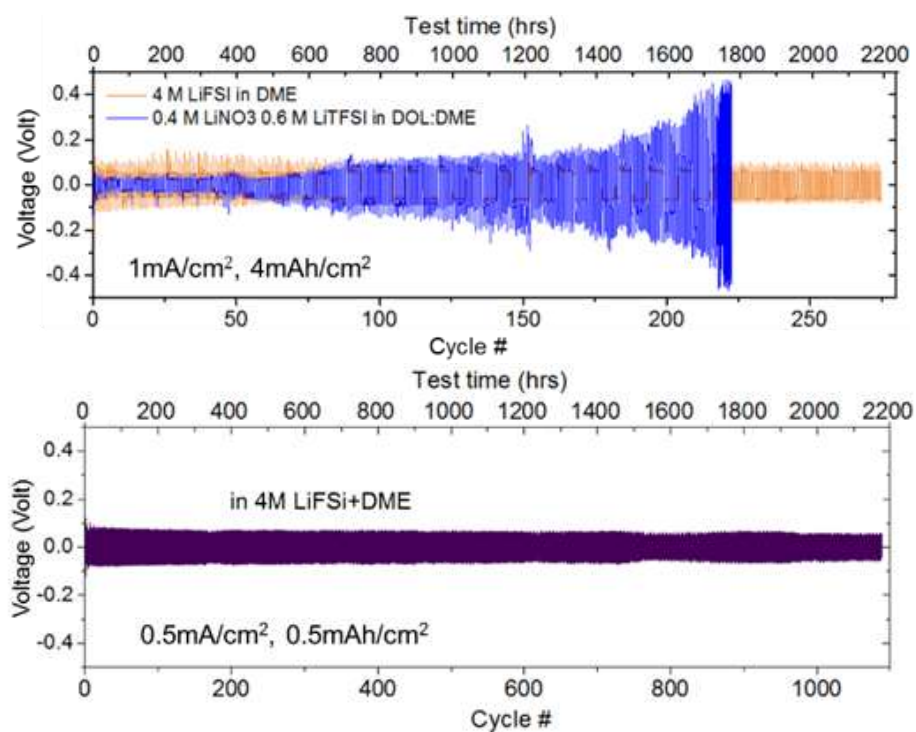


Figure 26. The combination of the protective coating with high-concentration LiFSI in dimethoxyethane enables long cycle stability.

Patents/Publications/Presentations

Patent

- Xiao, X. “Method of Applying Self-Forming Artificial Solid Electrolyte Interface (SEI) Layer to Stabilize Cycle Stability of Electrode in Lithium Batteries.” United States patent application P042557 (8540R-505), August 2017.

Publications

- Su, X., K. Guo, T. Ma, P. A. Tamirisa, H. Ye, H. Gao, and B. W. Sheldon. “Deformation and Chemomechanical Degradation at Solid Electrolyte–Electrode Interfaces.” *ACS Energy Letters* 2 (2017): 1729–1733.
- Guo, K., P. A. Tamirisa, B. W. Sheldon, X. Xiao, and H. Gao. “Pop-Up Delamination of Electrodes in Solid-State Batteries.” To be submitted to *Journal of Power Sources*.

Presentation

- 232nd ECS Meeting, National Harbor, Maryland (October 4, 2017): “Towards High Cycle Efficiency of High Energy Density Lithium Ion Batteries”; X. Xiao. Invited.

Award

- R&D 100 Award 2017: Xingcheng Xiao, Ultrathin Multifunctional Coating Technology for Next-Generation Lithium-Ion Batteries.

Task 2.7 – Microscopy Investigation on the Fading Mechanism of Electrode Materials (Chongmin Wang, Pacific Northwest National Laboratory)

Project Objective. The objective will be using a combination of *ex situ*, *in situ*, and *operando* HRTEM and spectroscopy to probe the fading mechanism of layer structured cathode under high-voltage operating condition. To complement the HRTEM study, *in situ* liquid cell SIMS and atom probe tomography (APT) will also be used to gain structural and chemical evolution of electrodes and correlate the structural and chemical evolution with battery performance.

Project Impact. The proposed characterization work focused on atomic level structural and chemical analysis and direct correlation with battery fading properties. The work can be directly used to guide the designing of electrode materials with tailored microstructure and chemistry for enhanced properties of increasing the energy density of Li-ion batteries and to accelerate market acceptance of EV, especially for PHEV required by the EV Everywhere Grand Challenge.

Approach. This project will use the unique *ex situ* and *in situ* TEM methods to probe the structure of Li-ion batteries, especially a biasing liquid electrochemical cell that uses a real electrolyte in a nano-battery configuration. It will also use various microscopic techniques, including *ex situ*, *in situ*, and especially the *operando* TEM system, to study the fading mechanism of electrode materials in batteries. This project will be closely integrated with other R&D efforts on high-capacity cathode and anode projects in the BMR Program to: (1) discover the origins of voltage and capacity fading in high-capacity layered cathodes, and (2) provide guidance for overcoming barriers to long cycle stability of electrode materials.

Out-Year-Goals. This project has the following out-year goals:

- Multi-scale (ranging from atomic-scale to meso-scale) *ex situ/in situ* and *operando* TEM investigation of failure mechanisms for energy-storage materials and devices. Atomic-level *in situ* TEM and STEM imaging to help develop fundamental understanding of electrochemical energy-storage processes and kinetics of electrodes.
- Extend the *in situ* TEM capability for energy storage technology beyond lithium ions, such as Li-S, Li-air, Li-metal, sodium ions, and multi-valence ions.

Collaborations. This project collaborates with Michael M. Thackeray and Jason Croy (ANL); Guoying Chen (LBNL); Jagjit Nanda (ORNL); Chunmei Ban (NREL); Khalil Amine (ANL); Donghai Wang (Pennsylvania State University); Arumugam Manthiram (University of Texas at Austin, UT Austin); Wei Tong (LBNL); Gao Liu (LBNL); Yi Cui (Stanford University); Jason Zhang (PNNL); Jun Liu (PNNL); Xingcheng Xiao (GM); Shirley Meng (UCSD); and Stan Whittingham (SUNY – Binghamton).

Milestones

1. Resolve the vacancy injection mechanism into the LM-NMC during the battery cycling and its correlation with battery fading mechanism. (Q2, March 31, 2018; In progress)
2. The functioning mechanism of electrolyte additive on the solid-liquid interphase in NMC cathode. (Q3, June 30, 2018; In progress)
3. Atomic level understanding of the mechanism of intergranular and intragranular cracking in NMC. (Q4, September 30, 2018; In progress)

Progress Report

The fundamental challenges for the layer structured cathode, typically such as NMC, are the capacity and voltage fading, especially at high voltage. It is known that the capacity fading in terms of cathode is related to the solid-liquid interfacial reaction, dissolution of the TM in the liquid, and layer to spinel/rocksalt phase transition. For the case of voltage fading, it is critically contributed by the layer to spinel/rocksalt phase transition. It has been generally realized that the layer to spinel/rocksalt phase transition is initiated from the surface of the particle and propagates only to a thickness of several nanometers with the progression of the cycling of the battery. Therefore, a thin layer of several nanometers on the particle surface cannot completely account for the continuous fading of both capacity and voltage for the layer structured cathode material.

This report documents observation of the propagation of layer to spinel/rock into the bulk lattice with the progression of the cycling of the battery for the case of $\text{LiNi}_{0.76}\text{Co}_{0.10}\text{Mn}_{0.14}\text{O}_2$ (Ni-rich NMC) cathode. This observation clearly demonstrates that for the case of Ni-rich NMC, the layer to spinel/rocksalt phase transition may be a bulk degradation process. Most importantly, it is further observed that such a phase transformation in Ni-rich NMC is affected by use of electrolyte, indicating that interfacial reaction process controls the bulk lattice transformation. This piece of new information provides critical insight on mitigating the bulk lattice transformation through controlling the interfacial reaction, which can be conveniently carried through adjusting the chemistry of electrolyte.

A combination of STEM imaging and *ab initio* computations reveals a two-stage picture for spinel/rocksalt phase propagation in Ni-rich layered materials: an initial growth along the periphery of surface and a feature of anisotropic growth into bulk (termed as branched growth). Based on the experimental clues, a comparative study was designed to build up the correlation between the anisotropic spinel/rocksalt growth and the battery degradation. In contrast to the regular electrolyte group that typically presents a branched growth on cycling, the optimized electrolyte group shows the absence of bulk spinel/rocksalt by reducing the surface side reactions, concomitantly with improvement of cycling performance. The benefits of suppressing the bulk growth clearly identify anisotropic growth dependent poor cyclability in the Ni-rich layered materials. The project's atomistic simulations reveal that the layered/rocksalt interface, which enhances interlayer diffusivity while it reduces the intralayer activity, is responsible for the favored anisotropic growth of spinel/rocksalt phase along the $\{104\}$ atomic planes direction. The introduction of oxygen vacancies, a parameter determined by the property of electrolyte, accelerates the nickel diffusions while it does not alter the anisotropic propagation manner, thereby promoting the phase transition at the reaction fronts.

The present results establish the connection between the spinel/rocksalt growth manner and the electrochemistry performance in the Ni-rich materials and provides insight into the optimization of the electrode/electrolyte interface reaction to control bulk lattice process.

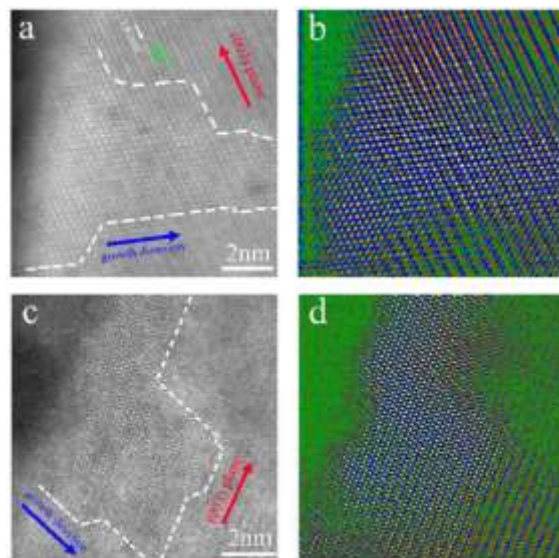


Figure 27. High-angle annular dark field scanning transmission electron microscopy (HAADF-STEM) images of cycled $\text{LiNi}_{0.76}\text{Co}_{0.10}\text{Mn}_{0.14}\text{O}_2$ in the regular electrolyte. STEM images of the surface structures at (a) $\{003\}$ exit surface and (c) the surface parallel to $\{003\}$ plane, respectively, seen along the $[010]$ zone axis. The white dashed lines outline the boundaries of the rocksalt phase, the red and blue arrows indicate the $\{003\}$ atomic plane direction and the rocksalt growth direction, respectively. (b/d) The colored maps correspond to (a/c), respectively.

Patents/Publications/Presentations

Publications

- Zhang, Hanlei, Fredrick Omenya, Pengfei Yan, Langli Luo, M. Stanley Whittingham, Chongmin Wang, and Guangwen Zhou. “Rock-Salt Growth-Induced (003) Cracking in a Layered Positive Electrode for Li-Ion Batteries.” *ACS Energy Letters* 2 (2017): 2607–2615.
- Zhang, Hanlei, Fredrick Omenya, M. Stanley Whittingham, Chongmin Wang, and Guangwen Zhou. “Formation of an Anti-Core–Shell Structure in Layered Oxide Cathodes for Li-Ion Batteries.” *ACS Energy Letters* 2 (2017): 2598–2606.

TASK 3 – MODELING

Summary and Highlights

Achieving the performance, life, and cost targets outlined in the EV Everywhere Grand Challenge will require moving to next-generation chemistries, such as higher capacity Li-ion intercalation cathodes, silicon and other alloy-based anodes, Li-metal anode, and sulfur cathodes. However, numerous problems plague development of these systems, from material-level challenges in ensuring reversibility to electrode-level issues in accommodating volume changes, to cell-level challenges in preventing cross talk between the electrodes. In this task, a mathematical perspective is applied to these challenges to provide an understanding of the underlying phenomenon and to suggest solutions that can be implemented by the material synthesis and electrode architecture groups.

The effort spans multiple length scales from *ab initio* methods to continuum-scale techniques. Models are combined with experiments, and extensive collaborations are established with experimental groups to ensure that the predictions match reality. Efforts are also focused on obtaining the parameters needed for the models, either from lower-length scale methods or from experiments. Projects also emphasize pushing the boundaries of the modeling techniques used to ensure that the task stays at the cutting edge.

In the area of intercalation cathodes, the effort is focused on understanding the working principles of the high nickel layered materials with an aim of understanding structural changes and the associated changes in transport properties. Coatings, an effective strategy for high-voltage operation, are being explored with the aim of providing a rational design approach for new coating materials. In addition, focus is paid to the assembling of porous electrodes with particles to predict the conduction behavior and developing tools to measure electronic conduction.

In the area of silicon anodes, the effort is in trying to understand the interfacial instability and suggest ways to improve the cyclability of the system.

In the area of Li-metal anodes, the focus is on understanding how materials can be designed to prevent dendrite growth using continuum modeling approaches, combined with calculations on mobility in solid conductors. The results are used to guide materials development by providing the properties needed to prevent dendrites while also achieving the energy and power goals. Models are also starting to examine the role of the SEI on the morphology of the dendrite and to describe the mechanical-electrochemical coupled effects that are critical for dendrite formation.

Task 3.1 – Design of High-Energy, High-Voltage Lithium Batteries through First-Principles Modeling (Kristin Persson, Lawrence Berkeley National Laboratory)

Project Objective. This project supports VTO programmatic goals by developing next-generation, high-energy cathode materials and enabling stable cathode operation at high voltages through target particle morphology design, functional coatings, and rational design of electrolytes. The end-of-project goals include: (1) novel disordered, high-rate Li-excess cathodes, (2) new fundamental understanding of the cathode/electrolyte interface and the factors that control the interfacial chemistry and interfacial impedance, (3) critical surface and coating design and optimization strategies that will improve cycling of Li-ion battery cathodes, and finally (4) understanding of the factors that govern stability in nonaqueous electrolytes for Li-ion and Li-S systems.

Project Impact. To enhance the performance of Li-ion systems, improvements on the cathode and the electrolyte side are needed. This project is aimed to result in an improved understanding of the atomistic mechanisms underlying the surface behavior and performance of the Li-ion cathode materials, with the ultimate goal being to suggest strategies, such as coatings, surface protection, and particle morphology design. Furthermore, fundamental studies of electrolyte stability, as a function of solvent and salt concentrations, and components will be conducted.

Out-Year Goals. Stable interfaces will be determined by focusing initially on degradation mechanisms related to the release of surface oxygen at high charge. Tuning particle morphology and coating materials—both of crystalline as well as amorphous structure—will be explored using the Materials Project. For the electrolyte development, work will be aimed toward understanding the atomistic interactions underlying the performance of lithium electrolytes specifically elucidating the solvation structure (as a function of salt concentration) and its impact on the stability of different liquid constituent species.

Collaborations. This project is highly collaborative between BMR PIs G. Chen (LBNL), G. Ceder (LBNL) and V. Srinivasan (ANL). Cathode design and synthesis will be performed by Chen and Ceder, surface design by Persson, and electrolyte design and testing by Persson and Srinivasan.

Milestones

1. Finish modeling of LiAsF_6 in weakly dissociating solvent. Identification of concentration limit causing change in Li^+ solvation structure between contact-ion-pair and free ion species. (Q1, December 2017; Completed)
2. Finish modeling of LiPF_6 in weakly dissociating solvent. Identification of concentration limit causing change in Li^+ solvation structure between contact-ion-pair and free ion species. (Q2, March 2018; Completed)
3. Modeling of dielectric constant of complex Li^+ electrolytes using MD. (Q3, June 2018; Ongoing)
4. *Go/No-Go Decision:* Test algorithm against experimental results to assess whether the project's model can quantitatively capture the change in dielectric behavior as a function of concentration and different solvation structures. If not, change approach. (Q3, June 2018; Ongoing)
5. Present simulated kinetic and thermodynamic evaluations of lithiation mechanisms of amorphous silicon and SiO_2 . (Q4, September 2018; Ongoing)

Progress Report

The project is aimed toward modeling linear carbonate-based electrolytes [for example, dimethyl carbonate (DMC) with the addition of LiAsF_6 or LiPF_6], where the associated salt is believed to increase the dielectric constant ϵ of the overall electrolyte, allowing an exponential increase in conductivity as the concentration is increased (see Figure 28).

To assess speciation of the electrolyte salt, the team employed first principles calculations to determine the free energy of dissociation. It uses a mean field polarizable continuum model (PCM), where the dielectric constant of the overall electrolyte is used to account for solvation effects. Figure 29 shows the free energy of dissociation for LiAsF_6 and LiPF_6 as a function of the overall permittivity of the electrolyte. Here, first-principles calculations results indicate that a higher dielectric constant promotes dissociation of contact ion pairs (CIPs) into free ions. An experimental value (black X) shows qualitative agreement for DMC ($\epsilon = 3.1$) with the calculated results such that CIPs are the majority species for sufficiently low concentrations of salt. This is in agreement with the hypothesis that CIPs could increase the overall permittivity of the electrolyte to allow a higher fraction of charge carriers as concentration is increased. The team notices a crossover for both LiAsF_6 and LiPF_6 , respectively at $\epsilon=13$ and $\epsilon=15$, indicating here that, upon addition of salt, there should be a change in the solvation structure in that the majority of added species should be free ions as opposed to CIPs. An inverse relationship fit to the free energy as a function of the dielectric constant ϵ shows that computed results agree with the theoretical expectation of such systems.^[1]

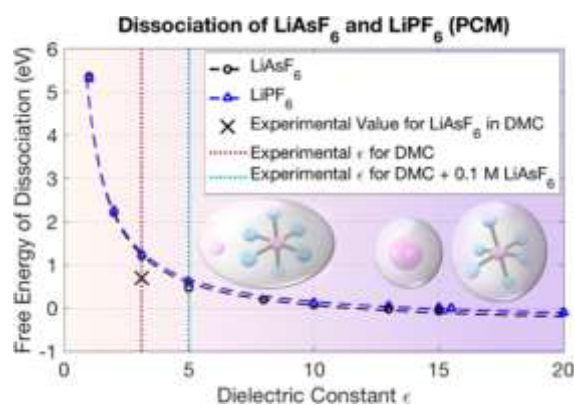


Figure 29. Free energy of dissociation for LiAsF_6 (black) and LiPF_6 (blue) into their respective free ions as computed from first principles using the polarizable continuum model.^[1]

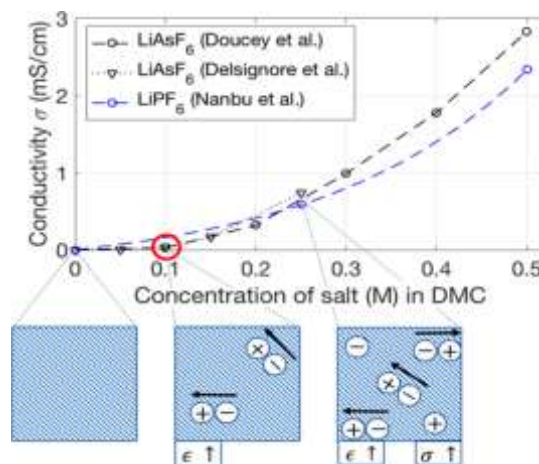


Figure 28. Experimentally measured conductivity as a function of salt concentration for LiAsF_6 and LiPF_6 in dimethyl carbonate. The bottom rectangles (left to right) illustrate the neat solvent, an electrolyte with only associated salt (with dipole moments drawn as directed arrows), and finally an electrolyte with both associated (arrows) and dissociated salt (no arrows).^[1]

In summary, the team's first-principles calculations have identified a concentration limit causing a change in Li^+ solvation structure between CIPs and solvent-separated ion pairs (SSIPs) for not only LiAsF_6 in DMC but LiPF_6 in DMC as well. This provides notable insight into the effect of the electrolyte dielectric constant on the speciation of salt, between neutral CIPs and charge-carrying free ions.

[1] Self, J., M. W. Brandon, N. N. Rajput, and K. A. Persson. "The Interplay between Salt Association and the Dielectric Properties of Low Permittivity Electrolytes: The Case of LiPF_6 and LiAsF_6 in Dimethyl Carbonate." *Journal of Physical Chemistry C* (2017).

Task 3.2 – Addressing Heterogeneity in Electrode Fabrication Processes (Dean Wheeler and Brian Mazzeo, Brigham Young University)

Project Objective. The project goal is to better understand connections between fabrication conditions and undesired heterogeneity of thin-film electrodes by means of new nondestructive inspection techniques and computer models. Two nondestructive inspection techniques will be developed or improved to characterize electrochemical and mechanical uniformity of the electrodes. The first tool will be a flexible contact probe on a polymer substrate for rapidly measuring local electrical conductivity across electrodes of any geometry. The second tool will be a new acoustic probe that measures local elasticity and density of the composite film. These two prototyping efforts will be tied together by a particle-based microstructure model that allows prediction and correlation of electrode conductive and mechanical properties with fabrication conditions.

Project Impact. This work will result in new diagnostic and modeling tools for rapidly and conveniently interrogating how well homogeneity has been maintained in electrodes during fabrication and in subsequent cycling. Real-time measurement of heterogeneity will enable manufacturer quality control improvements. The measurement and modeling tools will further enable researchers to compare different electrodes, improve formulations and processes, and anticipate cell performance of new designs.

Out-Year Goals. This project was initiated October 2016 and concludes September 2018. Overall goals by fiscal year are as follows:

- **2017.** Fabricate first-generation flexible conductivity probe and proof-of-concept of acoustic probe. Improve microstructure model to match experiment.
- **2018.** Integrate flex probe with test fixtures suitable for assessment of large or continuous samples. Demonstrate measurement of localized ionic conductivity.
- **2019.** Assess affect of heterogeneity on cell charge and discharge performance. Further improve accuracy and reliability of probe and modeling technologies.

Collaborations. Ram Subbaraman (Bosch), Daniel Abraham (ANL), Steve Harris (LBNL), Bryant Polzin (ANL), and Karim Zaghib (Hydro-Quebec, HQ) have provided battery materials for analysis. Other collaborations and the transfer of this technology to interested parties are being pursued.

Milestones

1. Integrate flex probe with off-the-shelf CNC positioning system to enable interrogation of large-format electrode films. (Q1, December 2017; Completed)
2. Integrate flex probe with prototype rolling apparatus to enable interrogation of continuous-roll electrode films. (Q2; In progress)
3. *Go/No-Go Decision:* Demonstrate that localized conductivity probe has adequate reliability for continued development. Criteria: Localized ionic conductivity probe can match macroscopic results for a representative electrode sample. (Q3; In progress)
4. Quantify the durability of multiple flex probes to validate suitability for industrial use. (Q4; In progress)

Progress Report

Milestone 1 (Complete)

The flexible N-line probe has been shown to be robust and achieves accurate results as compared with the previous rigid probe iterations. Despite the advantages of the old rigid probe, measurements of large-format electrodes have not been possible, and manufacturing of the probe was relatively time-consuming and costly. To make the N-line probe more attractive commercially, the first milestone of FY 2018 was to integrate an off-the-shelf solution to replace the high-resolution 3-axis stage. The result had to be less expensive and cover a larger interrogation area without compromising significantly on the usefulness of the measurement apparatus.

Due to the prevalence of do-it-yourself 3D printers and CNC devices, 3-axis stages have become both available and affordable. The stage seen in Figure 30 is an off-the-shelf CNC stage sold by Carbide 3D. Samples up to 15 inches by 20 inches can be measured easily.

Measurements of the ANL AC006 electrode materials were performed on both the old high-resolution stage and on the new low-cost stage. As shown in Figure 31, measurement results for the two stages are in statistical agreement. The results were further validated against the average film conductivity measured using the Van Der Pauw method and against initial results with the rigid 4-line probe.

Further improvements to the stage and measurement apparatus are under way to make the N-line probe viable for use in a production environment and to meet milestone 2.

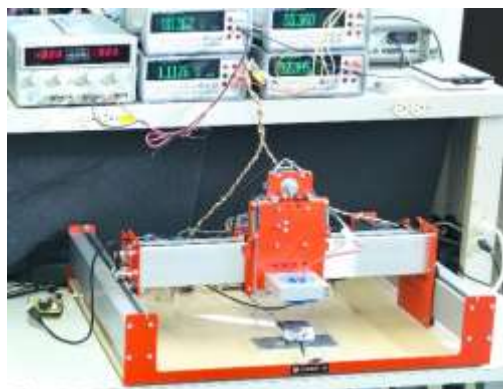


Figure 30. Large-format Shapeoko CNC stage produced by Carbide 3D, with a custom-made N-line probe attachment.

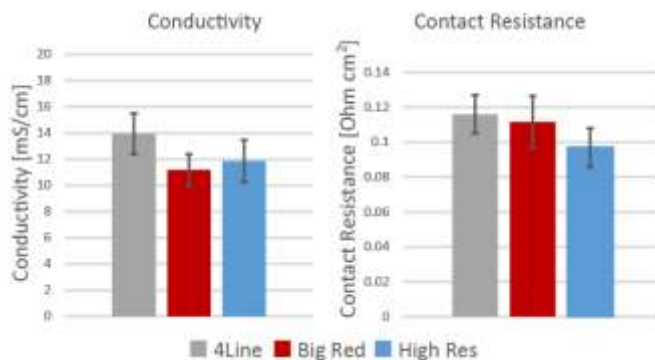


Figure 31. Measured bulk conductivity and contact resistance values (with 95% confidence intervals) on ANL AC006 cathode film using both large-format (“Big Red”) and high-resolution stages, compared to results from the (old) rigid 4-line probe.

Patents/Publications/Presentations

No publications or presentations were made this quarter. Two publications are under review, and four manuscripts are in preparation (expected to be done in Q2 of FY 2018). One patent application is being filed next quarter as well.

Task 3.3 – Understanding and Strategies for Controlled Interfacial Phenomena in Lithium-Ion Batteries and Beyond (Perla Balbuena, Jorge Seminario, and Partha Mukherjee, Texas A&M University)

Project Objective. The project objective is to evaluate and characterize interfacial phenomena in lithiated silicon and Li-metal anodes and to develop guidelines for potential solutions leading to controlled reactivity at electrode/electrolyte interfaces of rechargeable batteries using advanced modeling techniques based on first principles.

Project Impact. Understanding SEI growth on constantly evolving silicon surfaces and on highly reactive Li-metal surfaces is expected to define the electrolyte properties required in high-performance cells. Strategies to control the silicon anode instability and pulverization issues and the well-known safety and short effective lifetimes of Li-metal anodes will be developed by tuning the electrolyte composition, structure, dynamic, and stability, as well as that of the electrode morphology and interactions with the electrolyte, based on multiple characterizations of interfacial phenomena.

Approach. A comprehensive multiscale modeling approach including first-principles *ab initio* static and dynamics, classical MD, and coarse-grained mesoscopic models will focus on the roles of the electrolyte chemical, structural, and dynamical properties and of the electrode micro- and nano- structure on the formation and evolution of the SEI layer and associated electrochemical performance on silicon and on Li-metal anodes.

Out-Year Goals. Work will progress toward characterizing lithiation and SEI formation at silicon surfaces as well as the subsequent cracking and reforming events under the most realistic modeling conditions. Similarly, the project will investigate electrolyte effects on reactivity and dendrite formation in Li-metal surfaces. The project aims to capture how the chemistry of the various electrolyte components (mainly liquids, but also solid polymers and gels) affects the main issues that influence the electrode performance.

Collaborations. This project funds work at Texas A&M University (TAMU). Prof. G. Somorjai (UC Berkeley) and Prof. Shahbazian Yassar (University of Illinois at Chicago) have also contributed to the project.

Milestones

1. Complete analysis of effects of Li-substrate interactions on lithium deposition. (Q1, FY 2018; Completed)
2. Complete study of SEI reactions over lithium deposits. (Q2, FY 2018)
3. Complete analysis of operating conditions on dendrite growth. (Q3, FY 2018)
4. Complete evaluation of co-deposition effects. Establish comparisons with experimental trends. (Q4, FY 2018)

Progress Report

Lithium Deposition over Current Collector. The team demonstrated by combination of experimental and simulation techniques that two-dimensional (2D) films of graphene oxide (GO) can mitigate the dendrite growth by favoring a smooth deposition of lithium over the current collector. The experimental characterizations included microscopy, *in operando* optical observations, and electrochemical measurements, and were carried out by project collaborator Prof. Shahbazian Yassar, at the University of Illinois at Chicago. The *ab initio* molecular dynamics (AIMD) and DFT simulations evaluated the modes of lithium diffusion and deposition over the copper substrate. AIMD simulations suggested that lithium ions initially get adsorbed onto the lithiophilic GO film and then diffuse through defect sites. This delayed lithium transfer eliminates the “tip effect,” leading to a more homogeneous lithium nucleation. Meanwhile, the C-C bonds rupture that is observed in the GO during AIMD simulations creates more pathways for faster Li-ion transport. To understand Li-ion migration through the GO coating layer after the adsorption step, two scenarios were employed to simulate the early stages of lithium plating on the copper current collector. In scenario (i), the initial step of lithium plating is simulated by placing a thin layer of lithium above the GO layer existing on top of the copper current collector. After ~ 500 fs, the lithium ions start to migrate across the GO layer only through existing discontinuities, and after 2ps some lithium atoms have completely passed the GO layer and deposited on the copper surface (Figure 32a). Scenario (ii), which denotes the subsequent stage of lithium stripping/plating, is modeled with lithium layers above and underneath the GO layer. Similarly, lithium ions tend to pass only through the discontinuities of GO layer in this configuration (Figure 32b).

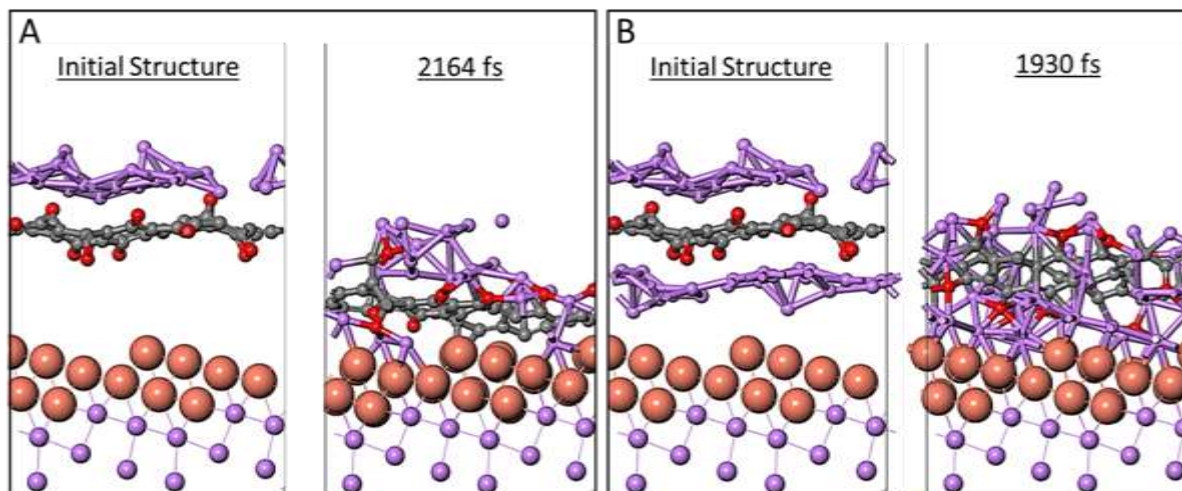


Figure 32. Snapshots of the lithiated graphene oxide/copper (221) interface model. Panels (a) and (b) show lithium diffusion in scenarios (i) and (ii), respectively (see text). Purple, orange, grey, and red spheres represent lithium, copper, carbon, and oxygen atoms, respectively.

An important conclusion is that GO will store lithium ions for a limited amount of time before releasing them to the metal surface. This confined transfer prevents adsorption of large flux of lithium ions to the amplified electric field existing at the surface perturbations, resulting in a more uniform delivery of lithium ions to the electrode surface and a homogenous and dense final lithium morphology.

In addition, classical MD simulations are used to simulate the dendrite growth by testing various charge distributions in a nanosized square representing a crack of the SEI, which is where the electrolyte solution gets in direct contact with the fresh anode. It is found that dendrites grow when there is an uneven distribution of charges on the electrode surface; especially, the concentration of charge in particular spots such as SEI cracks determines the dendrite formation. Moreover, 2D-Kinetic Monte Carlo (KMC) modeling is helping the team to map such uneven charge distribution into a nonuniform Li-ion distribution as a function of local overpotential and lithium surface diffusion kinetics.

Patents/Publications/Presentations

Publications

- Horowitz, Yonatan, and Hui-Ling Han, Fernando A. Soto, Walter T. Ralston, Perla B. Balbuena, and Gabor A. Somorjai. “Fluoroethylene Carbonate as a Directing Agent in Amorphous Silicon Anodes – Electrolyte Interface Structure Probed by Sum Frequency Vibrational Spectroscopy and *Ab Initio* Molecular Dynamics.” *Nano Letters*. In press.
- Hao, Feng, Zhixiao Liu, Perla B. Balbuena, and Partha Mukherjee. “Mesoscale Elucidation of Solid Electrolyte Interphase Layer Formation in Li-ion Battery Anode.” *Journal of Physical Chemistry C* 121 (2017): 26233–26240.
- Foroozan, Tara, Fernando A. Soto, Vitaliy Yurkiv, Soroosh Sharifi-Asl, Ramasubramonian Deivanayagam, Zhennan Huang, Ramin Rojaee, Farzad Mashayek, Perla B. Balbuena, and Reza Shahbazian-Yassar. “Synergistic Effect of Graphene Oxide for Impeding the Dendritic Plating of Lithium.” Under review.
- Camacho Forero, Luis E., and Perla B. Balbuena. “Elucidating Electrolyte Decomposition under Electron-Rich Environments at the Lithium-Metal Anode.” *Physical Chemistry Chemical Physics* 19 (2017): 30861–30873.
- Verma, A., and P. P. Mukherjee. “Mechanistic Analysis of Mechano-Electrochemical Interaction in Silicon Electrodes with Surface Film.” *Journal of the Electrochemical Society* 164, no. 14 (2017): A3570–A3581.
- Selis, L. A., and J. M. Seminario. “Dendrite Formation in Anodes of Lithium-Ion Batteries.” Under review.

Presentations

- 2nd International Computational Science and Engineering Conference, Doha, Qatar (October 23–24, 2017): “Interfacial Phenomena in Li-ion and Li-S Batteries and Beyond”; Perla B. Balbuena.
- 2nd International Computational Science and Engineering Conference, Doha, Qatar (October 23–24, 2017): “Molecular Dynamics Simulations of Nanobatteries for the Study of Cracks and Dendrites in Solid Electrolyte Interphases”; Jorge M. Seminario.
- University of Picardie, France (December 15, 2017): “Analysis and Design of Materials for Advanced Batteries”; Perla B. Balbuena.

Task 3.4 – Electrode Materials Design and Failure Prediction (Venkat Srinivasan, Argonne National Laboratory)

Project Objective. The project goal is to develop a continuum-based mathematical model to (i) investigate the impact of SEI layer on the growth of dendritic protrusions, and (ii) elucidate the deposition mechanism and deposit morphology observed on top of the carbon substrate in Li-S battery cathodes. Mechanical stiffness and transport mechanism of lithium through the SEI layer can significantly affect the nucleation of dendritic protrusions on top of Li-metal anodes. Effectiveness of protective layers in preventing the growth of lithium dendrites can also be studied by using this methodology. Next-generation, high-energy-density Li-S batteries experience limited capacity due to cathode surface passivation because of the precipitation of Li-sulfides during the discharge process. Understanding the morphology of precipitates can significantly help to develop strategies that can minimize the surface passivation and improve the practical specific capacity of Li-S batteries. The main focus will be to develop microscale models capable of successfully capturing the multiscale multiphysics phenomena that occurs during Li-metal and li-sulfide deposition processes.

Project Impact. Based on the work conducted as part of this project, better understanding of the different mechanisms responsible for degradation in Li-metal anodes and Li-S batteries can be developed. Based on these understandings, different strategies can also be devised to minimize the impact of degradation mechanisms and enhance the performance and lifetime of next-generation Li-ion batteries.

Out-Year Goals. At the end of this project, mathematical models will be developed that can capture the impact of diffusivity, conductivity, transference number, solubility and mechanical stiffness of various species on the morphology of lithium and Li-sulfide deposits on top of Li-metal and carbon substrates, respectively.

Collaborations. This project collaborates with Nitash Balsara of LBNL.

Milestones

1. Incorporate SEI layer in lithium dendrite growth model and analyze its influence on growth of dendritic protrusions. (Q1, December 31, 2017; Completed)
2. Evaluate the impact of mechanical properties and thickness of SEI layer on propensity for dendrite growth. (Q2, March 31, 2018; In progress)
3. Develop a model to examine the precipitation process of lithium sulfide during battery discharge. (Q3, June 30, 2018; In progress)
4. Complete model to describe sulfur redistribution. (Q4, September 30, 2018)

Progress Report

Incorporate SEI Layer in Lithium Metal Dendrite Model. Evaluate the impact of mechanical properties and thickness of SEI layer on propensity of dendrite growth. It has been argued by several researchers that inhomogeneous transport of lithium through the SEI layer leads to the formation and growth of dendritic protrusions. In this context, an SEI layer has been added at the lithium electrolyte interface, and its impact on the Butler-Volmer reaction current has been incorporated as an extra overpotential term. Transport of lithium through the extremely thin SEI layer has not been modeled. The Butler-Volmer equation is: $i_{BV} = Fk_{ref}c_e^{0.5} \exp(-gk\bar{V}_{Li}/2RT) [\exp(Fh/2RT) - \exp(-Fh/2RT)]$, that incorporates the effect of surface energy (g) and SEI resistance (R_f) within the overpotential term (h), defined as $h = \bar{f}_s - \bar{f}_e - i_{BV}R_f - (gk\bar{V}_{Li}/F)$. Figure 33a demonstrates possible inhomogeneities of SEI resistance in the form of “sharp” and “wide” variations. Starting from flat lithium (see Figure 33b), the corresponding dendrite morphologies have been depicted in Figure 33c-d, respectively.

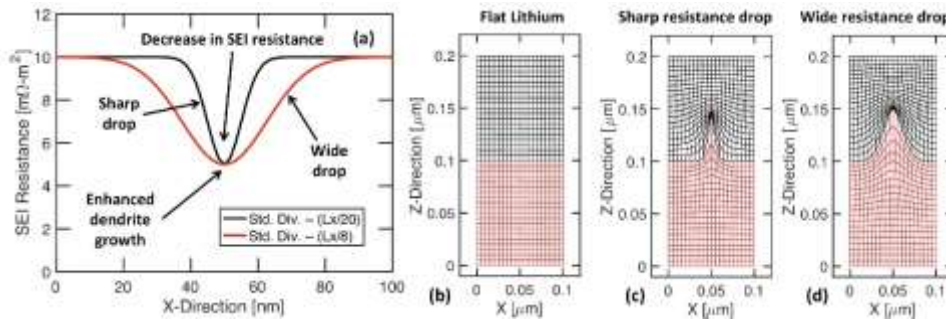


Figure 33. (a) Demonstration of inhomogeneous solid electrolyte interphase (SEI) resistance, which may have a sharp variation (black line) or a wide drop (red line). (b) Initial lithium electrolyte interface, which is flat. (c) Sharp drop in SEI resistance leads to growth of a thin dendritic protrusion. (d) Wider variation in SEI resistance forms a thick dendritic protrusion.

Heights of dendritic protrusions with increasing time have been demonstrated in Figure 34a. It is evident that the growth rate is not constant and decreases with time, which can be attributed to the increasing surface area of reaction and curvature induced suppression. Figure 34b clearly demonstrates that by increasing the surface energy density between lithium and electrolyte, size of the propagating dendritic protrusion can be altered significantly. Incorporation of SEI layer within the computational model and demonstration of its impact on the dendrite growth process completes the milestone for this quarter.

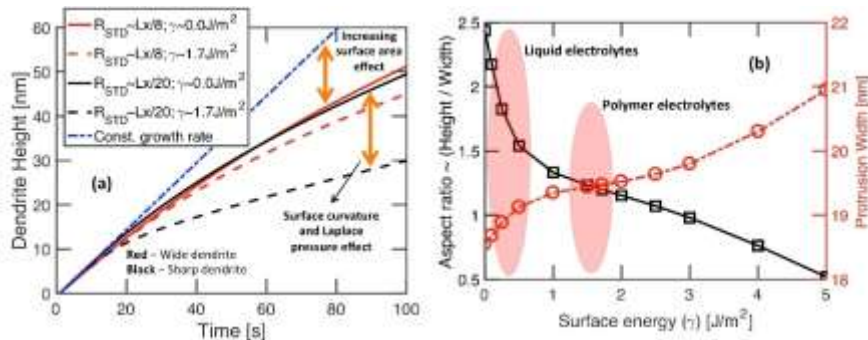


Figure 34. (a) Increase in height of dendritic protrusions with time for sharp and wide drop in solid electrolyte interphase resistance. Growth of dendrites decreases with time because of increase in surface area and surface curvature induced suppression mechanisms. (b) As the surface energy between lithium and electrolyte increases, the width of the dendritic protrusions increases (red circles), and the aspect ratio of the protrusions drops (black squares).

Task 3.5 – First Principles Calculations of Existing and Novel Electrode Materials (Gerbrand Ceder, Lawrence Berkeley National Laboratory)

Project Objective. The main project objectives are as follows: (1) develop very high-capacity, layered cathodes with high structural stability (> 250 mAh/g) and high surface stability; (2) clarify the role that Li-excess and cation disorder play in capacity and structural stability; (3) develop predictive modeling of oxygen charge transfer and oxygen loss, and find ways to make oxygen redox beneficial in terms of increase capacity; and (4) develop materials with engineered surface passivation that does not lead to impedance increase.

Project Impact. The project will lead to insight in how Li-excess materials work and ultimately to higher capacity cathode materials for Li-ion batteries. The project will help in the design of high-capacity cathode materials that are tolerant to TM migration.

Out-Year Goals. Future goals include the following: (1) develop higher capacity Li-ion cathode materials, and novel chemistries for higher energy density storage devices, and (2) guide the field in the search for higher energy density Li-ion materials.

Collaborations. This project collaborates with K. Persson (LBNL), C. Grey (Cambridge), G. Chen (LBNL), and B. McCloskey (UC Berkeley).

Milestones

1. Assess, through modeling, the viability of fluorination of disordered-rocksalt cathodes to reduce the oxygen activity. (Q1, FY 2018; Completed)
2. Synthesize one partially fluorinated cathode material and demonstrate fluorination through NMR, TEM, XRD or other characterization tool. (Q2, FY 2018)
3. Demonstrate viability of reducing TM valence in Li-excess materials to create higher capacity (for example, use Mn^{2+} or V^{3+} or more Ni^{2+}). (Q3, FY 2018)
4. Demonstrate capacity > 200 mAh/g in a novel fluorinated disordered rocksalt. (Q4, FY 2018)

Progress Report

The high capacity generally observed for Li-excess disordered (rocksalt) TM oxide (LEX-RS) cathodes relies on oxygen redox processes that can cause oxygen loss near the surface of the particles. In turn, this results in creation of high impedance surface layers and large polarization of the voltage profile, leading to poor cycling performance. The team recently showed that fluorine doping of LEX-RS materials is feasible and results in reduction of oxygen release as measured by DEMS [Lee et al., *Nature Communications* 8 (2017): 981].

The team has now used DFT and cluster expansion Monte Carlo simulation methods to study the thermodynamics of fluorine incorporation into TM oxides to produce Li-excess compositions.

Using *ab initio* simulations, the team constructed phase diagrams of the mixing of LiF into the Li-metal oxide phase for the titanium, vanadium, chromium, manganese, iron, cobalt, and nickel systems. Figure 35 shows an

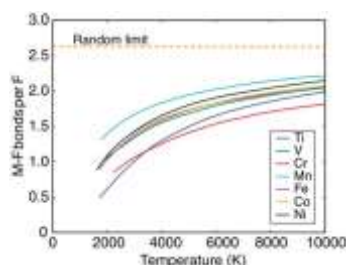


Figure 36. Local fluorine environments present in $\text{Li}_{1.125}\text{M}_{0.875}\text{O}_{1.75}\text{F}_{0.25}$ disordered rocksalt phases.

example phase diagram obtained for the LiCoO_2 -LiF system. The results indicate that, while fluorine solubility is very small in the cation ordered oxide phase (purple region on left of Figure 35), it is significantly increased upon disordering of the lithium and cobalt cations (dashed red region in Figure 35). Similar results were obtained for all the TM systems of interest to this study.

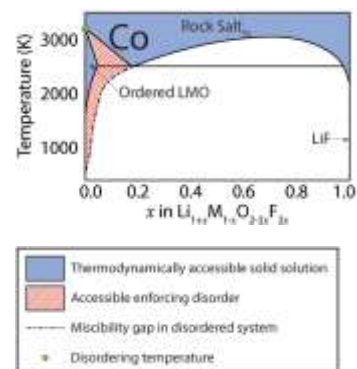


Figure 35. LiCoO_2 -LiF phase diagram.

The team also carried out Monte Carlo simulations to determine the distribution of fluorine environments in representative cation-disordered $\text{Li}_{1.125}\text{M}_{0.875}\text{O}_{1.75}\text{F}_{0.25}$ compositions as a function of temperature (Figure 36). While there are three M-F bonds per F dopant in cation-ordered LMO structures, fluorine environments have fewer M-F bonds on average in the cation-disordered compounds. At the solubility limit

(lowest temperature at which the disordered $\text{Li}_{1.125}\text{M}_{0.875}\text{O}_{1.75}\text{F}_{0.25}$ forms), most fluorine ions are surrounded by one TM and five lithium atoms to minimize the number of high-energy M-F interactions, while still allowing for reasonable entropy in the system. Since disordering of the cation sublattice creates more of these metal-poor, Li-rich local environments, it plays a central role in increasing LiF solubility in TM oxide systems.

Finally, due to the similar defect energetics of the disordered states, the miscibility gaps in the metastable disordered phase diagrams are very similar (Figure 37). The difference between the seven TM systems lies in the stability and disordering temperature of the stoichiometric LMO compound.

In summary, project results indicate that a major requirement for incorporation of fluorine into an oxide compound is the formation of metal-poor, Li-rich F dopant sites in the material, which can be achieved using a combination of Li-excess and disorder on the cation sublattice.

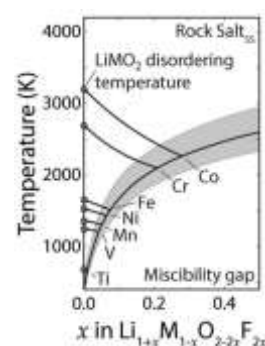


Figure 37. Superposition of the low fluorine region of the phase diagrams obtained for the titanium, vanadium, chromium, manganese, iron, cobalt, and nickel LMO systems.

Task 3.6 – Dendrite Growth Morphology Modeling in Liquid and Solid Electrolytes (Yue Qi, Michigan State University)

Project Objective. The project goal is to develop a validated model to predict lithium dendrite morphology evolution in both liquid and solid electrolytes during electrodeposition and stripping to accelerate the adoption of Li-metal electrodes in current and emerging battery technologies. To achieve this goal, the project has four objectives: (1) formulate a general framework that captures the electrochemical-mechanical driving forces for lithium morphology evolution; (2) consider the role of the nm-thin SEI in liquid electrolytes as well as the microstructures of mm-thick solid electrolytes for lithium morphology evolution; (3) connect micron-scale phase-field models and atomic-scale DFT-based simulations via parameter- and relationship-passing to predict lithium dendrite nucleation and growth kinetics and morphology; and (4) validate the key input parameters and main conclusions of the multi-scale model as new capabilities being developed step-by-step.

Project Impact. This atomically informed, fully coupled, electrochemical-mechanical dendrite morphology evolution model will allow the project to design the desired properties of artificial SEI coatings, the microstructure of solid electrolyte materials, and the corresponding battery operating conditions, so as to avoid dendrite growth during cycling. It will accelerate design of durable and safe lithium anodes for Li-S, Li-air, and all-solid Li-ion batteries. Thus, it directly impacts emerging technologies, such as Li-S, Li-air, and all-solid Li-ion batteries, which aim to meet the DOE target of the high-energy-density battery cells ($> 350 \text{ Wh/kg}$) for EV applications and to push the cost below $\$100/\text{kWh}_{\text{use}}$.

Out-Year Goals. The FY 2018 goal is to illuminate the role of SEI kinetics on lithium dendrite growth in liquid electrolytes. To achieve this goal, a phase-field model will be developed to capture the electrochemical-driven dendrite morphology evolution in a liquid electrolyte. The role of SEI will be modeled both implicitly and explicitly. The kinetic properties, as well as lithium diffusion coefficient along the Li/SEI interface will first be computed from DFT- and DFT binding (DFTB)- based atomic simulations. The validation of the model will come from experiments to correlate the distinctively different transport properties of artificial SEI layers with their impact on lithium dendrite morphology.

Collaborations. This project collaborates with UMD, Sandia National Laboratories (SNL) – Albuquerque, PNNL, University of Arkansas, and University of Houston.

Milestones

1. Compare the lithium morphology obtained from experiments and modeling. *Go/No-Go Decision:* Determine if effect of SEI on dendrite growth should be modeled implicitly or explicitly. (Q1, December 30, 2017; *Go*)
2. Identity the electronic pathway of lithium dendrite growth inside LLZO. (Q2, March 31, 2018; In Progress)
3. Identify the Li-ion pathway of lithium dendrite growth inside LLZO. (Q3, June 30, 2018; In progress)
4. Develop a multiphase multigrain phase-field model that incorporates mechanical and electrochemical driving forces for lithium dendrite growth in polycrystalline solid electrolyte. (Q4, October 31, 2018; In progress)

Progress Report

The project has determined that the effect of SEI on dendrite growth in the liquid electrolyte can be modeled implicitly; therefore, a *Go* decision was made this quarter.

The experiments for comparison were taken from the observation that lithium plating is more dendritic, but magnesium plating is more faceted (Figure 38). The difference in the morphology evolution of the plated lithium and magnesium is related to the charge transfer kinetics at the electrode/electrolyte interface. One major difference is that SEI always covers lithium surface, but not magnesium.

Using the multiscale modeling developed in this project, the team compared the two electrodes (Figure 38). At the atomistic scale, Li/Li₂CO₃/liquid-EC-electrolyte and Mg/liquid-THF-(with Cl⁻)-electrolyte interfaces were used to represent the two systems. The DFT results showed that the energy change for the reduction reaction is higher for magnesium than lithium (2.5 eV for Mg versus 1.2 eV for lithium) due to its larger solvation energy (1.1 eV for Mg²⁺ versus 0.6 eV for Li⁺). Coupling with atomistic calculations, phase-field simulations were performed to investigate the Li/Mg plating morphological evolution at mesoscale. With thermodynamic and kinetic parametric inputs from first-principles calculation (that is, interfacial energy and anisotropy of Li/Li₂CO₃, surface energy and anisotropy of magnesium, diffusion coefficient of Li⁺ in Li₂CO₃, and relative difference in charge-transfer energy barrier of Li/Mg plating), the implicit non-linear phase-field model captures the notable morphological evolution difference between dendritic lithium plating and faceted magnesium plating. Furthermore, the simulation results indicate that, among all possible parameters for Li/Mg electrodeposition processes, the plating charge-transfer energy barrier difference is the major contributing factor that accounts for the morphological discrepancy. Specifically, in the project's systematical tests on the impact of charge-transfer energy barrier on plating morphology (a range of 0.5 to 10 times the lithium plating reaction energy barrier height was tested), dendrites were prominently suppressed from around 2 times and faceted morphology (hexagonal for magnesium) was produced at about 4 times. This study result fundamentally explains the origin of the Li/Mg plating morphological difference and reveals that the proper elevation of the charge-transfer barrier height (for example, by anodic surface treatment, protective coating, and upgraded electrolyte) is a promising approach to dendrite suppression in Li-metal batteries.

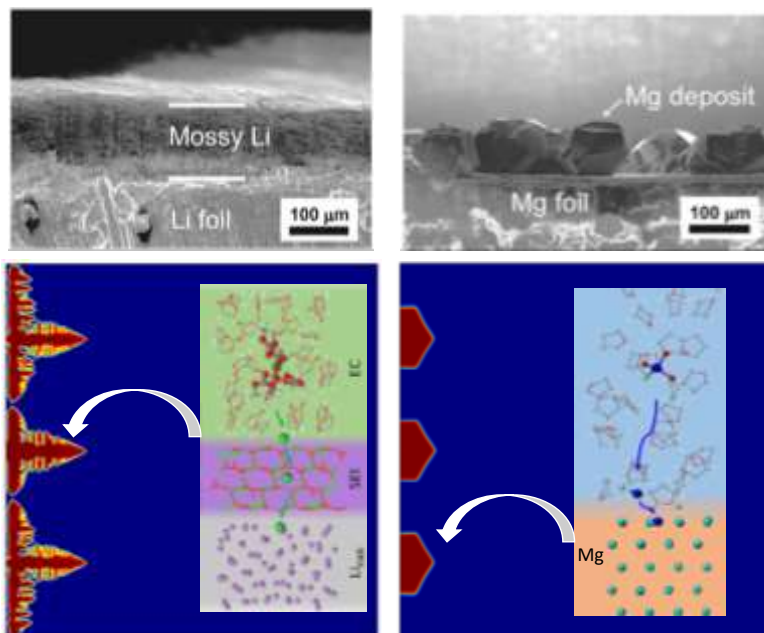


Figure 38. The observed lithium (upper left) and magnesium (upper right) plating morphology [Yoo et al., *ACS Appl. Mater. Interfaces* (2015): 7001]. The simulated morphology difference of lithium and magnesium plating (lower panels).

Patents/Publications/Presentations

Presentation

- Seminar at University of North Carolina, Charlotte, North Carolina: “The Thin Passivation Layer on Aluminum and Lithium Metals”; Yue Qi.

Task 3.7 – First Principles Modeling and Design of Solid-State Interfaces for the Protection and Use of Li-Metal Anodes (Gerbrand Ceder, UC Berkeley)

Project Objective. The project objective is to determine the design principles that control the solid electrolyte/lithium electrode interfaces by determining the reaction products stemming from pairing solid electrolytes and lithium metal. The project will conduct rigorous analysis based on computing electrolyte phase-diagrams closed and open to lithium. Li-ion transport properties in bulk electrolytes and interfacial products will be assessed through AIMD and nudged elastic band calculations. Simultaneously, a robust framework will be developed to identify factors controlling Li-dendrite propagation within solid electrolytes and interfacial products by accounting for irregularities, defects, and grain boundaries, through a model that includes elements of fracture mechanics, thermodynamics, and electrochemistry.

Project Impact. The project will lead to understanding of the complex evolution of lithium metal/SEI during electrochemical cycling. The understanding of this process is necessary to determine design principles to develop reliable all solid-state batteries.

Out-Year Goals. The out-year goals include the following: (1) obtain design criteria for solid electrolytes that can resist unstable lithium propagation by computing elastic properties surface energies and decohesion energies, and (2) adapt fracture mechanics models describing crack propagation to lithium dendrite propagation in different scenarios.

Collaborations. There are currently no collaborative activities.

Milestones

1. Development of metal-electrolyte electrochemical-mechanical interface model. (Q1, FY 2018; Completed)
2. Lithium conductivity screening using AIMD and nudged elastic band method to screen for materials with high Li-mobility. (Q2, FY 2018; In progress)
3. Evaluation of bulk elastic properties for candidate materials using first principles and atomistic calculations. (Q3, FY 2018; On target)
4. Determine critical stress conditions that yield fracture in ceramic electrolytes during lithium deposition. (Q4, FY 2018; On target)

Progress Report

Transport Properties of Solid Electrolyte Materials. Subsequent to assessing stability of electrode/electrolyte materials and screening for materials stable with lithium metal, as described previously, the team is studying Li-ion transport properties in these materials. It is vital to understand the ionic conduction mechanisms to properly account for sources of homogeneous Li-ion transport that plays a crucial role in Li-metal propagation across the solid electrolyte. Shown in Figure 39 are two possible ion transport scenarios that can lead to unstable lithium deposition. The team is computing transport properties using first-principles DFT with the nudged elastic band method as well as AIMD simulations.

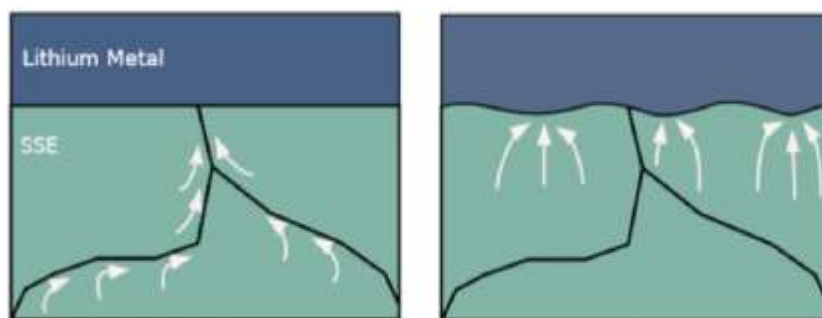


Figure 39. Destabilizing transport mechanisms. (a) Higher mobility along defects and grain boundaries. (b) Surface asperity flux concentration.

Mechanical Properties of Li-Metal and Solid Electrolyte Materials. In addition to quantifying Li-ion transport mechanisms, the mechanical properties of both Li-metal and solid-electrolyte materials need to be accurately computed. Bulk properties are readily obtained from DFT; however, the team is additionally studying the mechanical response in non-trivial scenarios present during electrochemical cycling. Understanding the mechanical response of both lithium metal and solid electrolyte requires knowledge of the materials' bulk mechanical properties and the effects of thermodynamic and chemical factors such as solute segregation, and possible interfacial reactions. To effectively address such phenomena, the team is employing macroscale models and atomic scale calculations in parallel.

Task 3.8 – Large-Scale *Ab Initio* Molecular Dynamics Simulations of Liquid and Solid Electrolytes (Lin-Wang Wang, Lawrence Berkeley National Laboratory)

Project Objective. The project goal is to use large-scale AIMD simulations and other computational approaches to study the discharging mechanism in Li-S battery, especially for polysulfur interaction with liquid electrolyte solvent molecules, and cathode materials, as well as lithium diffusion mechanisms in various systems. The long-term goal is to use such theoretical understanding to provide guidance to develop better electrolyte and cathode systems to overcome the bottlenecks that prevent commercialization of the Li-S battery. One major issue is solvation of Li_2S_n molecules in the electrolyte. The team is working to find the solution of this problem by both understanding the Li_2S_n -electrolyte interaction and discovering better cathode materials for optimal Li_2S_n -cathode binding. Specifically, the team seeks to: (1) develop reliable methods that combine classical force field (CFF) simulations with *ab initio* calculations to study thermal dynamic properties of Li_2S_n in different electrolytes, as well as interactions with different species within the electrolytes; and (2) study Li_2S_n interaction with different cathode materials, especially for 2D cathode materials consisted with light elements in the right-upper corner of the periodic table. The goal is to have sufficient binding energy between the Li_2S_n molecules and the cathode material, so, thermodynamically, the Li_2S_n will not be dissolved in the electrolyte. To study the Li_2S_n -electrolyte interaction, the team needs to accurately calculate the molecule entropy inside the solvent, which is a challenging task. The team plans to combine CFF with *ab initio* calculations for that study. To study Li_2S_n and cathode interaction, the team will calculate the phase diagrams of the systems with different number n and will hence obtain the binding energies and voltages at every step of the discharging process.

Project Impact. Making the Li-S battery a commercial reality will have a major impact in society, and also help to realize the VTO goal of 500 km per charge for EV. However, the nature of chemical reaction makes it different from the traditional intercalation-based Li-ion battery. The molecular nature of Li_2S_n also allows solvation in the electrolyte. To address these problems, it is essential to have fundamental studies and understandings of the underlying mechanisms. The theoretical simulation can also play an important role in discovering and designing new cathode materials.

Out-Year Goals. In the outgoing years, the team will further develop computational methods for more accurate entropy and interaction energy calculations for the electrolyte. This is a critical capability to study the battery system. The team will also explore different cathode materials and morphologies. In particular, there is a vast space to explore using 2D materials as Li-S battery cathodes and using curved amorphous structures to increase capacity. The key is to investigate all the effects and competitions of different reactions.

Collaborations. The project will collaborate with Gao Liu's group for cathode design. It has also collaborated with Prof. Feng Pan of Beijing University for lithium battery research in general.

Milestones

1. Set up the Li_2S_n calculation with charge polarization model (CPM) solvent model without explicit solvent molecule. (Completed).
2. Carrying out Li_2S_n /cathode structure calculations using CPM solvent model, with different cathode structures. (In progress).
3. Continue the Li_2S_n calculation with explicit solvent molecules; carry out direct CFF and AIMD simulations.
4. Continue calculation of Li_2S_n /cathode binding energies and phase diagrams, discovering new adequate cathode materials and morphologies.

Progress Report

This project has finished work for C_2N 2D material as Li-cathode material. It is found that the Li_xS_n cluster can anchor on the C_2N substrate and prevent the dissolution of lithium polysulfides. The theoretical weight energy capacity can be 1120 Wh/kg. The work has been published in *Journal of Materials Chemistry A* (2018), doi: 10.1039/C7TA10549E, as a HOT paper, or one recommended by referees.

The project has also worked on using oxidized black phosphorene as a 2D lithium battery cathode. The oxygen atoms on the 2D phosphorene can bind strongly with lithium, and thus serve as a solidified oxygen source of

Li-air battery. It overcomes many problems of Li-air battery (the source of oxygen, the mechanical stability, and the insulating nature of Li_2O). Its theoretical weight energy capacity is 1457 Wh/kg. It is thermally dynamically stable against decomposition into detached Li_2O . The system is conductive, thus overcoming the insulating issue in Li-air battery. The solid form of oxygen makes it possible to encapsulate the system.

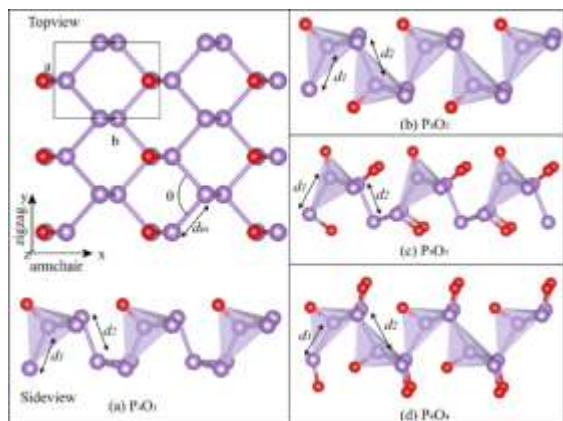


Figure 40. The different stages of oxidation of the back phosphorene.

Figure 40 shows the different stages of oxidation of the back phosphorene. It is found that the maximum composition of oxygen is P_4O_4 . Upon lithiation, the maximum number of lithium can be the same as that of oxygen. If more lithium is added, MD simulations show that the system becomes unstable. The formation energies of different lithiation states are shown in Figure 41a, while

Figure 42b-c shows the atomic structure after the systems are fully lithiated. The project notes that the lithium atoms bind with the oxygen atoms, and each oxygen atom can attach one lithium atom. The band structure of these systems is also calculated; it is shown that they are all semiconductors. AIMD is used to study the stability of these systems. It is found that as long as the number of lithium is smaller than the number of oxygen, the system is stable against the room-temperature vibration of the system. One manuscript has been submitted and is being reviewed.

The project has implemented a CPM in its own code. This is necessary to study Li_2S_n in the electrolyte. The team found that Li-electrolyte polarization interaction is particularly strong. The solvent model in the existing commercial code (like VASP) does not converge. This prompted the team to implement the model. The current

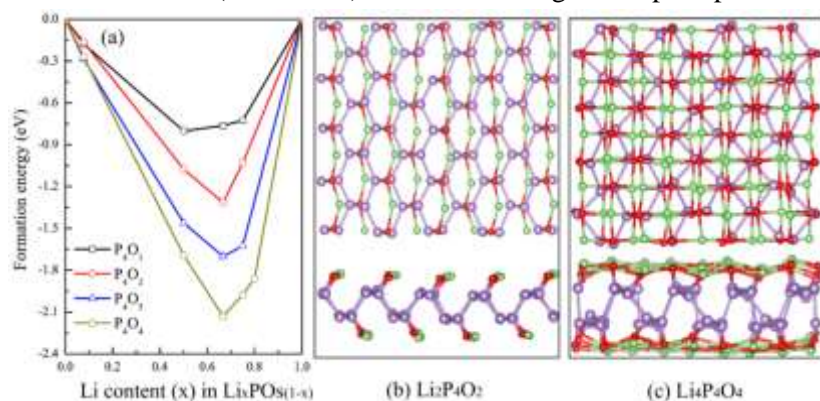


Figure 41. The formation energy of $Li_xPOs(1-x)$ for different POs ($s=1,2,3,4$) (a); the atomic structure of fully lithiated P_4O_2 (b) and P_4O_4 (c). The project found the system will become unstable if the number of lithium is larger than the number of oxygen.

CPM model runs well on the PWmat code, and the team has used it to study Li-electrolyte interaction. Using this code, the project has studied use of 2D coordination polymers, an emerging set of 2D organometallic frameworks, as the lithium cathode materials. A manuscript is being prepared.

The team has also studied the lithium diffusion in solid electrolytes, as well as stability of the solid electrolytes. They will be reported on next quarter.

Patents/Publications/Presentations

Publications

- Duan, Y., B. Zhang, J. Zheng, J. Hu, J. Wen, D. J. Miller, P. Yan, T. Liu, H. Guo, W. Li, X. Song, Z. Zhuo, C. Liu, H. Tang, R. Tan, Z. Chen, Y. Ren, Y. Lin, W. Yang, C. M. Wang, L.W. Wang, J. Lu, K. Amine, and F. Pan. “Excess Li-Ion Storage on Nanocrystal Reconstructed Surface to Boost Battery Performance.” *Nano Letters* 17 (2017): 6018.
- Yang, L., J. Zheng, M. Xu, Z. Zhuo, W. Yang, L. W. Wang, L. Dai, J. Lu, K. Amine, and F. Pan. “Short Hydrogen Bonds on Reconstructed Nanocrystal Surface Enhance Oxygen Evolution Activity.” *ACS Catalysis* 8 (2018): 466.
- Wu, J., and L. W. Wang. “2D Frameworks C₂N as a Potential Cathode for Lithium Sulfur Batteries: An *Ab Initio* Density Functional Study.” *Journal of Materials Chemistry A* (2018); doi: 10.1039/C7TA10549E.

Task 3.9 – *In Operando* Thermal Diagnostics of Electrochemical Cells (Ravi Prasher, Lawrence Berkeley National Laboratory)

Project Objective. Effective heat dissipation in batteries is important for multiple reasons including performance, reliability, and safety. Currently, the thermal management of battery cells is provided at the system level by either forced air or liquid cooling, leading to reduced system-level energy densities and more failure-prone complex system designs. Furthermore, even given theoretically infinite system level cooling applied to the external battery surface, peak temperature rise within a cell would still easily exceed acceptable threshold values due to the poor thermal transport properties within the cell itself. It has not yet been possible to thermally profile a real cell during operation to provide a spatially resolved map of heat transfer properties throughout the cell. The objective of this research is to create a metrology capable of spatially resolved *in operando* thermal property profiling, and then use this tool to reveal the largest thermal bottlenecks within a functioning Li-ion cell and create a complete materials-level cell thermal model.

Project Impact. The intrinsic thermal resistance of Li-ion cells is currently far higher than the theoretical value predicted by simply combining the known thermal properties of each macro component into an appropriate thermal model. The spatially resolved thermal transport property measurements from this project will reveal what key piece of information is missing. Preliminary data suggest that more than 75% of the total battery thermal resistance may be due to a single interface between the cathode and separator, previously unknown. An accurate understanding of the cell internal thermal transport is necessary to successfully optimize cell thermal performance to meet the challenges of extreme fast charging, mitigating thermal runaway, and improving battery performance, reliability, and safety.

Out-Year Goals. In the outgoing years, the project will adapt the established 3-omega technique to develop a new metrology that can measure thermal transport properties throughout the bulk of a Li-ion cell while it is in operation, without affecting cell operation. This will involve developing and testing the metrology itself, designing battery samples compatible with the metrology, and finally applying the technique to live cells. The project will also use the ultrafast optical time domain thermoreflectance (TDTR) technique to measure nanoscale thermal transport properties of constituent components of the cathode composite. It will then combine these results to create an “all-scale” accurate thermal model of the cell that—unlike existing models—agrees with the empirical measurements of cell thermal performance.

Collaborations. This project collaborates with two LBNL groups, Vincent Battaglia’s for cell assembly for 3-Omega studies and Robert Kostecki’s for pristine battery active material growths for TDTR studies.

Milestones

1. TDTR measurements of ideal battery samples. (Q1, FY 2018; Met)
2. 3-Omega sensing and heating lines fabricated, and metrology developed. (Q2, FY 2018; On schedule)
3. Electrochemical cells with 3-omega sensors integrated on the electrodes. (Q3; On schedule)
4. *Go/No-Go Decision*: Baseline *in operando* thermal diagnostics and measurement with 3-omega technique performed. (Q4, FY 2018; On schedule)

Progress Report

Q1 Milestone – Met. The team used PLD to grow 50-nm-thick epitaxial $\text{LiNi}_{0.5}\text{Mn}_{1.5}\text{O}_4$ (LNMO) pristine cathode material on the 0001 (C-plane) and 11(-2)0 (A-plane) faces of sapphire substrates (Figure 42). The different substrate orientations resulted in different crystal orientations of the deposited LNMO film. The team used TDTR to measure the cross-plane thermal conductivity of both samples. TDTR is an ultrafast pump-probe laser technique for measuring thermal transport properties at the nanoscale. Representative raw data are shown in Figure 43. The two different sample crystal orientations allowed the team to measure the LNMO thermal conductivity, k , in both principle directions. The team measured $k_{0001} = 1.4 \text{ W/m-K}$ and $k_{11(-2)0} = 3.8 \text{ W/m-K}$, yielding an anisotropy ratio of 2.7. This information helps the team understand the thermal transport through battery cathodes from the nanoscale up. When incorporated into a thermal model, it will also with prediction of changes to the bulk effective k of the system-level messy cathode composite as a result of changes to the active material. These nanoscale measurements will be combined with future microscale thermal measurements for a complete thermal transport picture of the battery.

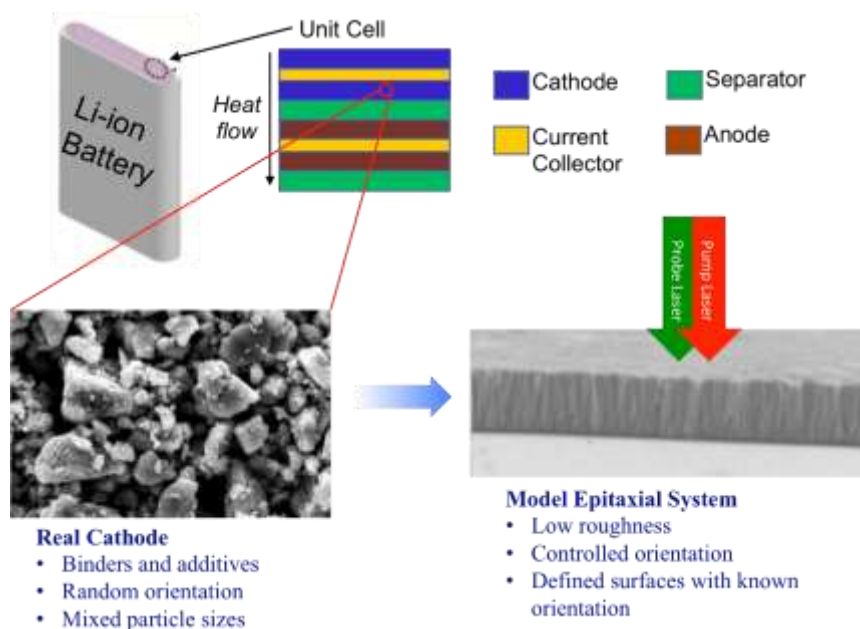


Figure 42. (Top) Heat must flow across all layers of the repeating unit cell to escape the Li-ion battery. (Bottom left) Scanning electron microscopy (SEM) image of a real cathode; too messy to get a controlled thermal transport measurement of the isolated active material. (Bottom right) SEM image of epitaxially grown pristine cathode material ideal for time domain thermoreflectance cross-plane thermal conductivity measurements.

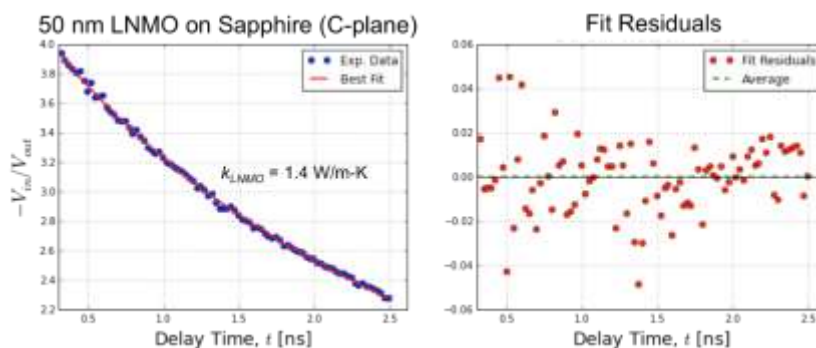


Figure 43. Representative raw time domain thermoreflectance data for one LNMO.

TASK 4 – METALLIC LITHIUM

Summary and Highlights

The use of a metallic lithium anode is required for advanced battery chemistries like Li-ion, Li-air, and Li-S to realize dramatic improvements in energy density, vehicle range, cost requirements, and safety. However, the use of metallic lithium with liquid and polymer electrolytes has so far been limited due to parasitic SEI reactions and dendrite formation. Adding excess lithium to compensate for such losses effectively negates the high energy density for lithium in the first place. For a long lifetime and safe anode, it is essential that no lithium capacity is lost either (1) to physical isolation from roughening, dendrites, or delamination processes, or (2) to chemical isolation from side reactions. The key risk and current limitation for this technology is the gradual loss of lithium over the cycle life of the battery.

BMR, Battery500, and other DOE programs are addressing this challenge with many innovative and diverse approaches. Key to all is the need for a much deeper analysis of the degradation processes and new strategies to maintain a dense, fully connected lithium and a dendrite-free electrolyte so that materials can be engineered to fulfill the target performance metrics for EV application, namely 1000 cycles and a 15-year lifetime, with adequate pulse power. Projecting the performance required in terms of just the lithium anode, this requires a high rate of lithium deposition and stripping reactions, specifically about 30 μm of lithium per cycle, with pulse rates up to 10 and 20 nm/s (15mA/cm²) charge and discharge, respectively with little or no excess lithium inventory. This is daunting in the total mass and rate of material transport that must be achieved without failures.

The efficient and safe use of metallic lithium for rechargeable batteries is then a great challenge, and one that has eluded R&D efforts for years. This Task takes a broad look at this challenge for both solid-state batteries and batteries continuing to use liquid electrolytes. For the liquid electrolyte batteries, steady improvement has been realized by PNNL researchers through use of dual lithium salts and organic additives to the typical organic solvent electrolytes to impede lithium corrosion and roughening. Now, Massachusetts Institute of Technology (MIT) is investigating halide and other additives to form self-healing SEI coatings. Engineered coating and 3D-anode structures continue to offer promising results. These include application of various 2D coating materials under investigation at Stanford University and use of 3D-copper-foam structures at University of Pittsburgh. An increasing number of programs are turning to various composites of polymer and ceramic electrolytes to address mechanical and ion transport challenges. ORNL is continuing investigation of spray-coated composite polymer electrolytes, while UT Austin and PNNL are also initiating work in this direction. A breakthrough is needed to promote facile Li-ion transport between the ceramic and organic polymer or liquid electrolytes. Two highly successful programs using ceramic solid electrolytes, specifically the LLZO garnets, were completed. Both demonstrated a great decrease in the area specific resistance (ASR) of the garnet-Li interface, *reaching values of just a few ohms*. This was accomplished variously using coating to promote wetting, treatments to ensure the surface is free of flaws and contamination, or higher interface areas to decrease the current density. As the ASR decreased, the interface adhesion and the critical current density achievable without forming Li-metal shorts increased. Fundamental aspects of this work on inorganic solid electrolytes are being continued by ANL researchers and others. The last project is focused on the properties of lithium metal itself. Past work using nanoindentation showed that lithium plating under high currents can exert large stresses at the lithium SEI. Following this, ORNL with Michigan Technological University (MTU) and University of Michigan will initiate work to create lithium stability maps to understand conditions where the lithium morphology becomes difficult to control. Each of these projects involves a collaborative team of experts with the skills needed to address the challenging materials studies of this dynamic electrochemical system.

Highlights. The highlights for this quarter are summarized below.

Stabilization of Lithium Metal in Liquid Electrolytes:

- The SEI formation and lithium morphology are profoundly sensitive to carbonate additive and use of dual lithium salts in the electrolyte formulation. The best so far cycles with 98.1% CE for extended times.
- Another liquid electrolyte study shows significantly improved CE with addition of fluorine-containing additives to create a self-healing SEI.
- Deposition of lithium onto copper foams modified with a graphene coating provides improved CE and a lower nucleation overpotential than for the uncoated foam or copper foil.

Formation of Barrier Materials at the Lithium Surface:

- Hexagonal-BN (h-BN) is formed on a copper current collector allowing ready electrodeposition of lithium metal under the h-BN coating and suppression of the occurrence of lithium dendrites. The performance of this structure is greatly improved using LiF deposited by atomic layer deposition (ALD) to selectively seal the edges of the BN platelets; it effectively seals cracks and pinholes and improves the mechanical robustness of the coating.

Lithium Batteries with Solid Electrolytes:

- Lithium batteries were fabricated using a practical and scalable aqueous spray coating of first the porous cathode layer (100 μm), followed by either a dense polymer or 50 vol% ceramic in polymer composite electrolyte coating (50 μm). A liquid catholyte, just sufficient to wet the pores, was added to the cathode.
- Similarly, solution cast polymer composites with 15 wt% alumina or lithium zirconium phosphate powders were compared side-by-side with symmetric cycling of Li||Li cells. The difference is attributed to a difference in the interfacial charge transfer resistance with the Li-metal contacts.
- XPS was used to evaluate the relative stability of LLZO with different dopants (aluminum, tantalum, and niobium) upon coating with lithium metal on a heat-treated, clean surface. The tantalum doped is most stable with no reduction of tantalum and only a small concentration of Zr^{4+} to Zr^{3+} reduction.
- Rationalization of the depth and strain rate dependent hardness of lithium metal has identified the conditions that a brittle solid electrolyte may be susceptible to failure by mode I fracture initiating at small-scale defects at the lithium/solid electrolyte interface.

Task 4.1 – Lithium Dendrite Prevention for Lithium Batteries (Wu Xu and Ji-Guang Zhang, Pacific Northwest National Laboratory)

Project Objective. The project objective is to enable lithium metal to be used as an effective anode in rechargeable Li-metal batteries for long cycle life at a reasonably high current density. The investigation in FY 2018 will focus on effects of various lithium salt mixtures, inorganic fillers and polymer types on ionic conductivity, lithium CE, Li-anode morphology, and battery performances in terms of long-term cycling stability at room temperature and elevated temperatures and at various current density conditions, rate capability, and low-temperature discharge behavior. The compatibility of such electrolytes with 4-V NMC cathode will be investigated.

Project Impact. Lithium metal is an ideal anode material for rechargeable batteries. Unfortunately, uncontrollable dendritic lithium growth and limited CE during repeated lithium stripping/deposition processes have prevented their practical applications. This work will explore the new hybrid composite electrolytes that can lead to dendrite-free lithium deposition with high CE. The success of this work will increase energy density of Li-metal and Li-ion batteries and accelerate market acceptance of EVs, especially for PHEVs as required by the EV Everywhere Grand Challenge.

Out-Year Goals. The long-term goal of the proposed work is to enable lithium and Li-ion batteries with > 120 Wh/kg (for PHEVs), 1000 deep-discharge cycles, 10-year calendar life, improved abuse tolerance, and less than 20% capacity fade over a 10-year period.

Collaborations. This project collaborates with Chongmin Wang, PNNL, on characterization by TEM/SEM.

Milestones

1. Develop a lithium salt mixture that has an ambient melting temperature and an ionic conductivity over 1 mS/cm. (Q1, December 31, 2017; Completed)
2. Investigate effects of inorganic fillers and polymers on hybrid composite electrolytes. (Q2, March 31, 2018)
3. Develop an inorganic/polymeric hybrid composite electrolyte with ionic conductivity over 1 mS/cm and lithium CE over 99%. (Q3, June 30, 2018; Ongoing)
4. Achieve over 300 cycles for 4-V Li||NMC batteries with ~ 2 mAh/cm² cathode loading. (Q4, September 30, 2018; Ongoing)

Progress Report

This quarter, the project further characterized the Li-metal anodes and the NMC cathodes from the disassembled Li||NMC cells after they were cycled in three electrolytes: (a) ELY-14, Dual-salt + LiPF₆ (EC/EMC = 4:6 by wt), (b) ELY-19, Dual-salt + LiPF₆ + VC + FEC (EC/EMC = 4:6 by wt), and (c) ELY-13, Dual-salt + LiPF₆ + VC + FEC (EC/EMC = 7:3 by wt). The Li-metal anode cycled in ELY-14 (Figure 44a) has mainly fibrous structure, which is consistent with the previous report. Further addition of VC + FEC additives (that is, ELY-19) leads to thicker lithium fibers with larger diameters (Figure 44b), suggesting that the addition of extra additives of VC + FEC could facilitate the formation of lithium fibers of larger diameter. In contrast, a remarkably different lithium morphology is generated in ELY-13 (EC/EMC ratio 7:3), Figure 44c, showing big particle structure and the further reduced surface area of the cycled Li-metal anode when compared to that of ELY-19 (EC/EMC ratio 4:6). The improved Li-metal stability in ELY-13 could be further confirmed by the thinnest surface film identified on the cycled Li-metal anode.

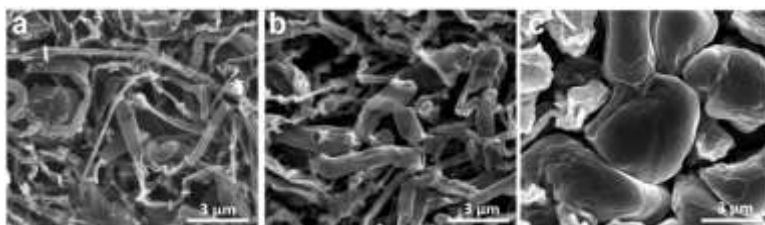


Figure 44. Top view scanning electron microscopy images of the Li-metal anodes in the Li||NMC cells after 100 cycles at the same charge and discharge current density of 2.0 mA cm⁻² after 3 formation cycles at 0.2 mA cm⁻² at 30°C using the electrolytes of (a) ELY-14, (b) ELY-19, and (c) ELY-13.

The impedance spectra of the Li||NMC cells using these three electrolytes at different stages of cycling reveal that the Li||NMC cell using ELY-13 exhibits the smallest interfacial resistances and charge transfer resistances after 3 formation cycles at 0.2 mA cm⁻² and after 100 regular cycles at 2.0 mA cm⁻², while the Li||NMC cell using ELY-14 shows the largest interfacial resistances and charge transfer resistances. The results evidence the good conductivity properties of the SEI layer formed in ELY-13. The XPS results demonstrate that there are many polycarbonates formed in the surface film on the Li-metal anode cycled in ELY-13, which is ascribed to the combinational effects of additives (LiPF₆, VC, and FEC) and the higher content of EC in the solvents, where the VC and FEC favor the formation of a more robust surface film and the LiPF₆ could induce more polymerization of the EC solvent in the surface film. Therefore, the excellent improvements in battery performances, such as dendrite-free, high lithium CE of 98.1% and long-term cycling stability of Li-metal batteries using the electrolyte of ELY-13, come from the formation of more polymeric, ionic conductive, compact and robust surface film on the surface of the Li-metal anode through the electrochemical reductive decompositions of the electrolytes components and the ring-opening polymerization of additives and EC solvent.

The team also worked on developing lithium salt mixtures that have an ambient melting temperature and an ionic conductivity over 1 mS/cm. The LiTFSI-LiFSI (2:8 by mol) mixture has a melting temperature at ca. 60°C and an ionic conductivity of ca. 0.1 mS/cm. With further mixing with a certain amount of room-temperature molten salts (that is, ionic liquids), the salt mixtures of (LiTFSI-LiFSI)_{0.2}-IL_{0.8} show an ionic conductivity of 1.0 ~ 1.4 mS/cm at 25°C (Figure 45). The electrochemical performances of the salt mixtures are being tested.

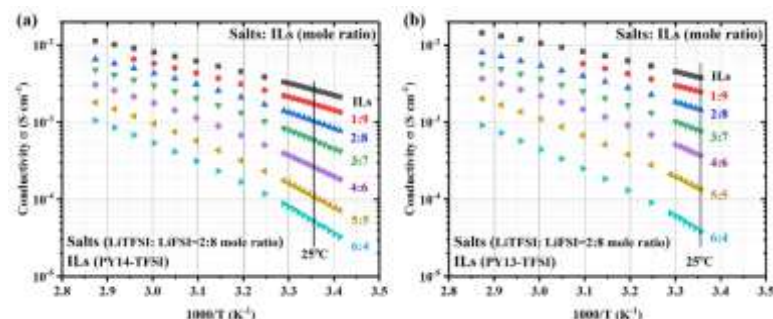


Figure 45. Temperature dependence of ionic conductivity of salt mixtures of LiTFSI-LiFSI (2:8 by mol) with ionic liquids PY14-TFSI (a) and PY13-TFSI (b) at different compositions.

Patents/Publications/Presentations

Publications

- Li, X., J. Zheng, X. Ren, M. H. Engelhard, W. Zhao, Q. Li, J.-G. Zhang, and W. Xu. “Dendrite-Free and Performance-Enhanced Lithium Metal Batteries through Optimizing Solvent Compositions and Adding Combinational Additives.” *Advanced Energy Materials*, revised version submitted.
- Li, X., J. Zheng, M. H. Engelhard, D. Mei, Q. Li, S. Jiao, N. Liu, W. Zhao, J.-G. Zhang, and W. Xu. “Effects of Imide-Orthoborate Dual-Salt Mixtures in Organic Carbonate Electrolytes on the Stability of Lithium Metal Batteries.” *ACS Applied Materials & Interfaces* (2018). doi: 10.1021/acsami.7b15117.
- Ren, X., Y. Zhang, M. H. Engelhard, Q. Li, J.-G. Zhang, and W. Xu. “Guided Lithium Metal Deposition and Improved Lithium Coulombic Efficiency through Synergistic Effects of LiAsF₆ and Cyclic Carbonate Additives.” *ACS Energy Letters* 3 (2018): 14–19. doi: 10.1021/acsenergylett.7b00982.
- Jiao, S., J. Zheng, Q. Li, X. Li, M. H. Engelhard, R. Cao, J.-G. Zhang, and W. Xu. “Behavior of Lithium Metal Anodes under Various Capacity Utilization and High Current Density in Lithium Metal Batteries.” *Joule* 2 (2018): 1–15. doi: 10.1016/j.joule.2017.10.007.

Presentation

- 232nd ECS Meeting, National Harbor, Maryland (October 4, 2017): “Effects of Imide-Orthoborate Dual-Salt Mixtures in Organic Carbonate Electrolytes on the Stability of Lithium Metal Batteries”; X. Li, J. Zheng, M. H. Engelhard, D. Mei, Q. Li, S. Jiao, N. Liu, W. Zhao, J.-G. Zhang, and W. Xu.

Task 4.2 – Self-Assembling and Self-Healing Rechargeable Lithium Batteries (Yet-Ming Chiang, Massachusetts Institute of Technology; Venkat Viswanathan, Carnegie Mellon University)

Project Objective. The project objectives are as follows: (1) investigate formation of lithium halide containing SEI, (2) characterize the structure and composition of the SEI surface film and morphology of the electrochemically deposited lithium, and (3) develop combinations of electrolytes (solvents + salts) and electrolyte additives that produce a highly Li-ion conducting, mechanically robust, and self-healing SEI to suppress lithium dendrite formation and improve CE.

Project Impact. Efforts to achieve practical use of the Li-metal anode in rechargeable lithium batteries have long been plagued by lithium dendrite formation and low CE. Lithium dendrites cause battery short-circuits, leading to serious safety hazards. The low CE of Li-metal anodes demands use of excess lithium to offset the lithium loss during cycling, which lowers the overall energy density of the battery. If successful, this project will enable self-forming and self-healing SEI containing alkali and/or alkaline earth halides that can suppress dendrite formation and improve CE. This will eventually enable high-energy-density (> 400 Wh/kg) and long-cycle-life (> 500 cycles, 80% capacity retention) Li-metal batteries.

Approach. The project approach involves the following: (1) identifying suitable combinations of solvents, Li-electrolyte salts, and halide and other additives that can produce highly Li-ion conducting, mechanically robust, and self-healing SEI, (2) using integrated theory and experiment, and (3) assembling and testing symmetric and asymmetric cells and Li-metal batteries comprising a high areal-capacity cathode (> 3 mAh/cm²) and a capacity-limited Li-metal anode ($< 130\%$ lithium excess).

Out-Year Goals. The project will down-select electrolyte compositions, develop designs for prototype full cells of > 10 mAh capacity, and fabricate and deliver cells to DOE-specified laboratories for testing and evaluation.

Collaborations. This project collaborates with 24M Technologies Inc. (18 cm²/80 cm² pouch cell fabrication and tests).

Milestones

1. Demonstrate Li-Li asymmetric cell using halide additives that outperforms additive-free cell according to criteria in Q3 and Q4. (Q1, December 2017; Completed)
2. Deliver structural and chemical characterization results for baseline halide films on lithium metal. (Q2, March 31, 2018; Ongoing)
3. Deliver structural and chemical characterization results for self-healed halide films on lithium metal. (Q3, June 30, 2018)
4. Establish quantitative theoretical criteria for effectiveness and reproducibility in dendrite-suppression experiments. (Q4, September 30, 2018)
5. *Go/No-Go Decision:* Demonstrate Li-Li symmetric cells that meet established criteria cycling at ≥ 3 mAh/cm² at C/5 rate over 30 cycles. (Q1, FY 2019)

Progress Report

This quarter, results are reported that the Li-Li asymmetric cell using halide additives outperforms the additive-free cell according to criteria in Q3 and Q4. The team has also carried out DFT simulations looking at the decomposition pathways for fluorinated electrolytes to guide the electrolyte design. These results will be reported next quarter.

The asymmetric cell consists of two Li-metal electrodes that have different thickness and areal capacity. The working electrode is a 20- μm -thick lithium film coated on a copper foil (areal capacity $\sim 4.12 \text{ mAh/cm}^2$), while the counter electrode is a 750- μm -thick lithium foil. The two electrodes are assembled into a CR2032-type coin-cell with a Tonen polyethylene separator and 40- μL electrolyte. The cell is cycled at a current density of 0.6 mA/cm^2 , and the cycling capacity is 3.0 mAh/cm^2 per deposition/stripping cycle. The cell is cycled until the overpotential for Li-stripping reaches 0.5 V versus Li^+/Li . The average lithium cycling CE is calculated using a method similar to that previously reported by Doron Aurbach et al.:

$$E_{\text{average}} = 1 - \frac{Q_D}{nQ_T}$$

Q_T is the cycling capacity (3 mAh/cm^2 in the project's tests); Q_D is total lithium capacity ($Q_D = Q_T + Q_{\text{excess}} \sim 7.12 \text{ mAh/cm}^2$); and n is the number of completed deposition/stripping cycles when the test is stopped.

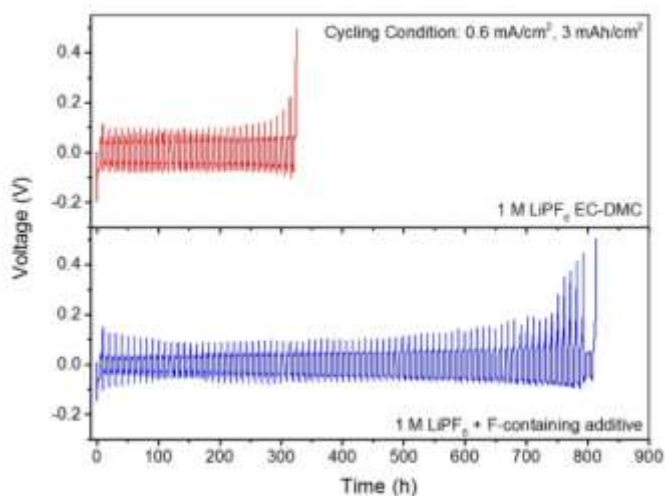


Figure 46. Li-Li asymmetric cell cycling with 1 M LiPF_6 EC-DMC (1:1) and 1 M LiPF_6 + F-containing additive electrolytes. Cycling condition is 0.6 mA/cm^2 current density and 3.0 mAh/cm^2 areal capacity.

The Li-Li asymmetric cell using conventional 1 M LiPF_6 EC-DMC (1:1 by volume, Sigma-Aldrich) only lasts 32 cycles (Figure 46). The average lithium cycling CE ($\text{Li CE}_{\text{average}}$) is calculated to be 92.6%. With the addition of a fluorine-containing additive, the cycle life of the Li-Li asymmetric cell improves to 80 cycles. The $\text{Li CE}_{\text{average}}$ is calculated to be 97.0%. This test is also carried out at a higher current density of 1 mA/cm^2 and the same areal capacity of 3.0 mAh/cm^2 . The results are $88.8 \pm 2.3\%$ (4 experiments) for the conventional 1 M LiPF_6 EC-DMC electrolyte and $95.4 \pm 1.6\%$ (4 experiments) for the electrolyte with the F-containing additive. These results meet this quarter's milestone.

Task 4.3 – Engineering Approaches to Dendrite-Free Lithium Anodes (Prashant Kumta, University of Pittsburgh)

Project Objective. This project will yield Li-metal anodes with specific capacity ≥ 2000 mAh/g (≥ 10 mAh/cm²), ~ 1000 cycles, CE loss $\leq 0.01\%$, and CE $\geq 99.99\%$ with superior rate capability. The goal is to (1) systematically characterize different approaches for generation of dendrite-free Li-metal anodes while also providing understanding of the scientific underpinnings, and (2) evaluate the microstructure and electrochemical performance of dendrite-free Li-metal anodes. Generation of high-performance, dendrite-free Li-metal anodes will successfully demonstrate generation of novel sulfur cathodes, affording fabrication of Li-S batteries meeting the targeted gravimetric energy densities ≥ 350 Wh/kg and ≥ 750 Wh/l with a cost target \$125/kWh and cycle life of at least 1000 cycles for meeting the EV Everywhere Grand Challenge blueprint.

Project Impact. Dendrite formation in electrochemical systems occurs due to inhomogeneous current densities coupled with local diffusion gradients, surface roughness, and kinetic roughening. Lithium dendrite formation and growth are, however, not well understood; adding to the complexity is SEI formation. Control and elimination of Li-metal dendrite formation is a veritable challenge. If overcome, it would render universal adoption of Li-anode batteries for stationary and mobile applications. This project is a scientific study of novel approaches to address dendrite formation in Li-anode batteries, electrolyte decomposition, and associated cell failure. Development of dendrite-free, high-performance lithium anodes will enable the use of Li-free cathodes, opening myriad possibilities to push the envelope in terms of cathode capacity and battery energy density.

Out-Year Goals. This project comprises three major phases to be successfully completed in three years:

- Year 1 – Synthesis, characterization, and scale up of suitable PF (porous foams) for use as current collectors for lithium anodes and Li-ion conductor (LIC) materials to prepare multilayer porous foams (MPF).
- Year 2 – Development of Li-rich structurally isomorphous alloy (SIA) anodes. Generation of composite multilayer anodes (CMAs).
- Year 3 – Advanced high-energy-density, high-rate, extremely cyclable cell development.

Collaborations. The project will collaborate with Dr. Moni Kanchan Datta and Dr. Oleg I. Velikokhatnyi (University of Pittsburgh, U Pitt) as co-PIs. It will collaborate with Dr. A Manivannan (Global Pragmatic Materials) for XPS analysis. It will also collaborate with Dr. D. Krishnan Achary (U Pitt) for solid-state magic angle spinning NMR (MAS-NMR) characterization.

Milestones

1. Synthesis of MPFs exhibiting: specific capacity ≥ 1000 mAh/g (≥ 4 mAh/cm²), > 400 cycles without cell failure), and initial CE of $\geq 95\%$ with $\leq 0.05\%$ loss per cycle. (Q1, October 2017; Ongoing)
2. Perform first-principles investigations into identifying electronically and ionically conductive materials capable of acting as SIA compositions over a range of lithium compositions. (Q1, October 2017; Ongoing)
3. Fabrication and characterization of suitable thick electrodes for 10-mAh cell configurations. (Q1, October 2017; Ongoing)
4. Synthesis and testing of SIA electrodes. (Q3, April 2018; Ongoing)
5. Optimization of MPFs to improve capacity and stability for scaling. (Q4, July 2018; Ongoing)

Progress Report

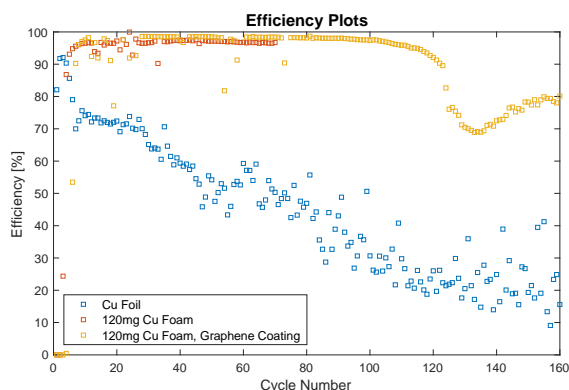


Figure 47. Coulombic efficiency of multilayer porous foams with graphene coating, without graphene coating, and of unmodified copper foil serving as reference.

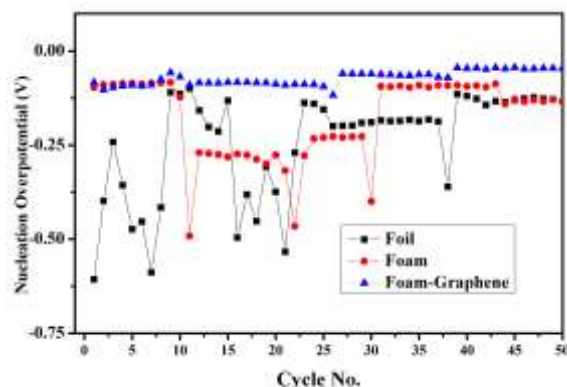


Figure 48. Nucleation overpotential for copper foil, copper foam, and graphene-Cu foam during the first 50 cycles.

Current phase-2 efforts focus on surface modifications of MPFs to control SEI formation and growth using thin graphene coatings. Figure 47 shows graphene embedded MPF improving the electrode CE, and the stability achieved before fade (~70 cycles for unmodified MPF to ~120 cycles for graphene MPF). Furthermore, a reduction in the lithium nucleation overpotential (~0.09 V) is seen with graphene (Figure 48). The erratic behavior of the nucleation overpotential for the unmodified foam and foil can be attributed to the instabilities of the SEI formed on the metallic copper surface. Introduction of graphene provides a more stable SEI layer coupled with solid-state Li^+ diffusion pathway resulting in improved reversible lithium plating and lower resistance to ionic conduction. The growth of a thick SEI layer leads to efficiency fade. Additional research to improve the graphene coating, as well as examine other surface functionalization strategies to assist in stable SEI generation, is being explored.

Another approach focuses on modifying nucleation and growth of lithium employing patterning methods. Figure 49 shows SEM images of two surface patterns. Modification of the surface roughness leads to high energy sites for preferential nucleation and plating, preventing high surface area lithium dendrite formation. Reduction in nucleation overpotential is observed for the coarser pattern, with no effect on the finer patterns. The deep sites for the former provide pre-active high energy sites for nucleation, thus reducing the overpotential. Lithium plating studies on various textured patterns, along with SEM analysis to study the deposition morphology and location, are in progress and will be discussed in future reports.

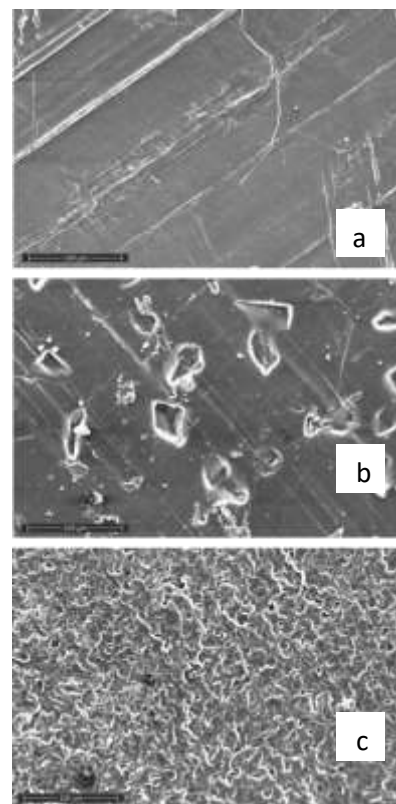


Figure 49. Scanning electron microscopy images of (a) pristine lithium foil and lithium foil imprinted with (b) coarse and (c) fine patterns. Scale Bar = 100 nm.

Patents/Publications/Presentations

Publication

- Day, B. A., M. K. Datta, P. M. Shanthi, B. Gattu, and P. N. Kumta. “Highly Porous Metal Foam Electrodes as Dendrite-Free Anodes for Li-Metal Batteries.” In preparation.

Presentation

- 232nd ECS Meeting, National Harbor, Maryland (October 1–5, 2017): “Engineered Porous Foam Electrodes: New Approaches to Dendrite-Free Li-Metal Batteries”; B. A. Day, P. H. Jampani, M. K. Datta, P. M. Shanthi, B. Gattu, and P. N. Kumta.

Task 4.4 – Nanoscale Interfacial Engineering for Stable Lithium-Metal Anodes (Yi Cui, Stanford University)

Project Objective. This study aims to render Li-metal anode with high capacity and reliability by developing chemically and mechanically stable interfacial layers between lithium metal and electrolytes, which is essential to couple with sulfur cathode for high-energy, Li-S batteries. With the nanoscale interfacial engineering approach, various kinds of advanced thin films will be introduced to overcome issues related to dendritic growth, reactive surface, and virtually “infinite” volume expansion of Li-metal anode.

Project Impact. Cycling life and stability of Li-metal anode will be dramatically increased. The success of this project, together with breakthroughs of sulfur cathode, will significantly increase the specific capacity of lithium batteries and also decrease cost, thereby stimulating the popularity of EVs.

Out-Year Goals. Along with suppressing dendrite growth, the cycle life, CE, and current density of Li-metal anode will be greatly improved (that is, no dendrite growth for current density up to 3.0 mA/cm², with CE greater than 99.5%) by choosing the appropriate interfacial nanomaterial along with rational electrode material design.

Milestones

1. Further improve the efficacy of Li-metal protection layers. (Q1, December 2017; Completed)
2. Improve the CE > 99.2%. (In progress)
3. Demonstrate > 800 cycles of Li-metal anode with stable host and interphase. (In progress)

Progress Report

Hexagonal-BN, a 2D atomic crystal with superior chemical inertness and mechanical strength has shown recent success as a stable coating to suppress dendrite formation during electrochemical Li-metal plating.^[1] However, the h-BN grown by chemical vapor deposition (CVD) has numerous defects intrinsic to the synthesis and transfer processes, which may compromise the effectiveness of h-BN as a stable interfacial layer. To further improve the efficacy of the Li-metal protection layer, herein, the project takes the advantage of the dangling bonds at the defective sites to selectively stitch CVD grown h-BN domains by ALD. This project demonstrated selective ALD of LiF primarily on the line and point defects of h-BN. The protected lithium electrodes exhibited good cycling behavior with more than 300 cycles at relatively high CE (> 95%) in an additive-free carbonate electrolyte.

ALD of LiF in this project was carried out using lithium tert-butoxide and titanium fluoride as precursors at a growth temperature of 250°C. ALD is typically known for its ability to achieve a conformal coating. Conversely, the ALD LiF deposition on h-BN is selective and does not cover the entire substrate. For comparison, h-BN before and after ALD LiF deposition was characterized by SEM (Figure 50). Although pristine h-BN appears to form complete coverage on silicon (Figure 50b, left), point and line defects cannot be revealed by SEM due to the limitation of resolution. After LiF deposition, there were considerable numbers of nanowires and nanoparticles deposited on the continuous h-BN layer (Figure 50b, right), indicating the nature of selective ALD LiF deposition on h-BN. The formation of nanowires and nanoparticles might relate to the preferred nucleation of LiF on the line and point defects of CVD h-BN.

The project's previous results have also shown that h-BN can be lifted by the lithium plated underneath. However, despite a high theoretical in-plane Young's modulus, the grain boundaries are predicted to be the weak points of h-BN when tensile stress is applied. Although the team started with a continuous CVD h-BN film, holes appeared after plating. Using the LiF/h-BN hybrid film as the interfacial layer combines the advantages of both components. First, the weak physical interaction between h-BN and copper allows lithium to be plated in between h-BN and copper. Second, with the addition of chemically stable LiF linkers, the overall mechanical strength of LiF/h-BN is improved. It also helps to seal any pinholes or cracks induced in the CVD synthesis and transfer. The superior chemical and mechanical stability of the LiF/h-BN combination effectively suppressed the dendrite formation. Long-term lithium plating/stripping experiments were also conducted in corrosive carbonate electrolyte without any additives (1 mAh cm⁻² capacity at a rate of 0.5 mA cm⁻²). The lithium plating/stripping on the LiF/h-BN/Cu substrate maintained a high average CE above 96% for over 300 cycles, which improved significantly compared to pristine h-BN without sealing the defects.

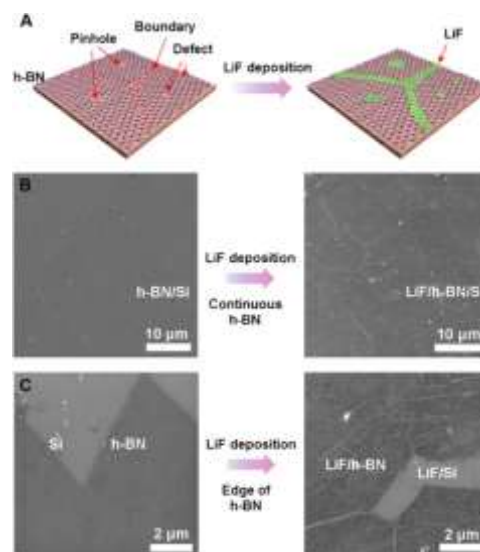


Figure 50. (a) Schematics of selective atomic layer deposition (ALD) LiF deposition on h-BN. (b) Scanning electron microscopy (SEM) characterization of 50 cycles of ALD LiF deposition on continuous h-BN. (c) SEM characterization of 50 cycles of ALD LiF deposition on the edge of h-BN.

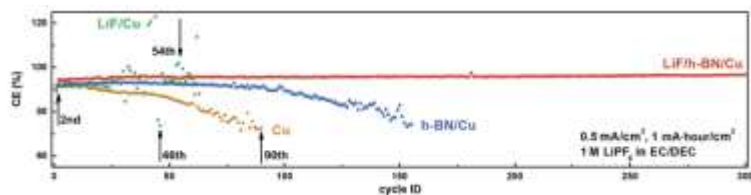


Figure 51. Coulombic efficiency during long-term cycling.

[1] Yan, K., et. al. *Nano Letters* 14, no. 10 (2014): 6016–6022.

Patents/Publications/Presentations

Publication

- Xie, J., L. Liao, Y. Gong, Y. Li, F. Shi, A. Pei, J. Sun, R. Zhang, B. Kong, R. Subbaraman, J. Christensen, and Y. Cui. “Stitching h-BN by Atomic Layer Deposition of LiF as a Stable Interface for Lithium Metal Anode.” *Science Advances* 3, no. 11 (2017): eaao3170.

Task 4.5 – Composite Electrolytes to Stabilize Metallic Lithium Anodes (Nancy Dudney and X. Chelsea Chen, Oak Ridge National Laboratory)

Project Objective. The project has several objectives: (1) prepare composites of representative polymer and ceramic electrolyte materials to achieve thin membranes that have the unique combination of electrochemical and mechanical properties required to stabilize the metallic lithium anode while providing for good power performance and long cycle life, (2) understand the Li-ion transport at the interface between polymer and ceramic solid electrolytes, which is critical to effective conductivity of the composite membrane, (3) identify key features of composite composition, architecture, and fabrication that optimize performance, and (4) using practical and scalable processing, fabricate thin electrolyte membranes to use with a thin metallic lithium anode to provide good power performance and long cycle life.

Project Impact. A stable lithium anode is critical to achieve high energy density with excellent safety, lifetime, and cycling efficiency. This study will identify key design strategies that should be used to prepare composite electrolytes to meet the challenging combination of physical, chemical, and manufacturing requirements to protect and stabilize the Li-metal anode for advanced batteries. By utilizing well characterized and controlled component phases, design rules developed for composite structures will be generally applicable toward substitution of alternative and improved solid electrolyte component phases as they become available. Success will enable DOE technical targets: 500-700 Wh/kg, 3000-5000 deep discharge cycles, and robust operation.

Approach. This project seeks to develop practical solid electrolytes that will provide stable, long-lived protection for the Li-metal anode. Current electrolytes have serious challenges when used alone: oxide ceramics are brittle, sulfide ceramics are air sensitive, polymers are too resistive and soft, and many electrolytes react with lithium. Composites provide a clear route to address these issues. This project does not seek discovery of new electrolytes; rather, the goal is to study combinations of well-known electrolytes. The project emphasizes investigation of polymer-ceramic interfaces formed as bilayers and as simple composite mixtures where the effects of interface properties can be readily isolated. In general, the ceramic phase is several orders of magnitude more conductive than the polymer electrolyte, and interfaces can contribute an additional source of resistance. Using finite element simulations as a guide, composites with promising compositions and architectures are fabricated and evaluated for Li-transport properties using AC impedance and DC cycling with lithium in symmetric or half cells. General design rules will be determined that can be widely applied to other combinations of solid electrolytes.

Out-Year Goal. The goal is to use advanced manufacturing processes where the architecture of the composite membrane can be developed and tailored to maximize performance and cost-effective manufacturing.

Collaborations. Work is conducted by Dr. A. Samuthira Pandian and Dr. Xi Chen. Dr. Jihua Chen (ORNL) assisted with electron microscopic characterization and Dr. Rose Ruther (ORNL) with Raman spectroscopy. Electrolyte powders are obtained from Ohara Corporation and Prof. Sakamoto (University of Michigan).

Milestones

1. Fabricate a full battery using aqueous spray coating for both the composite electrolyte and cathode incorporating a protected Li-metal anode. (Q4 FY 2017 stretch goal; Completed)
2. Accurately determine the polymer/ceramic electrolyte interface resistance for PEO and Ohara. Revisit effect of DMC on interface ASR. (Q1, FY 2018; Completed – detailed report next quarter)
3. Minimize interface ASR by chemical and mechanical treatment with a goal of < 100 ohm. (Q2, FY 2018)
4. Move beyond model materials like Ohara and PEO, to include polymer gels. Identify promising polymer ceramic systems with interfacial ASR less than 10 ohm. (Q3, FY 2018)
5. Assess the feasibility of slurry spray coating to form the thin membrane of new materials. (Q4, FY 2018)

Progress Report

An automatic desktop spray coater (Prism 400, Ultrasonic Systems, Inc., Figure 52) was installed in the lab to investigate this route to cost-effective manufacturing. The spray coater features programmable x-y-z positioning and uses an ultrasonic spray head instead of the conventional nozzle spray head. It delivers thinner, more precise coatings. Full batteries using aqueous spray coating for both a thick NMC (5:3:2) cathode, with carbon and binder, followed by a spray coating of the composite electrolyte are reported. The bilayer was fully dried and calendered, punched, and assembled to cells. This fulfills the milestone to demonstrate a promising approach.

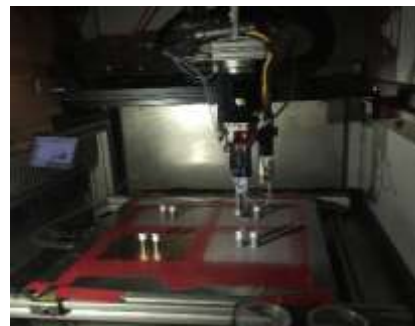


Figure 52. A picture of the spray coater.

The table below lists the batteries assembled/tested and the analysis. The first entry, reported last quarter, shows that the spray-coated cathode cycled well in a flooded cell. The composite polymer electrolyte (CPE) is composed of 50 vol% Ohara ceramic powder in PEO+LiTf+TEGDME (CPE-P, P for plasticized). The intent of additional cells and tests was to probe the stability of the lithium protected by dry CPE-P, but the assessment is that the cathode is limiting the performance for most cells. To cycle the thick NMC cathode, its pores must be wet with a liquid electrolyte (LE), here being EC-DMC-LiPF₆(1.2M); however, the team determined that the CPE-P delaminates from the NMC cathode upon addition of even a very small volume of LE. Without excess LE, for contact and to prevent drying, the cells could not cycle. Omitting the Ohara powder and the TEGDE from the polymer electrolyte (PE), provided improved adhesion to the NMC, but still only 2 cycles. This points to spraying a thin PE contact layer between the NMC and CPE-P in future cells. Also, ongoing tests seek to identify the side reaction(s) limiting cycling; indeed, limiting the charge to 3.8 V appears to avoid decomposition of the PEO in contact with the cathode, as one deleterious reaction.

Table 3. Cells fabricated in Q1 FY 2018. Tests by electrochemical impedance spectroscopy and cycling at 0.1 or 0.01C.

Cathode electrolyte assembly anode	T (°C)	Cyclability	Analysis and details
NMC - LE CPE-P (10µm) Celgard-LE Li	27	20 cycles, no capacity fade	<ul style="list-style-type: none"> Spray coated NMC works well on expanded aluminum foil NMC is cast to ~ 100 µm, calendered with thin CPE-P Cell is flooded with liquid electrolyte (LE)
NMC- LE CPE-P (50µm) Celgard-LE Li	27, 50	20 cycles at 27°, 3 cycles at 50°C	<ul style="list-style-type: none"> A thicker CPE-P limits the LE access to cathode pores, although the cell is flooded with liquid electrolyte The LE may be drying; PEO may decompose
NMC, dry CPE-P (50µm) Li	27	Cannot cycle	<ul style="list-style-type: none"> Dry cell has high cell resistance. Poor adhesion of CPE-P to NMC when disassembled
NMC-LE (6-12 µL) CPE-P (50µm) Li	27	Cannot cycle	<ul style="list-style-type: none"> Lower resistance (~ 200 Ω) achieved with little LE Reaction occurs upon charging
NMC-LE (12 µL) CPE-P (50µm) Lipon (200 nm) Li	27	Cannot cycle	<ul style="list-style-type: none"> CPE delaminated from NMC as soon as LE is added Lipon appears to limit reactions and darkening of CPE and lithium
NMC-LE (6-8 µL) PE (200µm) Li	50	2 cycles to 4.2V, then reaction	<ul style="list-style-type: none"> PE penetrated the porous cathode for better adhesion Limited cycling indicates a side reaction, at NMC-PE or Li-PE

Patents/Publications/Presentations

Publication

- Pandian, Amaresh Samuthira, X. Chelsea Chen, Jihua Chen, Bradley S. Lokitz, Rose E. Ruther, Guang Yang, Kun Lou, Jagjit Nanda, Frank M. Delnick, and Nancy J. Dudney. “Facile and Scalable Fabrication of Composite Polymer-Ceramic Electrolyte with High Ceramic Loadings.” In review, January 2018.

Presentation

- Materials Research Society (MRS) Fall Meeting, Boston, Massachusetts (November 2017): “(PEO)₁₆.LiCF₃SO₃+Ohara LICGC® Composite Polymer Ceramic Electrolyte for Lithium Secondary Batteries”; Amaresh Samuthira Pandian, Frank M. Delnick, and Nancy J. Dudney.

Task 4.6 – Lithium Batteries with Higher Capacity and Voltage (John B. Goodenough, University of Texas – Austin)

Project Objective. The project objective is to develop an electrochemically stable alkali-metal anode that can avoid the SEI layer formation and the alkali-metal dendrites during charge/discharge. To achieve the goal, a thin and elastic solid electrolyte membrane with a Fermi energy above that of metallic lithium and an ionic conductivity $\sigma > 10^{-4} \text{ S cm}^{-1}$ will be tested in contact with alkali-metal surface. The interface between the alkali-metal and the electrolyte membrane should be free from liquid electrolyte, have a low impedance for alkali-metal transport and plating, and keep a good mechanical contact during electrochemical reactions.

Project Impact. A safe alkali-metal anode that can be plated/stripped reversibly at low resistance and high rates over many thousands of charge/discharge cycles would maximize the volumetric energy density for a given cathode of a rechargeable battery for powering an all-electric road vehicle. Such a battery could also be used for stationary back-up storage of electric power from energy sources other than fossil fuels.

Approach. The project will design, make, and test cells. The approach is to introduce a solid-electrolyte interfacing the anode and a coating on the anode current collector that is wet by a lithium anode. The solid electrolyte should also be wet by the anode to create a bond that is strong enough to constrain the anode volume changes to be perpendicular to the anode/electrolyte interface.

Out-Year Goals. The out-year goal is to develop coin cells that are safe and low-cost with a long cycle life at a voltage $V > 3.0 \text{ V}$ that can compete with the internal combustion engine for powering a road vehicle.

Collaborations. This project collaborates with A. Manthiram at UT Austin and Karim Zaghib at HQ.

Milestones

1. Test the cyclability of plating of metallic lithium through a conventional polymer/ceramic or ceramic Li^+ electrolyte. (Q1, FY 2018; Ongoing)
2. Test relative energies of Cu^+/Cu^0 redox couple and energy of plating/stripping of lithium on/from copper. (Q2, FY 2018)
3. Test plating/stripping of metallic lithium on a carbon-coated copper current collector with different electrolytes. (Q3, FY 2018)
4. Demonstrate a low-cost, 3V cell with a copper current collector as cathode. (Q4, FY 2018)

Progress Report

The project has fabricated and tested ceramic/polymer composite membranes as a solid-state Li^+ conductor to evaluate the effect of ceramic fillers on the ionic conductivity and charge-transfer resistance. Al_2O_3 and $\text{LiZr}_2(\text{PO}_4)_3$ powder (15 wt%) were added to LiTFSI:PEO (1:2 weight ratio) to contrast the ionic conductivity with the different fillers. The composite membranes were fabricated with the solution casting method on a Teflon dish, and the final film had a thickness of ~ 0.2 mm.

First, Li^+ conductivity at 60°C was measured with AC impedance spectroscopy in the blocking electrode configuration. The impedance plot has no semicircle component, which suggests that (i) the charge carriers are ions and (ii) the total conductivity is mainly the Li^+ conductivity. The bulk resistance (R_b) of the membrane was obtained from the Z' -intercept of the low-frequency straight line, and the Li^+ conductivity was calculated. Both the separator membranes have almost identical Li^+ conductivities of ~ 0.3 mS cm^{-1} at 60°C , which indicates that the Li^+ conductivities of the ceramic fillers do not have an immediate impact on the total ionic conductivity.

Second, lithium plating/stripping cycle properties of the membranes were characterized with Li//Li symmetric coin cells. Figure 53 shows the charge/discharge voltage curves of the cells at the 10th cycle and 60°C . The team has studied the voltage drop (iR drop) upon the current switch from charge to discharge to compare the charge-transfer resistances at the membranes/Li interfaces instead of the AC impedance technique. The overpotential occurs owing to the ohmic, charge-transfer, and mass-transport resistances. The initial voltage drop at the extreme beginning of the discharge reflects the ohmic resistance of the cell. In the following discharge at the early stage, the voltage drop owing to the charge-transfer resistance (R_{ct}) dominates. In this analysis, the team has only focused on the iR_{ct} during initial 60 seconds because the iR_i in Figure 53 has complicated contributions from ohmic, charge-transfer, and mass-transport resistances during both charge and discharge. The calculated R_{ct} values are $335.6\ \Omega$ and $165.3\ \Omega$ for the Al_2O_3 - and $\text{LiZr}_2(\text{PO}_4)_3$ -filled LiTFSI:PEO membranes, respectively. Although the measured bulk Li^+ conductivity is almost the same, the interfacial charge transfer resistance is very different. The Li^+ conducting ceramic particles help the interfacial Li^+ transfer not only by increasing the electrochemical surface area, but also by providing Li^+ ions directly to the interface.

Finally, the cycle life in Figure 54 also shows an interesting contrast. The Al_2O_3 -filled sample failed at 57th cycle, but the $\text{LiZr}_2(\text{PO}_4)_3$ -filled sample runs > 440 cycles. Since surface morphology change of the Li-metal electrode during cycling is a critical factor for long-term cycling, the enhanced charge transfer kinetics may have played a key role to stabilize the surface morphology change and the resulting cycle life. The team will monitor evolution of the surface morphology of the lithium metal during cycling in the future.

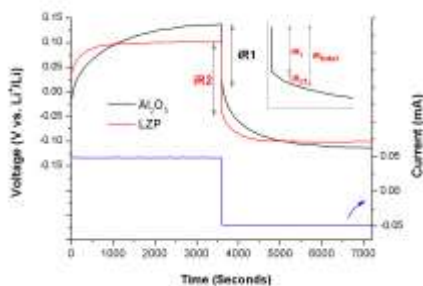


Figure 53. Charge/discharge voltage curves of the Li//Li symmetric cells with the Al_2O_3 - and $\text{LiZr}_2(\text{PO}_4)_3$ -filled LiTFSI:PEO membranes at the 10th cycle and 60°C .

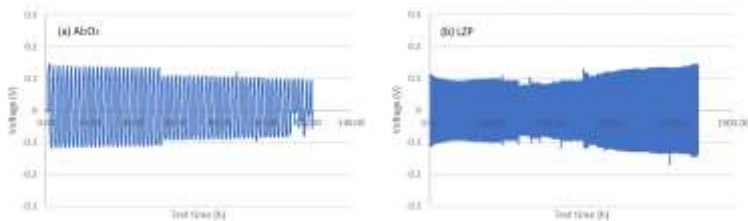


Figure 54. Charge/discharge cycle performance of the Li//Li symmetric cells with the (a) Al_2O_3 - and (b) $\text{LiZr}_2(\text{PO}_4)_3$ -filled LiTFSI:PEO membranes at 60°C .

Task 4.7 – Advancing Solid-State Interfaces in Lithium-Ion Batteries (Nenad M. Markovic and Larry Curtiss, Argonne National Laboratory)

Project Objective. The project objectives are multifaceted, including development of a new mechanically and chemically stable and Li-ion conductive ($\geq 2 \times 10^{-4}$ S/cm at 298 K) solid electrolyte for a solid-state battery encompassing a Li-metal anode, Li-oxide-based cathode, and nonflammable crystalline and amorphous solid electrolytes that can operate at cathode potentials > 5 V (denoted as a S_{Li}-SEL-SC system).

Project Impact. Protective organic and inorganic compounds can enhance stability of the interface, improve Li-ion interfacial transport, minimize dendrite formation, and increase safety in Li-ion batteries.

Approach. The project proposes to develop and use interdisciplinary, atomic-/molecular-level insight obtained from integrating both experimental- and computational-based methodologies to define the landscape of parameters that control interfacial properties for a new generation of the Li-ion solid-solid battery systems. The strategy will involve transferring knowledge gained from well-characterized thin-film materials to real-world materials. This strategy forms a closed loop wherein the knowledge gained from model systems is used to design more complex, real-world materials, and vice versa. The work will focus on utilizing existing in-house synthesis and characterization methods to enable rapid transition from fundamental science to realistic cells.

Out-Year Goals. The out-year goals are to use and develop the physical and chemical synthesis methods for design of solid-solid interfaces with unique chemical/mechanical/conductivity properties. The proposed work will develop and exploit a variety of *ex situ* and *in situ* experimental optical and surface sensitive techniques and electrochemical methods to explore and explain bulk and interfacial properties of the selected materials. The results will serve to unravel many puzzling bulk and interfacial properties of S_{Li}-SEL-SC systems, including various types of ceramic and glass materials.

Collaborations. This project funds work at ANL. It will establish collaboration with Jeff Sakamoto at University of Michigan.

Milestones

1. Development of new synthesis and characterization methods for controlled deposition of lithium on crystalline LLZMO (M = Nb, Ta, Al) materials on the appropriate substrate. (Q1, FY 2018; Completed)
2. Use electrochemical methods to investigate the efficiency as well as charge-discharge cyclability for selected LLZMO materials. (Q2, FY 2018)
3. Development of chemical- and physical-based synthesis method to make amorphous Li₂S-P₂S₅ ($\sim 10^{-3}$ S/cm at room temperature) and LLZMO solid electrolytes with fast ionic transport of lithium and to elucidate the chemical interaction of lithium with such a glass material. (Q3, FY 2018)
4. Introduce new experimental and computational tools for characterizing *ex situ* and *in situ* interaction of lithium and LiCoO₂ with amorphous solid electrolytes. (Q4, FY 2018)

Progress Report

LLZO Thermal Stability. Due to high reactivity of lithium and formation of various types of oxygen/carbon species on the LLZO surface, interfacial impedance can dramatically increase depending on surface chemistry. Consequently, it is critical to understand Li-LLZO interfacial properties with and without these surface layers. An effective way to remove such surface contamination layers is heating the sample to burn off the reaction layer; however, heat treatment can induce formation of secondary phases. To determine the window of structural stability on annealing, the team heated LLZO up to 1173 K in ultra-high vacuum (UHV) using a specially designed chamber at the Advanced Photon Source (APS) at ANL. Using synchrotron X-rays, it was possible to simultaneously monitor, *in situ*, both the structural evolution via X-ray scattering and the surface (5 nm) versus bulk (50 nm) chemistry of LLZO via angle-resolved hard XPS (AR-HAXPES).

Figure 55a shows the X-ray scattering data during heating. From room temperature up to 923 K, the LLZO is in a pure cubic garnet phase, as drawn in blue line. Above 923 K, a lithium deficient $\text{La}_2\text{Zr}_2\text{O}_7$ phase appears, as evidenced by a growing peak at 22.5° due to the loss of lithium and oxygen at high temperature. From the *in situ* XPS spectra, the team monitored surface oxidation states during heating, as shown in Figure 55b-c. Before heating (blue line), the relative intensity of the carbonate peak in the carbon 1s core level is high, indicating that the surface is covered in Li_2CO_3 . In addition to the Li_2CO_3 oxidation layer, the oxygen 1s peak also indicates that there are hydroxyl adsorption species on surface, with a characteristic peak at 530.7 eV that disappears above 353 K. When heated to 773 K, both carbon C 1s and oxygen 1s spectra (red line) show a clean LLZO surface with no carbonate or hydroxide peaks. The valence state of zirconium and lanthanum was unchanged during heating, indicating that chemical environment is not significantly affected by removal of Li_2CO_3 or surface OH.

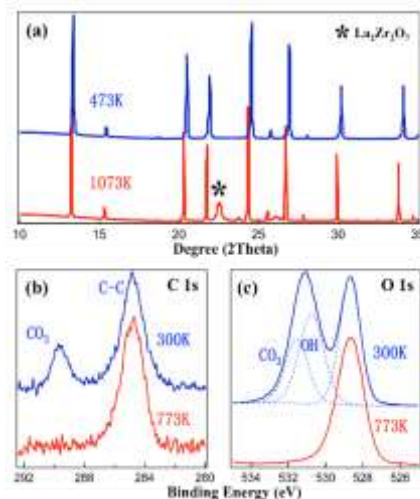


Figure 55. (a) X-ray scattering spectrum of LLZO heated to 473 K and 1073 K, respectively. (b) Carbon 1s and (c) oxygen 1s X-ray photoelectron spectroscopy core level before (blue) and after (red) heating to 773 K to burn off surface contamination species.

LLZO-Li Interface Stability. Niobium, tantalum, and aluminum are commonly used dopants in highly-conductive LLZO electrolytes. To understand the influence of dopant species on the intrinsic stability of the doped LLZO surface in contact with lithium metal, Nb-, Ta- and Al-doped LLZO were first heat treated in UHV at 500°C to completely remove surface contamination layers while still maintaining the pure cubic-garnet phase. Metallic lithium was sputtered on the LLZO after cooling down to room temperature, followed by XPS to characterize the chemistry of the LLZO-Li interface. Figure 56a-b shows significant niobium reduction from 5+ to 4+ (ca. 40%), and mild zirconium reduction from 4+ to 3+, as well (ca. 7.5%). As depicted in Figure 56c, ~10% of the zirconium is reduced to 3+ in the Al-doped LLZO, and ca. 2.5% is further reduced to 2+. Ta-doped LLZO was found to be the most stable surface, with no reduction of tantalum and only a small amount (~3.4%) of zirconium reduction (Figure 56d). The team concludes that the stability of the Li-LLZO interface is strongly dependent on the dopant.

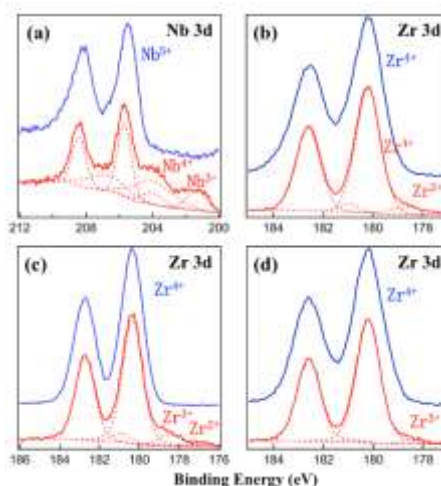


Figure 56. X-ray photoelectron spectroscopy core level spectra before (blue) and after (red) lithium deposition on clean LLZO surface. Reduction of: (a) niobium in Nb:LLZO; (b) zirconium in Nb:LLZO; (c) zirconium in Al:LLZO; and (d) zirconium in Ta:LLZO.

Patents/Publications/Presentations

Publications

- Connell, Justin G., Yisi Zhu, Peter Zapol, Sanja Tepavcevic, Jeff Sakamoto, Larry A. Curtiss, Dillon D. Fong, John W. Freeland, and Nenad M. Markovic. “Crystal Orientation-Dependent Reactivity of Oxide Surfaces in Contact with Lithium Metal.” Under review.
- Zhu, Yisi, Justin G. Connell, Peter Zapol, Sanja Tepavcevic, Jeff Sakamoto, Larry A. Curtiss, Dillon D. Fong, John W. Freeland, and Nenad M. Markovic. “Surface Chemistry and Intrinsic Stability of Doped Lithium Lanthanum Zirconium Oxides.” In preparation.

Task 4.8 – Mechanical and Defect Properties at the Protected Lithium Interface (Nancy Dudney, Oak Ridge National Laboratory; Erik Herbert, Michigan Technological University; Jeff Sakamoto, University of Michigan)

Project Objective. A new objective for this project will be to understand the evolution of lithium metal upon cycling in contact with a generic solid electrolyte under various intrinsic and extrinsic conditions. The team plans to construct a set of stability maps that will describe the predominate mass transport process and defect structure evolution in the lithium metal. Simple maps may address the current density, areal capacity, and layer thickness. Then, maps extending to many other cell designs, interfacial factors, and duty cycle parameters are envisioned. A key activity in FY 2018 will be to develop experimental tools with which to probe the lithium morphology in real time. While initial work will focus on experimental characterization, modeling will be introduced to interpret the kinetic processes and extrapolate for alternative properties and designs and extended cycling.

Project Impact. Stability maps can guide realistic design choices for solid electrolytes and cell design. Ideally, lithium is deposited and removed uniformly to maintain a fully dense anode in good contact with the solid electrolyte. However, in practice, this may not be realized depending on cycling conditions, nature of the electrolyte, nature of the lithium, and cell architecture. Mapping the lithium defect evolution will offer insight for when, how, and why the lithium structure is altered, along with a much deeper analysis of the degradation. With this insight, the team can realistically project the performance of optimized Li-metal anodes. Materials and cells can be engineered to fulfill the target level of performance for EV batteries, namely 1000 cycles, 15-year lifetime, with adequate pulse power.

Approach. For the initial one-year effort, the project will work to develop experimental tools to probe the lithium structure and its interfaces with mechanical, imaging, and electrochemical methods during mass transport and relaxation. Different constructions for the stability maps will be explored to identify the most useful graphical representation of what is expected to be a rich and detailed analysis of the formation and annealing of lattice and extended defects in the lithium metal.

Out-Year Goals. In the out-years, modeling efforts will be integrated to interpret and extrapolate the results to wide cycling conditions and detailed analysis of the solid electrolytes being used to stabilize the lithium metal.

Collaborations. This project funds work at ORNL, MTU, and University of Michigan.

Milestones

1. Characterize *in situ* changes in lithium anode from a single stripping/plating half cycle. (FY 2017; Ongoing)
2. Identify two experimental tools to probe the defect structure of lithium created under cycling. (Q2, FY 2018)
3. Cycle lithium under conditions expected to create different defect structures and morphologies to begin creation of stability maps. (Q3, FY 2018)
4. Design and construct stability diagrams to map the evolution of the defects structure and morphology for lithium metal under a variety of cycling conditions and with different model solid electrolytes. (Q4, FY 2018)

Progress Report

This quarter was devoted to completing studies and manuscripts for publication for both the elastic and plastic properties of lithium metal as studied by nanoindentation, and the adhesion strength of lithium metal with the garnet LLZO solid electrolyte.

Lithium Indentation Studies. As part of the series of manuscripts under revision, the authors have discussed the implication of lithium's mechanical behavior in relation to potential failure mechanisms of solid electrolytes. Some excerpts are below:

The unique mechanical behavior of lithium at small length scales and high homologous temperature is of particular interest because of its potential impact on the performance of energy storage devices. During charging (lithium deposition), gradients in the chemical potential will force lithium to preferentially diffuse into defects at the lithium / solid electrolyte interface. In a manner that depends on the length scale of the defect and the imposed strain rate, for an initially low dislocation density ($\rho \leq 1.1 \times 10^{12} \text{ m}^{-2}$), *lithium can support pressures ranging from ~46 to 350 times higher than the nominal yield strength of bulk polycrystalline lithium.* The highest pressures develop in the smallest interfacial defects exposed to the highest strain rates (coupled to the charging current density).

Grain boundaries, grain boundary grooving, porosity, and scratches in the solid electrolyte (SE) are among the potential small-scale ($\leq 500 \text{ nm}$) defects disrupting the local Li/SE interface morphology. During charging, these defects would become filled with metallic lithium. The team assumes the constraint afforded by the high elastic modulus of the SE separator inhibits volume expansion of the lithium inside the defect and results in a hydrostatic pressure. As the hydrostatically stressed lithium is open to the planar lithium film outside the defect, stress will be relieved by diffusion or dislocation-mediated flow. Some defects at the SE interface may be physically too small to activate glide-controlled dislocation mechanisms such as Frank-Reed sources. Under these conditions, dislocation plasticity will not be an efficient stress relief mechanism, allowing the hoop stress within the interfacial defect to initiate mode I fracture in the SE. Diffusional creep would also be expected to relieve stress. When the diffusion distance through the planar lithium is much greater than the interface defect, pressure grows with higher currents.

Li/LLZO Interface Studies. In other mechanics testing, the team used a precision Instron housed in an inert glove box to assess the Li/LLZO interface. Results of the lap shear and tensile adhesive strength show that the adhesive strength of interfaces associated with low interfacial resistance exceed the yield strength of the lithium metal itself.

There is a clear correlation between the area specific ionic resistance and the tensile adhesive strength of the Li/LLZO interface, as shown in Figure 57. The tensile strength was determined as Li/LLZO/Li cells were pulled in tension. Analysis of the fracture surfaces showed that at high ASRs, there is a clean separation of the lithium from the LLZO surface, leaving behind negligible lithium residue. In contrast, at the lowest ASRs reported, the *adhesive strength of the Li/LLZO interface exceeds the tensile strength of the lithium metal.* To support these results, the tensile strength of lithium foil was measured to be $\sim 8 \text{ MPa}$, which is the maximum interface strength observed in Li/LLZO/Li stacks (red-dashed line in Figure 57). The fact that the strength of the interface is stronger than the lithium metal itself at low ASRs suggests that there is good surface chemistry and wettability of lithium on LLZO. From these studies, it can be concluded that both the adhesive strength and ASR of the interface are governed by the surface chemistry and wettability of the LLZO surface.

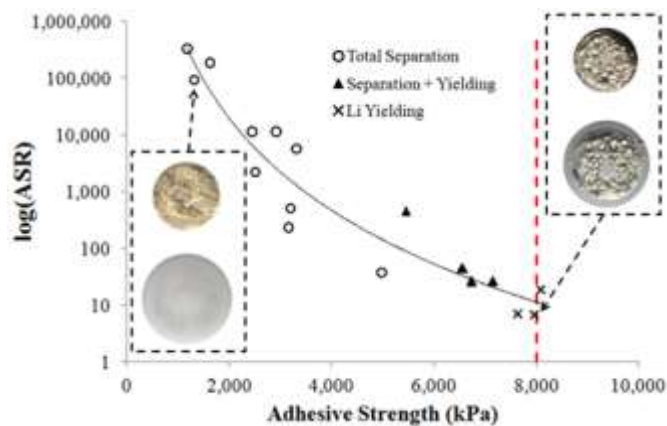


Figure 57. Area specific resistance as a function of the adhesion strength of the Li-LLZO interface. Optical microscope images show the fracture surface of the lithium and LLZO disks at low and high area specific ionic resistance. The red dashed line indicates the measured tensile strength of lithium metal.

Patents/Publications/Presentations

Publications

- Herbert, E. G., P. S. Phani, N. J. Dudney, and S. A. Hackney. “Nanoindentation of High Purity Vapor Deposited Lithium Films: The Elastic Modulus.” Reviewed; under revision.
- Herbert, E. G., S. A. Hackney, N. J. Dudney, V. Thole, and P. S. Phani. “Nanoindentation of High Purity Vapor Deposited Lithium Films: A Mechanistic Rationalization of Diffusion-Mediated Flow.” Reviewed; under revision.
- Herbert, E. G., S. A. Hackney, N. J. Dudney, V. Thole, and P. S. Phani. “Nanoindentation of High Purity Vapor Deposited Lithium Films: A Mechanistic Rationalization of the Transition to Dislocation-Mediated Flow.” Reviewed; under revision.
- Wang, M., and J. Sakamoto. “Correlating the Interface Resistance and Surface Adhesion of the Li Metal-Solid Electrolyte Interface.” *Journal of Power Sources* 377 (2018): 7–11.

TASK 5 –SULFUR ELECTRODES

Summary and Highlights

Advances in Li-ion technology have been stymied by challenges involved in developing high reversible capacity cathodes and stable anodes. Hence, there is a critical need for development of alternate battery technologies with superior energy densities and cycling capabilities. In this regard, Li-S batteries have been identified as the next flagship technology, holding much promise due to the attractive theoretical specific energy densities of 2,567 Wh/kg. In addition, realization of the high theoretical specific capacity of 1,675 mAh/g corresponding to formation of Li_2S using earth-abundant sulfur renders the system highly promising compared to other available cathode systems. Thus, the research focus has shifted to developing Li-S batteries. This system, however, suffers from major drawbacks, as elucidated below:

- Limited inherent electronic conductivity of sulfur-based and sulfur-compound-based cathodes;
- Volumetric expansion and contraction of both the sulfur cathode and lithium anode;
- Soluble polysulfide formation/dissolution and sluggish kinetics of subsequent conversion of polysulfides to Li_2S , resulting in poor cycling life;
- Particle fracture and delamination resulting from the repeated volumetric expansion and contraction;
- Irreversible loss of lithium at the sulfur cathode, resulting in poor CE; and
- High diffusivity of polysulfides in the electrolyte, resulting in plating at the anode and consequent loss of driving force for lithium diffusion (that is, drop in cell voltage).

These major issues cause sulfur loss from the cathode, leading to mechanical disintegration. Additionally, surface passivation of anode and cathode systems results in a decrease in the overall specific capacity and CE upon cycling. Consequently, the battery becomes inactive within the first few charge-discharge cycles. Achievement of stable, high capacity Li-S batteries requires execution of fundamental studies to understand the degradation mechanisms in conjunction with devising engineered solutions.

This Task addresses both aspects with execution of esoteric, fundamental *in situ* XAS and *in situ* electron paramagnetic resonance (EPR) studies juxtaposed with conducting innovative applied research comprising use of suitable additives, coatings, and exploration of composite morphologies as well as appropriate engineered strategies. Both ANL and LBNL use X-ray based techniques to study phase evolution and loss of CE in S-based and S-Se-based electrodes, primarily by the former during lithiation/delithiation while understanding polysulfide formation in sulfur and oligomeric PEO solvent by the latter, respectively. Work from PNNL, U Pitt, and Stanford demonstrates high areal capacity electrodes exceeding 4 mAh/cm². Following loading studies reported this quarter, PNNL performed *in situ* EPR to study reaction pathways mediated by sulfur radical formation. Coating/encapsulation approaches adopted by U Pitt and Stanford comprise flexible sulfur wire electrodes coated with LIC by U Pitt, and TiS_2 encapsulation of Li_2S in the latter, both ensuring polysulfide retention at sulfur cathodes. BNL work, on the other hand, has focused on benchmarking of pouch-cell testing by optimization of the voltage window and study of additives such as LiI and LiNO_3 . *Ab initio* studies at Stanford and U Pitt involve calculation of binding energies, diffusion coefficients, ionic conductivities, and reaction pathways determination, augmenting the experimental results. Similarly, AIMD simulations performed at TAMU reveal multiple details regarding electrolyte decomposition reactions and the role of soluble polysulfides on such reactions. Using KMC simulations, electrode morphology evolution and mesostructured transport interaction studies were also executed. Studies over the last quarter at PNNL suggest that proper control of electrode porosity/thickness is essential for obtaining high-energy Li-S batteries.

Porosity shows strong dependence on calendering pressure because of low tap densities of electrode components such as sulfur and carbon. Increasing the calendering-pressure from 0.2 to 1.5 ton (T) leads to rapid decrease of electrode porosity, resulting in improvement of electrode volumetric energy density.

Measured electrode volumetric energy density increased from 650 Wh L⁻¹ for as-cast electrode (120- μ m thick) to 1300 Wh L⁻¹ for electrode compressed to 60 μ m. Additionally, Pennsylvania State University has shown use of dimethyl disulfide as a functional co-solvent, demonstrating its ability to show an alternate electrochemical reaction pathway for sulfur cathodes by formation of dimethyl polysulfides and lithium organosulfides as intermediates and reduction products. Further, University of Wisconsin has conducted high-performance liquid chromatography (HPLC)-MS studies and has determined the distribution of polysulfides at various discharge and recharge reactions. UT Austin, at the same time, has shown that by integrating polysulfide-filter-coated separators fabricated with CNF, the cells retain 50% of the initial capacity after storing for one year and exhibit a low self-discharge rate of only 0.14% per day.

Each of these projects has a collaborative team of experts with the required skill set needed to address the EV Everywhere Grand Challenge of 350 Wh/kg and 750 Wh/l and cycle life of at least 1000 cycles.

Highlights. This Task reports the following project highlights for this quarter:

- Classical reactive MD simulations were used by Dr. Perla Balbuena (TAMU) to evaluate novel sulfur/graphene architectures that emulate the electrochemical behavior of the Li-S battery cathode. The sulfur/graphene model proposed in the work provides new understanding of the graphene effects on the sulfur reduction behavior and the role that van der Waals interactions may play in favoring sulfur reduction reactions and enhanced polysulfide trapping.
- Dr. Arumugam Manthiram (UT Austin) used a coating of a ceramic-polymer composite on anode and cathode sides of a commercial Celgard 2500 separator as an excellent artificial SEI with low resistance and high flexibility, which enabled a uniform Li-ion flux on the anode surface.
- Dr. Donghai Wang (Pennsylvania State University) has used (poly (sulfur-random-1, 3-diisopropenyl-benzene (PSD) as an electrolyte additive to facilitate stable SEI layer formation. This additive demonstrates best performance and cycling stability.

Task 5.1 – Novel Chemistry: Lithium Selenium and Selenium Sulfur Couple (Khalil Amine, Argonne National Laboratory)

Project Objective. The project objective is to develop a novel S_xSe_y cathode material for rechargeable lithium batteries with high energy density and long life, as well as low cost and high safety.

Project Impact. Development of a new battery chemistry is promising to support the goal of PHEV and EV applications.

Approach. The dissolution of lithium polysulfides in nonaqueous electrolytes has been the major contribution to the low energy efficiency and short life of Li-S batteries. In addition, the insulating characteristics of both end members during charge/discharge (S and Li_2S) limit their rate capacity. To overcome this problem, sulfur or Li_2S are generally impregnated in a carbon-conducting matrix for better electronic conductivity. However, this makes it difficult to increase the loading density of practical electrodes. It is proposed here to solve the above barriers using the following approaches: (1) partially replace S with Se, (2) nano-confine the S_xSe_y in a nano-porous conductive matrix, and (3) explore advanced electrolytes with suppressed shuttle effect.

Out-Year Goals. This new cathode will be optimized with the following goals:

- A cell with nominal voltage of 2 V and energy density of 600 Wh/kg.
- A battery capable of operating for 500 cycles with low capacity fade.

Collaborations. This project engages in collaboration with the following: Professor Chunsheng Wang of UMD, Dr. Yang Ren and Dr. Chengjun Sun of APS at ANL, and Dr. Larry Curtiss at ANL.

Milestones

1. Exploration of novel Siloxane-based electrolytes for Li-Se and Se-S systems. (Q1, FY 2018; Completed)
2. Development of high-performance Li/Se-S batteries using optimized Siloxane-based electrolytes. (Q2, FY 2018)
3. *In operando* XAS study on the working mechanism of Siloxane-based electrolytes. (Q3, FY 2018)
4. Computational modeling on the working mechanism of Siloxane-based electrolytes. (Q4, FY 2018)

Progress Report

This quarter, the team further worked on the optimization of Siloxane-based electrolytes for Li-Se and Se-S systems to achieve high reversible capacity and good cycle stability. The team has evaluated the effect of lithium salt concentration and additional cosolvents such as dioxolane (DOL) and dimethoxyethane (DME) on the electrochemical performance of Li/Se-S battery.

High-concentration electrolytes have recently attracted increased attention in the application of rechargeable batteries due to unique properties such as increased reductive stability, enhanced oxidative stability, and low solvent volatility. High-concentration electrolytes can also decrease the amount of free solvent in the electrolyte to solvate with polysulfides and thus decrease the dissolution. Hence, the team has prepared an electrolyte composed of 3M LiTFSI/ANL-2.

As shown in Figure 58, compared to the low-concentration LiTFSI/ANL-2, the polysulfides/polyselenides shuttle effect was significantly suppressed; however, the team can see that capacity fading and voltage polarization are both deteriorated. This could be due to the decreased ionic conductivity and increased viscosity of high-concentration electrolytes, which will inhibit the diffusion of lithium ions and thus decrease the electrochemical reactivity.

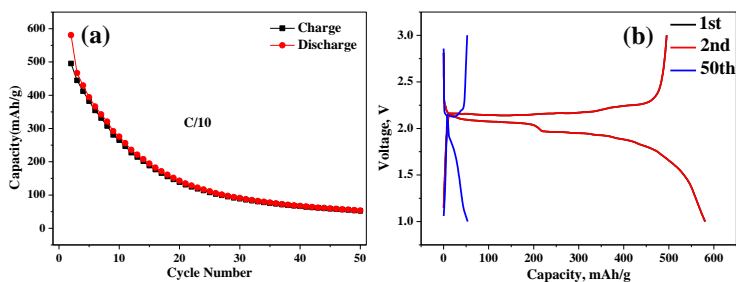


Figure 58. (a) Cycle performance and (b) charge/discharge voltage profiles of Li/Se-S battery with 45 wt% Se-S loading in 3M LiTFSI/ANL-2 at C/10.

Therefore, the team has further studied the effect of additional cosolvents with higher solvation capability with lithium species to partially dilute the electrolytes to balance the polysulfides dissolution and lithium ionic conductivity. Figure 59a shows that after the addition of DME in the electrolyte, the cell delivers high reversible capacity up to 900 mAh/g. However, a rapid capacity fade after the initial 5 cycles was observed. In the case of 5M LiTFSI/DOL+ANL-2 (Figure 59), the reversible capacity is increased to 1200 mAh/. The cell retained about 800 mAh/g after 50 cycles at C/10 rate, showing much improved electrochemical performance. Moreover, the charge/discharge capacities during cycling are almost overlapped, indicating there is no shuttle effect. The team has prepared another electrolyte, which is based on DOL and DME that are the mostly used solvents for Li-S batteries. Compared to 5M LiTFSI/DOL+DME, the team can see that the DOL/ANL-2 based electrolyte showed much higher reversible capacities within 50 cycles. These results demonstrated the advantages of siloxane-based solvents as electrolytes for Li-Se and Se-S systems.

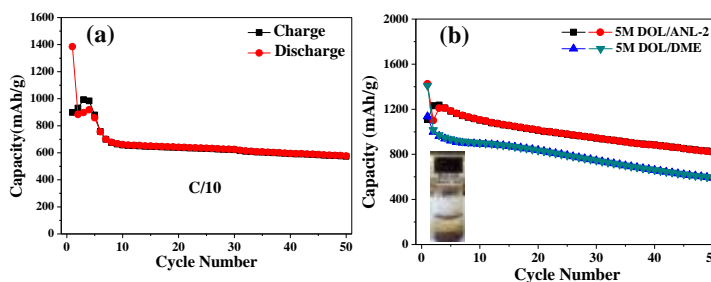


Figure 59. Cycle performance of Li/Se-S battery with 45 wt% Se-S loading in (a) 5M LiTFSI/DME+ANL-2, (b) 5M LiTFSI/DOL+DME and (c) 5M LiTFSI/DOL+ANL-2 at C/10.

Next quarter, the team will work on the rational design of cathode structures and electrolytes to achieve better electrochemical performance for high-loading Se-S systems.

Patents/Publications/Presentations

Patent

- Xu, Guiliang, Zonghai Chen, Jianzhao Liu, and Khalil Amine. US. Patent Application No. 15/760,295. Pending.

Task 5.2 – Development of High-Energy Lithium-Sulfur Batteries (Jun Liu and Dongping Lu, Pacific Northwest National Laboratory)

Project Objective. The project objective is to develop high-energy, low-cost Li-S batteries with long lifespan. All proposed work will employ thick sulfur cathode (≥ 2 mAh/cm² of sulfur) at a relevant scale for practical applications. The diffusion process of soluble polysulfide out of thick cathode will be revisited to investigate cell failure mechanism at different cycling. Alternative anode will be explored to address the lithium anode issue. The fundamental reaction mechanism of polysulfide under the electrical field will be explored by applying advanced characterization techniques to accelerate development of Li-S battery technology.

Project Impact. The theoretical specific energy of Li-S batteries is ~ 2300 Wh/kg, which is almost three times higher than that of state-of-the-art Li-ion batteries. The major challenge for Li-S batteries is polysulfide shuttle reactions, which initiate a series of chain reactions that significantly shorten battery life. The proposed work will design novel approaches to enable Li-S battery technology and accelerate market acceptance of long-range EVs required by the EV Everywhere Grand Challenge.

Out-Year Goals. This project has the following out-year goals:

- Fabricate Li-S pouch cells with thick electrodes to understand sulfur chemistry/electrochemistry in the environments similar to real application.
- Leverage the Li-metal protection project funded by the DOE and PNNL advanced characterization facilities to accelerate development of Li-S battery technology.
- Develop Li-S batteries with a specific energy of 400 Wh/kg at cell level, 1000 deep-discharge cycles, improved abuse tolerance, and less than 20% capacity fade over a 10-year period to accelerate commercialization of electrical vehicles.

Collaborations. This project engages in collaboration with the following:

- Dr. Xiao-Qing Yang (LBNL) – *In situ* characterization,
- Dr. Deyang Qu (University of Wisconsin at Milwaukee) – Electrolyte analysis,
- Dr. Xingcheng Xiao (GM) – Materials testing, and
- Dr. Jim De Yoreo (PNNL) – *In situ* characterization.

Milestones

1. Study of electrolyte compatibility with different carbon host materials and binders and their effects on reversible sulfur utilization. (Q1, December 31, 2017; Completed)
2. Design and demonstration of an electrochemical cell by using ceramics Li⁺ conductive separator for focused cathode or anode mechanism study for Li-S. (Q2, March 31, 2018; In progress)
3. Study failure mechanism of Li-S cell under lean amount of liquid electrolyte by decoupling the interference of lithium anode using liquid/solid electrolyte hybrid cell. (Q3, June 30, 2018; In progress)
4. Develop functionalized separators to suppress polysulfide shuttle and improve interfacial stability of lithium anode. (Q4, September 30, 2018; In progress)

Progress Report

It is a challenge to improve rate capability and sulfur utilization of high-loading sulfur cathodes because of electrode wetting and electrolyte mass transfer issues. This is exacerbated when reducing electrode porosity for high energy density. The electrode wetting process comprises electrolyte diffusion through the voids in between the secondary particles and also infiltration into the internal part of individual particles. The latter process is more sluggish than the former because of higher tortuosity inside the particles. Binder coats the electrode components and stabilizes electrode architectures, but it may also negatively affect electrolyte penetration. This quarter, the team studied impacts of solution- and emulsion-based binders on electrode active area, electrolyte penetration, and sulfur utilization rate in high-loading electrodes.

Integrated Ketjen Black (IKB) and CNF, used as sulfur host and electronic conductor, respectively, were mixed with 10 wt% of different binders as target electrode. The project took polyarylamide (PAA) and polytetrafluoroethylene (PTFE) as examples of solution- and emulsion-based binders, respectively. It was found that both solution and emulsion binders have significant coating effects on the IKB/CNF carbon materials. As shown in Figure 60a, the Brunauer–Emmett–Teller (BET) surface area of IKB/CNF decreases significantly, from the original 650 m²/g to 195 m²/g with PTFE binder, and further reduces to only 107 m²/g with PAA. The pore volume of IKB/CNF follows the same trend and decreases from 2.01 cc/g (no binder) to 1.05 and 0.8 cc/g using a binder of PTFE and of PAA, respectively. In both cases, micropores are completely filled or blocked.

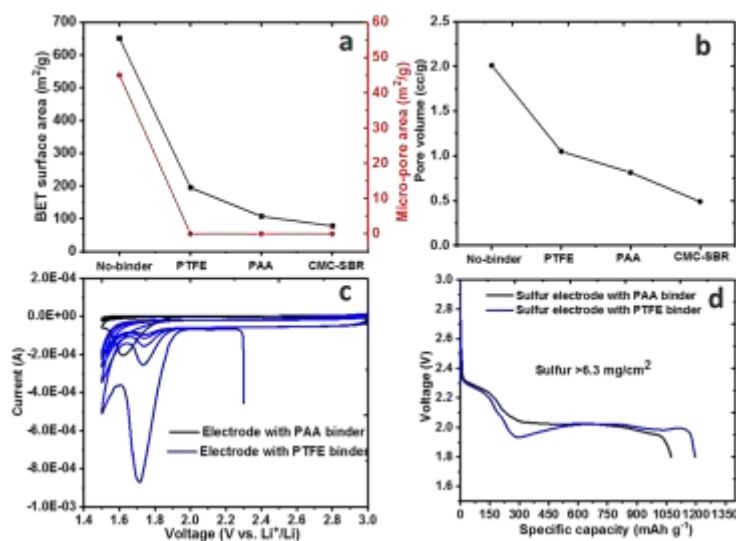


Figure 60. (a) Comparison of Brunauer–Emmett–Teller surface areas of pristine Integrated Ketjen Black / carbon nanofiber (IKB/CNF) carbon materials and after mixed with 10 wt% of different binders and (b) corresponding pore volume. (c) Cyclic voltammetry of IKB/CNF electrodes with polyarylamide and polytetrafluoroethylene (PAA and PTFE) binders (1.5–3.0 V, 0.05 mV/s), and (d) first discharge curves of sulfur electrodes with PAA and PTFE binders (sulfur loading > 6.3 mg/cm², E/S=4 µL /mg, 0.05C).

the electrode. But, for the electrode comprised of PTFE binder, the reduction peak is much higher (0.85 mA) in the first scan and reduces gradually in subsequent scans, indicating more extensive reaction but slower electrode passivation. This is consistent with results of both BET surface and pore volume analysis. Figure 60d compares sulfur utilization rate of high-loading sulfur electrodes (> 6.3 mg/cm²) with those two binders. The sulfur electrode with PAA binder exhibits a discharge capacity of 1073 mAh/g, while the PTFE-based electrode shows a much higher capacity of 1196 mAh/g. This is attributed to the noted coating effects of different binders. This study suggests that a rational electrode architecture design taking advantage of both solution- and emulsion-based binders should be considered for high-loading sulfur cathodes.

Patents/Publications/Presentations

Publication

- Wang, Y., D. Lu, M. Bowden, P. Z. El Khoury, K. S. Han, Z. D. Deng, et al. “Formation Mechanism of $\text{Li}_7\text{P}_3\text{S}_{11}$ Solid Electrolytes through Liquid Phase Synthesis.” *Chemistry of Materials* (2018). doi: 10.1021/acs.chemmater.7b04842.

Task 5.3 – Nanostructured Design of Sulfur Cathodes for High-Energy Lithium-Sulfur Batteries (Yi Cui, Stanford University)

Project Objective. The charge capacity limitations of conventional TM oxide cathodes are overcome by designing optimized nano-architected sulfur cathodes. This study aims to enable sulfur cathodes with high capacity and long cycle life by developing sulfur cathodes from the perspective of nanostructured materials design, which will be used to combine with Li-metal anodes to generate high-energy Li-S batteries. Novel sulfur nanostructures as well as multi-functional coatings will be designed and fabricated to overcome issues related to volume expansion, polysulfide dissolution, and the insulating nature of sulfur.

Project Impact. The capacity and the cycling stability of sulfur cathode will be dramatically increased. This project's success will make Li-S batteries to power EVs and decrease the high cost of batteries.

Out-Year Goals. The cycle life, capacity retention, and capacity loading of sulfur cathodes will be greatly improved (200 cycles with 80% capacity retention, $> 0.3 \text{ mAh/cm}^2$ capacity loading) by optimizing material design, synthesis, and electrode assembly.

Collaborations. This project engages in collaboration with the following:

- BMR PIs,
- SLAC National Accelerator Laboratory: *In situ* X-ray, Dr. Michael Toney, and
- Stanford: Professor Nix, mechanics; and Professor Bao, materials.

Milestones

1. Demonstrate the catalytic effect of Li_2S_x species on metal sulfides, enabling good performance of Li-S batteries. (FY 2017, April 2017; Completed)
2. Establish a standard procedure to quantitatively compare the polysulfide adsorption capability of candidate materials. (FY 2017, July 2017; Completed)
3. Quantitatively approximate the polysulfide adsorption amount of candidate materials. (Q1, FY 2018, October 2017; Completed)
4. Elucidate different adsorption mechanisms and probe possible adsorption species. (Q2, FY 2018, January 2018; Completed)
5. Develop multi-functional sulfur cathode binder capable of controlling the polysulfide shuttling and facilitating Li-ion transport. (Q3, FY 2018, April 2018; Ongoing)
6. Demonstrate the flame-retardant property of binder to improve safety and propose flame-retardant mechanism. (Q4, FY 2018, July 2018; On schedule)
7. Build *in situ* characterization platform to monitor nucleation/dissolution of sulfur/ Li_2Sn . (Q1, FY 2019, October 2018; On schedule)

Progress Report

Last quarter, the team quantitatively approximated the polysulfide adsorption capabilities employing the Beer-Lambert law. This quarter's report elucidates different adsorption mechanisms and probes possible adsorption of sulfide species. The team expects this work to provide a useful strategy to screen for suitable candidate materials and valuable information for rational design of long cycle life Li-S batteries.

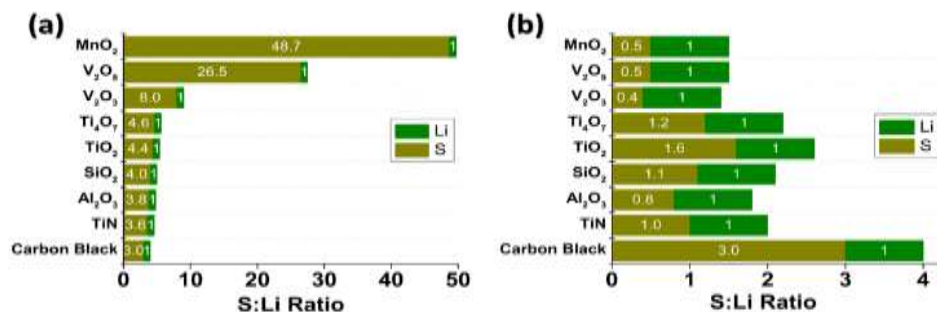


Figure 61. Inductively coupled plasma – atomic emission spectroscopy data of sulfur-to-lithium atoms concentration ratio (a) remaining in supernatant solutions and (b) adsorbed onto candidate materials, after 3-mM Li₂S₆ adsorption test.

It is commonly assumed that the Li₂S₆ species stays intact and is the adsorbed species. This may not be true, as the adsorbed species could be a mixture of different species, for example, Li₂S₄ and Li₂S₂. Different candidate materials can have different preferences and mechanisms for the species adsorbed. Figure 61a illustrates the sulfur-to-lithium content ratio of the supernatant solutions after Li₂S₆ adsorption tests. Based on the sulfur-to-lithium content, speculations can be made about the species present. A sulfur-to-lithium ratio of 3 corresponds with the original introduced species Li₂S₆, a ratio of 4 implies possible formation of the species Li₂S₈, while even higher ratios may suggest a mixture of S₈ and lithium polysulfide species such as Li₂S₆ and Li₂S₈. Figure 61b illustrates the calculated sulfur-to-lithium content ratio of the adsorbed species based on ICP-AES data. For carbon black, a S:Li ratio of 3 for both the remaining supernatant solution and the adsorbed species suggests that Li₂S₆ may be the adsorbed species. For Al₂O₃, SiO₂, TiN, TiO₂, and Ti₄O₇, a S:Li ratio of higher than 3 remaining in the supernatant solution suggests relatively more sulfur is left behind than lithium; thus, the adsorbed species should have a lower S:Li ratio than 3. This may correspond to a S:Li ratio of 2 for Li₂S₄, a ratio of 1 for Li₂S₂, and a ratio of 0.5 for Li₂S. For MnO₂, V₂O₅, and V₂O₃, S:Li ratios of much higher than 3 remain in the supernatant solution, suggesting the adsorbed species would proportionally have higher lithium than the original Li₂S₆ species, and thus S:Li ratios much lower than 3. Therefore, it can be seen that the candidate materials can have different preferences for the proportional amount of sulfur and lithium adsorbed. In general, stronger candidate materials seem to adsorb relatively more lithium than sulfur, compared to weaker candidate materials. This is particularly evident in MnO₂, V₂O₅, and V₂O₃. The trend is also consistent in metal sulfides, with TiS₂, FeS, and MoS₂ also exhibiting much higher preferences for lithium; however, the S:Li ratios are not reported here because the metal sulfides themselves are a source of

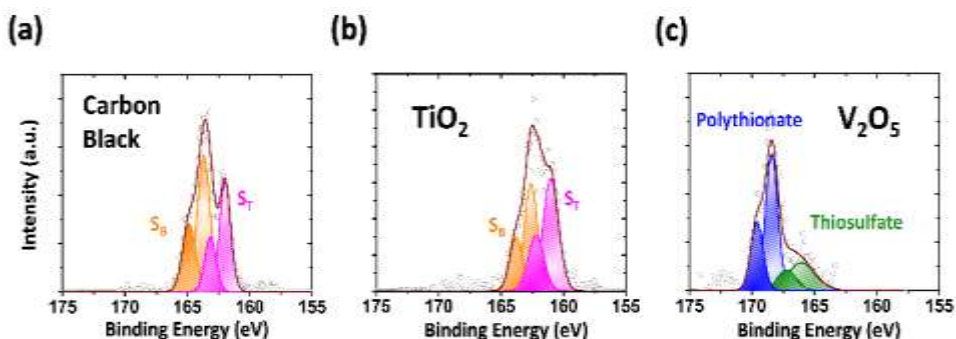


Figure 62. X-ray photoelectron spectroscopy sulfur 2p spectra of candidate materials surface after Li₂S₆ adsorption test for (a) carbon black, (b) TiO₂, and (c) V₂O₅.

sulfur atoms. Thus, any powder particles that are suspended in supernatant solutions would severely undermine the validity of the S:Li ratio data for speculations of species adsorbed. It should also be noted that these ratios give the overall proportions of sulfur and lithium atoms, but do not provide information about the particular species present.

To further probe the interaction of candidate materials with polysulfides, XPS studies are performed on the surface of candidate materials after adsorption tests. These give insight of the species adsorbed, and Figure 62 depicts a few representative cases. In the case of weak to moderate adsorption materials such as carbon black and TiO₂, polysulfides are the predominantly observed species for sulfur 2p spectra, exhibiting “bridging” (S_B, 163.1 eV) sulfur and “terminal” (S_T, 161.7 eV) sulfur. This agrees with previous ICP-AES speculations that polysulfide species are adsorbed. For strong adsorption materials such as V₂O₅, polythionate (168.2 eV) and thiosulfate (167.2 eV) species are observed. This is also in agreement with published reports.

Patents/Publications/Presentations

Publication

- Wu, David, Feifei Shi, Guangmin Zhou, Chenxi Zu, Chong Liu, Kai Liu, Yayuan Liu, Jiangyan Wang, Yucan Peng, and Yi Cui. “Quantitative Investigation of Polysulfide Adsorption Capability of Candidate Materials for Li-S Batteries.” Under revision.

Task 5.4 – Addressing Internal “Shuttle” Effect: Electrolyte Design and Cathode Morphology Evolution in Lithium-Sulfur Batteries (Perla Balbuena, Texas A&M University)

Project Objective. The project objective is to overcome the Li-metal anode deterioration issues through advanced Li-anode protection/stabilization strategies including (1) *in situ* chemical formation of a protective passivation layer and (2) alleviation of the “aggressiveness” of the environment at the anode by minimizing the polysulfide shuttle with advanced cathode structure design.

Project Impact. Through formulation of alternative electrolyte chemistries as well as design, fabrication, and test of improved cathode architectures, it is expected that this project will deliver Li/S cells operating for 500 cycles at efficiency greater than 80%.

Approach. A mesoscale model including different realizations of electrode mesoporous structures generated based on a stochastic reconstruction method will allow virtual screening of the cathode microstructural features and the corresponding effects on electronic/ionic conductivity and morphological evolution. Interfacial reactions at the anode due to the presence of polysulfide species will be characterized with *ab initio* methods. For the cathode interfacial reactions, data and detailed structural and energetic information obtained from atomistic-level studies will be used in a mesoscopic-level analysis. A novel sonochemical fabrication method is expected to generate controlled cathode mesoporous structures that will be tested along with new electrolyte formulations based on the knowledge gained from the mesoscale and atomistic modeling efforts.

Out-Year Goals. By determining reasons for successes or failures of specific electrolyte chemistries, and assessing relative effects of composite cathode microstructure and internal shuttle chemistry versus that of electrolyte chemistry on cell performance, expected results are as follows: (1) develop an improved understanding of the Li-S chemistry and ways to control it, (2) develop electrolyte formulations able to stabilize the lithium anode, (3) develop new composite cathode microstructures with enhanced cathode performance, and (4) develop a Li-S cell operating for 500 cycles at an efficiency greater than 80%.

Collaborations. This is a collaborative work combining first-principles modeling (Perla Balbuena, TAMU), mesoscopic level modeling (Partha Mukherjee, TAMU), and synthesis, fabrication, and test of Li/S materials and cells (Vilas Pol, Purdue University). Balbuena also collaborates with M. Vijayakumar from PNNL.

Milestones

1. Elucidate concentrated solution effects in Li-S battery electrolyte transport.
2. Investigate effects of carbon-sulfur morphology on cathode electrochemical performance.

Progress Report

Elucidating Concentrated Solution Effects in Li-S Battery Electrolyte Transport. The electrolyte in a Li-S system is a continuously evolving system, given the successive reduction of sulfur during discharge (or oxidation during charge). This leads to a coexistence of multiple species, and the presence of each species influences the transport of the rest. Such coupled interactions are modeled here using a concentrated solution theory. A distinguishing feature of such involved interactions is the decline in ionic conductivity at high enough ion concentrations. For the Li-S, the ionic concentration is highest when high-order polysulfides (PS) nearly completely convert to medium chain PS (shorter chain PS precipitate almost instantaneously, thus limiting their concentration), which takes place around the transition from an upper voltage to a lower voltage plateau. This sudden decrease in ionic conductivity reflects on increased overpotential and correspondingly a dip joining the two plateaus (Figure 63a). When evolution of different cell resistances is plotted (Figure 63b), it is revealed that the electrolyte phase resistance (transport and concentration) is most dominant during this transitional portion, while microstructural resistances (passivation and blockage) are most influential during voltage plateaus.

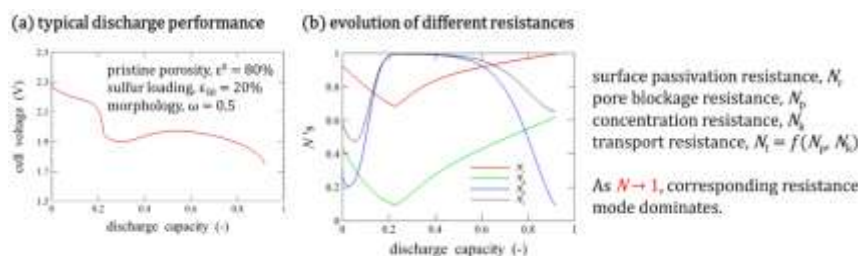


Figure 63. (a) Effects of porosity, sulfur loading, and morphology on cell performance. (b) Evolution of different resistance modes during discharge. As the resistance value goes to 1, the mode becomes dominant.

Effects of Carbon-Sulfur Morphology on Cathode Electrochemical Performance. Classical reactive MD simulations were used to evaluate novel sulfur/graphene architectures that emulate the electrochemical behavior of the Li-S battery cathode, promoting S-C interaction through the edges of graphene sheets. A random mixture of 8-membered sulfur rings and small graphene sheets was simulated at 64 wt% sulfur loading. Structural stabilization and sulfur reduction calculations are performed with classical reactive MD. This methodology allowed accounting for the collective behavior of the sulfur and graphene structures. The sulfur encapsulation induces ring opening, and the sulfur phase evolves into a distribution of small chain-like structures interacting with carbon through the graphene edges. This new arrangement of the sulfur phase not only leads to less pronounced volume expansion during sulfur reduction, but also to a different discharge voltage profile, in qualitative agreement with earlier reports on sulfur encapsulation in microporous carbon structures.

The Li_2S phase was found to grow around ensembles of parallel graphene sheets during sulfur reduction. No diffusion of sulfur or lithium between graphene sheets was observed, and extended Li_2S domains bridging the space between carbon ensembles were suppressed. The results emphasize the importance of morphology on the electrochemical performance of the composite material. The sulfur/graphene model outlined here provides new understanding of the graphene effects on sulfur reduction behavior and the role that van der Waals interactions may play in favoring sulfur reduction reactions and enhanced polysulfide trapping.

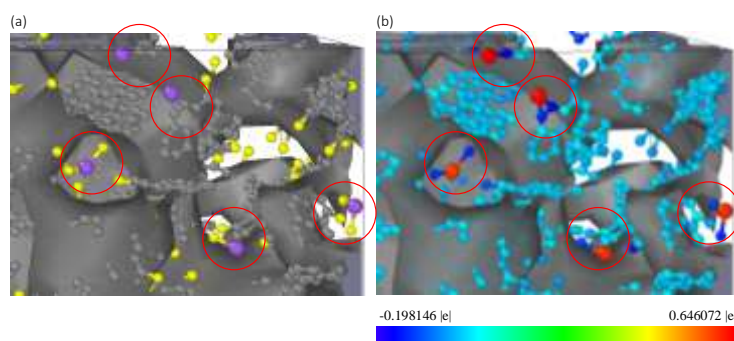


Figure 64. (a) Lithium-sulfur bonding and lithium-carbon interaction at low lithium contents. (b) Electronic charge distribution at low lithium contents. Color code: carbon, grey; sulfur, yellow; and lithium, purple. In part (b) atoms are colored according to their electrostatic charge shown in the color bar.

Patents/Publications/Presentations

Publications

- Mistry, Aashutosh, and Partha P. Mukherjee. “Precipitation – Microstructure Interactions in the Li-S Battery Electrode.” *Journal of Physical Chemistry C* 121 (2017): 26256–26264.
- Beltran, Saul Perez, and Perla B. Balbuena. “Formation of Multi-Layer Graphene Domains with Strong Sulfur-Carbon Interaction and Enhanced Sulfur Reduction Zones for Lithium-Sulfur Battery Cathodes.” Under review.
- Liu, Zhixiao, Huiqiu Deng, Wangyu Hu, Fei Gao, Shiguo Zhang, Perla B. Balbuena, and Partha P. Mukherjee. “Revealing Reaction Mechanisms of Nanoconfined Li₂S: Implications for Lithium-Sulfur Batteries.” Under review.

Presentations

- University of Houston, Houston, Texas (October 4, 2017): “Analysis and Design of Materials for Advanced Batteries”; Perla B. Balbuena.
- University of Picardie, France (December 15, 2017): “Analysis and Design of Materials for Advanced Batteries”; Perla B. Balbuena.

Task 5.5 – Investigation of Sulfur Reaction Mechanisms (Deyang Qu, University of Wisconsin Milwaukee; Xiao-Qing Yang, Brookhaven National Laboratory)

Project Objective. The primary objectives are (1) to conduct focused fundamental research on the mechanism of “shuttle effect” inhibition for the rechargeable Li-S batteries, and (2) to develop the electrode and electrolyte systems that can mitigate the “shuttle effect” so the low self-discharge and long cycle life can be achieved. Special attention will be paid to the following: investigating chemical interactions between the additives and dissolved polysulfides, management for solubility of polysulfide ions, formation of SEI layer and dead lithium on the surface of lithium anode, and exploration of electrode and cell designs. Through such investigations, the Li-S chemistry will be studied systematically, and the scientific understanding of the inhibition mechanism for “shuttle effect” can be well utilized to guide system engineering design. The ultimate goal for the project is to develop a practical rechargeable Li-S battery to meet the challenges of powering the next-generation EVs beyond Li-ion technologies.

Project Impact. With the unique *in situ* electrochemical-HPLC/MS technique developed in this program, the mechanisms of all reactions in a Li-S cell can be revealed. The interactions between additives and the soluble polysulfides can be investigated real-time toward mitigation of “shuttle effect.” The results will guide development of sulfur cathode and Li-S designs for EVs.

Approach. This project will use *in situ* electrochemical-MS, electrochemical-HPLC/MS, XPS, SEM, and XRD to study electrochemical reactions associated with sulfur electrodes. Electrochemical techniques such as AC impedance, rotation ring disk electrode, and galvanostat will be used to study the electrode process kinetics. The project will use an *in situ* electrochemical optical method to investigate the surface of lithium anode during cycling of a Li-S cell.

One-Year Goals. The one-year goals include the following: (1) complete preliminary investigations of the inhibition mechanism for the “shuttle effect” and evaluation of “shuttle effect” inhibitors, and (2) complete preliminary design and tests of sulfur-containing electrodes and electrolytes.

Collaborations. The PI, Deyang Qu, is the Johnson Control Endowed Chair Professor; thus, the University of Wisconsin at Milwaukee and BNL team have close collaboration with Johnson Controls’ scientists and engineers. This collaboration enables the team to validate the outcomes of fundamental research in pilot-scale cells. This team has been closely working with top scientists on new material synthesis at ANL, LBNL, and PNNL, with U.S. industrial collaborators at GM, Duracell, and Johnson Control as well as international collaborators in China, Japan, and South Korea. These collaborations will be strengthened and expanded to give this project a vision on both today’s state-of-the-art technology and tomorrow’s technology in development, with feedback from the material designer and synthesizers upstream, and from industrial end users downstream.

Milestones

1. Complete the investigation and determination of the possible chemical reactions between dissolved polysulfide ions with the materials in a Li-S cell, both active and non-active during the storage, and thus the stability of battery components. (Q1, December 31, 2017; Completed)
2. Complete tabulating the list of materials to be tested as the inhibitive additives to mitigate “shuttle effect”; start the tests and develop understanding of the mechanism of such effects. (Q2, FY 2018)
3. Complete testing the inhibitive additives; start to explore and design sulfur-containing electrode materials. (Q3, FY 2018)
4. Complete the preliminary engineering design and test for the new sulfur-containing electrode materials. (Q4, FY 2018)

Progress Report

This quarter, the team used its established HPLC method and XPS to study chemical stability of different battery components with highly reactive polysulfide species in Li-S battery electrolytes. The side reaction between polysulfides and battery components (such as current collectors, separators, and binders) along with the well-known “shuttle reaction” could negatively influence the battery performance of rechargeable Li-S batteries with nonaqueous electrolytes. Consequently, to utilize the high energy density of Li-S battery, it is required that battery components be chemically stable against polysulfides.

In current work, chemical stabilities of eight kinds of battery components against polysulfides were investigated by comparing the HPLC chromatograms (as shown in figure 65a) of stock electrolyte with 25-mM polysulfides (Li_2S_6 stoichiometrically), including five current collectors, one separator, and two binders. To correlate the chromatographic observations, the spectroscopic analysis, XPS (as shown in figure 65b) and SEM/EDS were also performed. It was found that three current collectors (aluminum, stainless steel 304, and titanium), Celgard polypropylene separator (Celgard 2400), and two binders (CMC and PVDF) are stable with polysulfides up to 180 days at room temperature. Both copper and nickel current collectors are unstable with polysulfides, though copper current collector is more reactive with polysulfide than nickel current collector. Furthermore, the chemical stabilities of these stable battery components at elevated temperature as well in different solvents will be studied since it is known that polysulfide species in different solvents are different (more radical species in electrophoretic deposition solvents), and the reactivity typically increases as temperature increases.

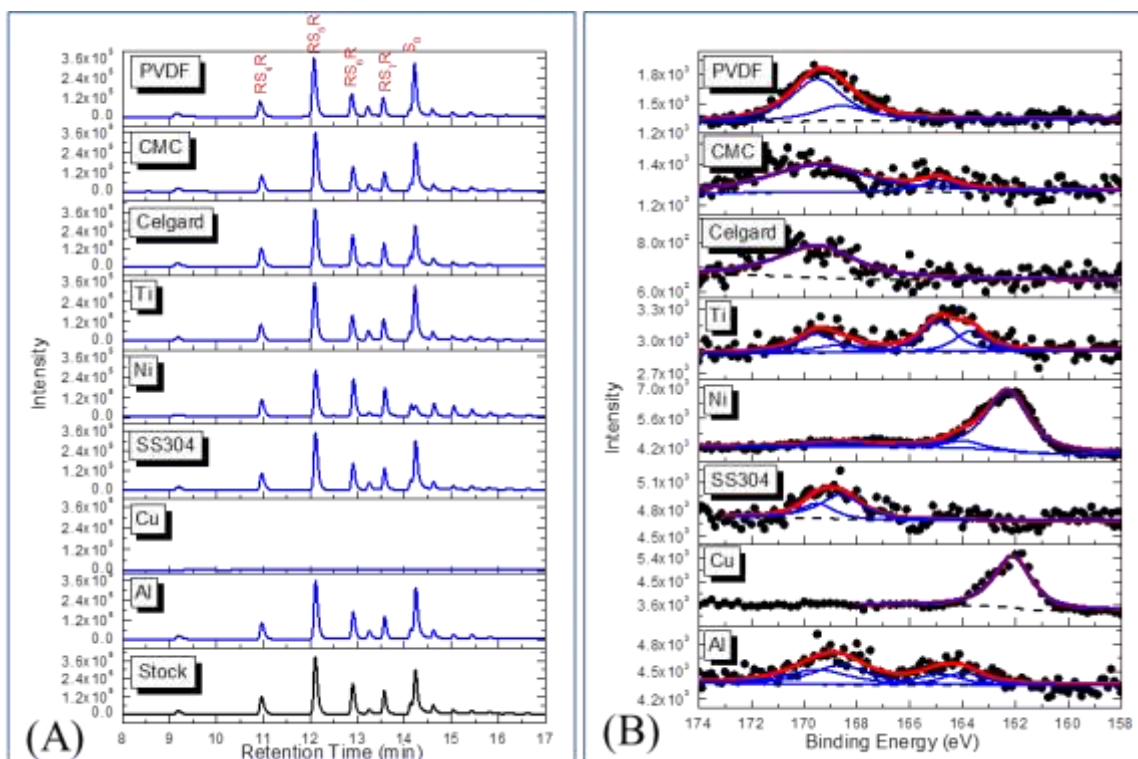


Figure 65. (a) High-performance liquid chromatography/ultraviolet chromatograms for electrolytes with polysulfides after contacted with different current collectors for 180 days and for stock electrolyte with polysulfides after rest for 180 days at room temperature. (b) X-ray photoelectron spectroscopy measurements of sulfur 2p for five current collectors after contacted with electrolyte (containing 25-mM polysulfides) for 180 days. Black dot: raw data; black dash: baseline; red line: fitted data; blue line: different fitting sulfur 2p species.

Task 5.6 – Statically and Dynamically Stable Lithium-Sulfur Batteries (Arumugam Manthiram, University of Texas – Austin)

Project Objective. The project objective is to develop statically and dynamically stable Li-S batteries by integrating polysulfide-filter-coated separators with a protected Li-metal anode through additives or a modified Li_2S cathode with little or no charge barrier during first charge. The project includes demonstration of electrochemically stable cells with sulfur capacities of $> 1000 \text{ mA h g}^{-1}$ and cycle life in excess of 500 cycles (dynamic stability) along with positive storage properties (static stability) at $> 70 \text{ wt\%}$ sulfur content and $\sim 5 \text{ mg cm}^{-2}$ loading.

Project Impact. The combination of polysulfide-filter (PS-filter)-coated separator, Li-metal-protection additives, and Li_2S cathode modifications offers a viable approach to overcome the persistent problems of Li-S batteries. This project is systematically integrating the basic science understanding gained in its laboratory of these three aspects to develop the Li-S technology as the next-generation power source for EVs. The project targets demonstrating cells with sulfur capacities of over 1000 mA h g^{-1} and cycle life in excess of 500 cycles along with good storage properties at high sulfur content and loading that will make the Li-S technology superior to the present-day Li-ion technology in terms of cost and cell performance.

Approach. Electrochemical stability of the Li-S cells is improved by three complementary approaches. The first approach focuses on establishment of an electrochemically stable cathode environment by employing PS-filter-coated separators. The PS-filter coatings aim to suppress the severe polysulfide diffusion and improve the redox capability of Li-S cells with high-sulfur loadings. The study includes an understanding of materials characteristics, fabrication parameters, electrochemical properties, and battery performance of the PS-filter-coated separators. The second approach focuses on electrode engineering from two aspects. First, investigation of a Li-metal anode with coating- and additive-supporting approaches is aimed at improving the safety of Li-S cells. Second, research on activated- Li_2S cathode with little or no charge-barrier will promote performance and safety of the C- Li_2S cells. Integration of the first two approaches would create statically and dynamically stable Li-S batteries for EVs.

Out-Year Goals. The overall goal is to develop statically and dynamically stable Li-S batteries with custom cathode and stabilized anode active materials. In addition to developing a high-performance battery system, a fundamental understanding of the structure-configuration-performance relationships will be established. Specifically, the optimization of the electrochemical and engineering parameters of PS-filter-coated separators aims at comprehensively investigating different coating materials and their corresponding coating techniques for realizing various high-performance custom separators. The developed PS-filter-coated separators can be coupled with pure sulfur cathodes with high-sulfur loading and content. Multi-functional PS-filter-coated separators, high-loading sulfur cathodes, stabilized-Li-metal anodes, activated- Li_2S cathodes, and novel cell design are anticipated to provide an in-depth understanding of the Li-S battery chemistry and to realize statically and dynamically stable Li-S batteries.

Collaborations. There are currently no collaborative activities.

Milestones

1. Develop Li-metal anodes with high electrochemical stability. (Q1, December 2017; Completed)
2. Develop Li_2S cathodes with low activation barrier and polarization. (Q2, March 2018; Ongoing)
3. Demonstrate high-loading coin cells and pouch cell prototypes. (Q3, June 2018; Ongoing)
4. *Go/No Go Decision:* Study cost and environmental impact assessment of the technology. (Q4, September 2018; Ongoing)

Progress Report

To enhance stability of the reacted Li-metal electrode during long-term cycling, the team has demonstrated this quarter two methods for stabilizing Li-metal anodes. The team applied a Kimwipe (KW) paper on the surface of Li-metal anode as a stabilization layer. The KW-stabilization layer aimed to create a uniform, smooth lithium redeposition with no lithium dendrites. Moreover, the fresh cellulose fibers of the KW paper had abundant polar functional groups like $-OH$ and $C-O-C$, which can adhere to lithium ions, improve wettability with the electrolyte, and impede the inhomogeneous aggregation of lithium ions around the protrusions of the deposited lithium. To demonstrate these physical and chemical functions, Li-Li symmetric cells without the KW-stabilization layer were assembled as a control. The control cell showed a typical high and increasing voltage polarization (~ 700 mV) with unstable voltage fluctuations in the voltage versus cycling time profile during 400-hour cycling (Figure 66a). In contrast, the symmetric cell with the KW-stabilization layer showed excellent cycling stability for 400 hours with a low polarization (~ 200 mV) at the same current density of 2 mA cm^{-2} (Figure 66b). The high reversibility of the KW-protected cell suggests that the KW paper provides a polar lithiophilic interface for the Li-metal anode, which effectively eliminates inhomogeneous Li-ion distribution on the surface, resulting in a dendrite-free morphology of the deposited lithium.

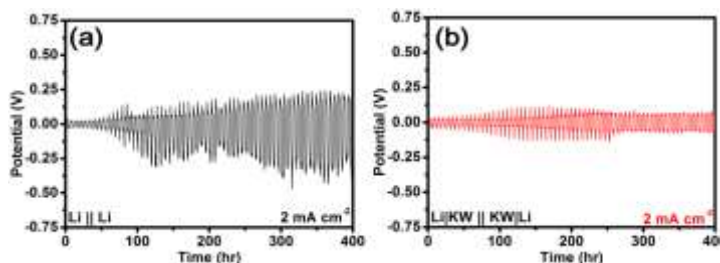


Figure 66. Overpotential of lithium-lithium symmetric cells (a) with and (b) without the KW-stabilization layer at 2 mA cm^{-2} .

The second approach involved a coating of a ceramic-polymer composite on both the anode and cathode sides of a commercial Celgard 2500 separator. The composite coating had PVDF HFP and fumed silica (SiO_2) in a 10:1 weight ratio and formed a porous structure onto the coated-separator. The combination of a polymer and ceramic served as an excellent artificial SEI with low resistance and high flexibility, which enabled a uniform Li-ion flux on the anode surface. The abundant polar functional groups in the composite, such as $-F$ and $O-Si-O$, interact strongly with lithium ions and help reduce the surface roughness of the deposited lithium, thus improving electrolyte retention and CE. This improvement is demonstrated by the low overpotential of the symmetric cell fabricated with the composite-coated separator (Figure 67a). The team next applied the composite-coated separator in Li-S cells with a sulfur loading of 5 mg cm^{-2} . Figure 67b demonstrates a clear improvement in cycling stability and consistently a high CE. This improvement can be attributed to a couple of factors: improvement in efficiency of lithium plating and stripping due to reduced mossy growth and thus lithium loss, and a reduction in polysulfide crossover and shuttling due to the presence of polar functional groups in the coating. The results demonstrate the promise of the ceramic-polymer composite coating on the separator in leading to a remarkable improvement in the electrochemical performance of Li-metal anode-based systems, particularly Li-S batteries.

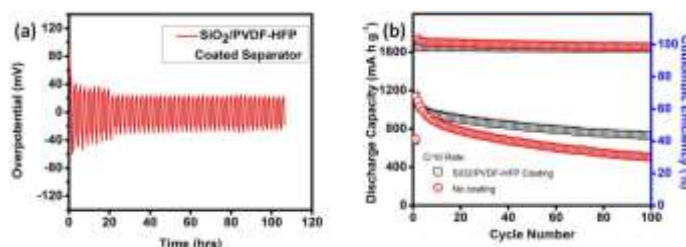


Figure 67. (a) Overpotential of a symmetric cell with composite-coated separator for over 100 hours. (b) Cycling performance of the composite-coated separator in Li-S cells.

The abundant polar functional groups in the composite, such as $-F$ and $O-Si-O$, interact strongly with lithium ions and help reduce the surface roughness of the deposited lithium, thus improving electrolyte retention and CE. This improvement is demonstrated by the low overpotential of the symmetric cell fabricated with the composite-coated separator (Figure 67a). The team next applied the composite-coated separator in Li-S cells with a sulfur loading of 5 mg cm^{-2} . Figure 67b demonstrates a clear improvement in cycling stability and consistently a high CE. This improvement can be attributed to a couple of factors: improvement in efficiency of lithium plating and stripping due to reduced mossy growth and thus lithium loss, and a reduction in polysulfide crossover and shuttling due to the presence of polar functional groups in the coating. The results demonstrate the promise of the ceramic-polymer composite coating on the separator in leading to a remarkable improvement in the electrochemical performance of Li-metal anode-based systems, particularly Li-S batteries.

Patents/Publications/Presentations

Publications

- Chang, C.-H., and A. Manthiram. “Covalently-Grafted Polysulfur-Graphene Nanocomposites for Ultrahigh Sulfur-Loading Lithium-Polysulfur Batteries.” *ACS Energy Letters* 3 (2018): 72.
- Chung, S.-H., and A. Manthiram. “Rational Design of Statically and Dynamically Stable Lithium-Sulfur Batteries with High Sulfur Loading and Low Electrolyte/Sulfur Ratio.” *Advanced Materials*. doi: 10.1002/adma.201705951.

Presentations

- King Abdullah University of Science and Technology (KAUST), Thuwal, Saudi Arabia (October 26, 2017): “Electrical Energy Storage: Next Generation Battery Technologies”; A. Manthiram. Invited.
- 2017 MRS Fall Meeting, Boston, Massachusetts (November 26 – December 1, 2017): “Oligoanilines as a Suppressor of Polysulfide Shuttling in Lithium-Sulfur Batteries”; C.-H. Chang, S.-H. Chung, and A. Manthiram.
- 2017 MRS Fall Meeting, Boston, Massachusetts (November 26 – December 1, 2017): “Polymeric Sulfur-Graphene Nanocomposites for High Areal Capacity Lithium-Sulfur Batteries”; C.-H. Chang and A. Manthiram.
- 2017 MRS Fall Meeting, Boston, Massachusetts (November 26 – December 1, 2017): “Lithium-Sulfur Batteries with the High Sulfur Loading/Content and Low Electrolyte/Sulfur Ratio”; S.-H. Chung and A. Manthiram.
- 2017 MRS Fall Meeting, Boston, Massachusetts (November 26 – December 1, 2017): “Lithium-Sulfur Batteries with the Lowest Self-Discharge and the Longest Shelf-Life”; S.-H. Chung and A. Manthiram.
- School on Clean and Renewable Energy Technologies via Chemical Route, International Institute for Complex Adaptive Matter, Jawaharlal Nehru Centre for Advanced Scientific Research, Bangalore, India (November 27 – December 2, 2017): “Electrical Energy Storage: Next Generation Battery Chemistries”; A. Manthiram. Invited.
- Ford Motor Company, Dearborn, Michigan (December 13, 2017): “Next-Generation Battery Technologies”; A. Manthiram. Invited.

Task 5.7 – Electrochemically Responsive, Self-Formed, Lithium-Ion Conductors for High-Performance Lithium-Metal Anodes (Donghai Wang, Pennsylvania State University)

Project Objective. The project objective is to develop and deliver an electrochemically responsive self-formed hybrid Li-ion conductor as a protective layer for Li-metal anodes, enabling Li-metal anodes to cycle with a high efficiency of ~ 99.7% at high electrode capacity ($> 6 \text{ mAh/cm}^2$) and high current density ($> 2 \text{ mA/cm}^2$) for over 500 cycles. The project will also demonstrate prototype ~ 300 mAh Li-S battery cells with energy densities of ~ 200 Wh/kg and ~ 80% capacity retention for ~ 300 cycles at ~ 80% depth of discharge using Li-metal anodes with this protective layer.

Project Impact. This project aims to develop a new hybrid Li-ion conductor that enables safe and high-performance Li-metal anodes. The use of these high-performance Li-metal anodes in turn enables Li-S batteries with high energy density and long cycling life. Such anodes can also lead to a 50% increase in the energy density of conventional Li-ion batteries with Li-metal oxide cathodes. Meeting the technical targets will potentially develop a new high-energy-density lithium battery, promote increased adoption of EVs and PHEVs, and reduce petroleum consumption in the transportation sector by helping battery-powered vehicles become accepted by consumers as a reliable source of transportation.

Approach. The novel multiphase organo- Li_xS_y or organo- $\text{Li}_x\text{P}_y\text{S}_z$ hybrid ion conductors with tunable multi-functional organic components and controlled Li_xS_y and $\text{Li}_x\text{P}_y\text{S}_z$ inorganic components will be designed and prepared, and thus enable safe use of lithium metal with high CE. In the second year, the team will develop the 2nd generation of organo- Li_xS_y lithium protection layers with tuned functionality: (1) finding appropriate composition, (2) developing appropriate synthesis and fabrication methods, and (3) optimizing organic components in a protection layer to further improve CE and Li-S battery performance.

Out-Year Goals. Work will progress toward development of the 2nd generation of organo- Li_xS_y lithium protection layers with tuned functionality. Characterization, performance, and compatibility tests on materials and systems will be conducted. Uniform and dendrite-free lithium deposition under the protection of the 2nd generation of organo- Li_xS_y lithium protective layers will be demonstrated, and CE will be further improved.

Collaborations. There are no active collaborations.

Milestones

1. Development of the 2nd generation of organo- Li_xS_y lithium protection layers with tuned functionality. Conduct characterization and performance tests on the materials. (Q1, FY 2018)
2. Demonstrate uniform and dendrite-free lithium deposition under protection of the 2nd generation of organo- Li_xS_y lithium protective layers. (Q2, FY 2018)
3. Optimize the 2nd generation of organo- Li_xS_y lithium protective layer and demonstrate lithium anodes cycling with ~ 98.8% CE for ~ 200 cycles. (Q3, FY 2018)
4. Demonstrate lithium anodes with optimized 2nd-generation organo- Li_xS_y lithium protective layer and ~ 99.2% CE for ~ 300 cycles. (Q4, FY 2018)

Progress Report

To further strengthen the organo- Li_xS_y lithium protective layer, the team has screened the organic species based on molecular conformation. Because the planar backbone conformation facilitates fabrication of the flat and uniform structure of the SEI layer during co-deposition of organic and inorganic components, aromatic-based organic components with planar backbone conformation should be beneficial to preparing a more stable lithium protection layer. The team used aromatic compound (1, 3-diisopropenylbenzene (DIB)) that can react with sulfur to prepare the sulfur-containing polymer PSD. This polymer retains the electrochemical properties of elemental sulfur and can generate inorganic lithium salt ($\text{Li}_2\text{S}/\text{Li}_2\text{S}_2$) and aromatic-based organic components during the charge/discharge process; the aromatic-based organic components could be co-deposited with $\text{Li}_2\text{S}/\text{Li}_2\text{S}_2$ to form a more stable inorganic/organic hybrid film. Figure 68 shows possible molecular conformation of different lithium organosulfides; aromatic-based organic components show planar backbone conformation (Figure 68a-b) rather than a branched structure of PST polymer (used for preparing the 1st-generation organo- Li_xS_y lithium protective layer, Figure 68c-d). These kinds of organic components facilitate the initial “growth” of a flat and uniform morphology of a hybrid protective layer and formation of a planar and smooth structure.

The team prepared PSD polymers with various sulfur contents, as shown in Table 4. PSDs with different sulfur contents (50 wt%, 70 wt%, and 90 wt%, designated as PSD-50, PSD-70, and PSD-90, respectively) were used as additives in the electrolyte. The solubility of PSDs in electrolyte decreases with the increment in sulfur content of the polymer. When PSD-90 is added in the electrolyte, a mixture is formed. However, it becomes homogeneous after the first cycle of lithium plating/stripping due to the chemical/electrochemical reaction with lithium metal (Figure 69). The corresponding cycling performance of lithium plating/stripping was first investigated. The electrolyte used here was 1 M LiTFSI (lithium bis(trifluoromethanesulfonyl)imide) and 1 wt% LiNO_3 in the DOL/DME, V/V = 1. It is found that cells using PSD-90 as an additive exhibit the best performance, and cycling stability drops with decrease of sulfur content in the PSDs (for example, PSD-70 and PSD-50), as shown in Figure 70.

Table 4. Prepared sulfur-containing polymers with different sulfur content.

Samples	Content (wt%)	
	Sulfur	DIB
PSD-50	50	50
PSD-70	70	30
PSD-90	90	10

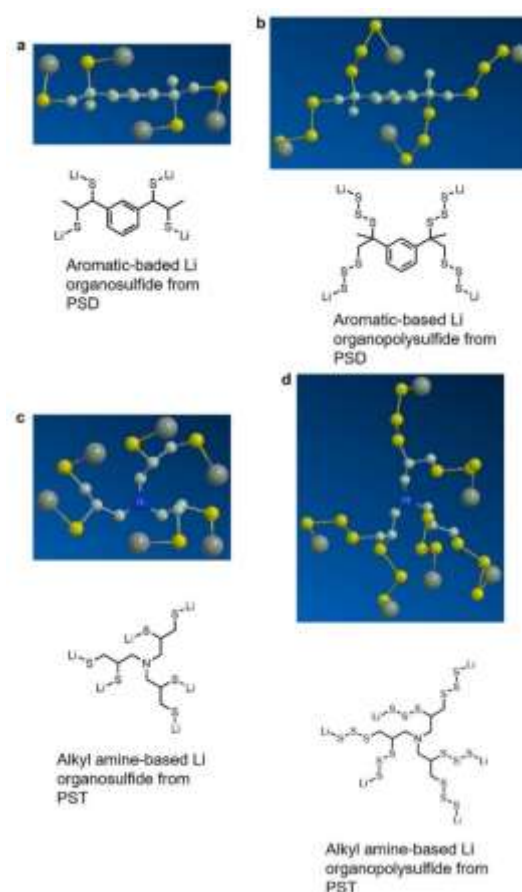


Figure 68. Possible molecular conformation of aromatic-based lithium organosulfide (a) and lithium organopolysulfide (b) originating from PSD polymer; alkyl amine-based lithium organosulfide (c) and lithium organopolysulfide (d) originating from PST polymer.

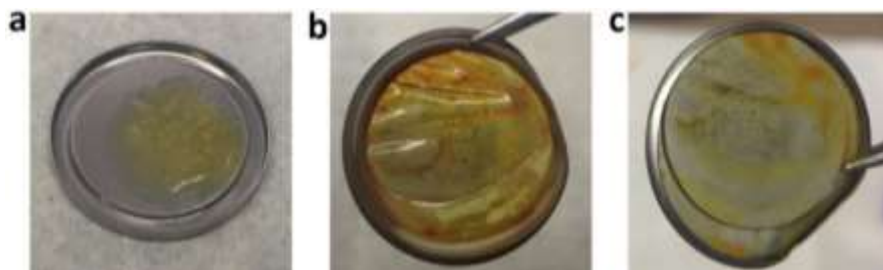


Figure 69. The photos of PSD-90-Ely before cycling (a) and after 1st cycle of lithium plating/stripping: (b) with separator covering on stainless steel, and (c) separator was peeled off.

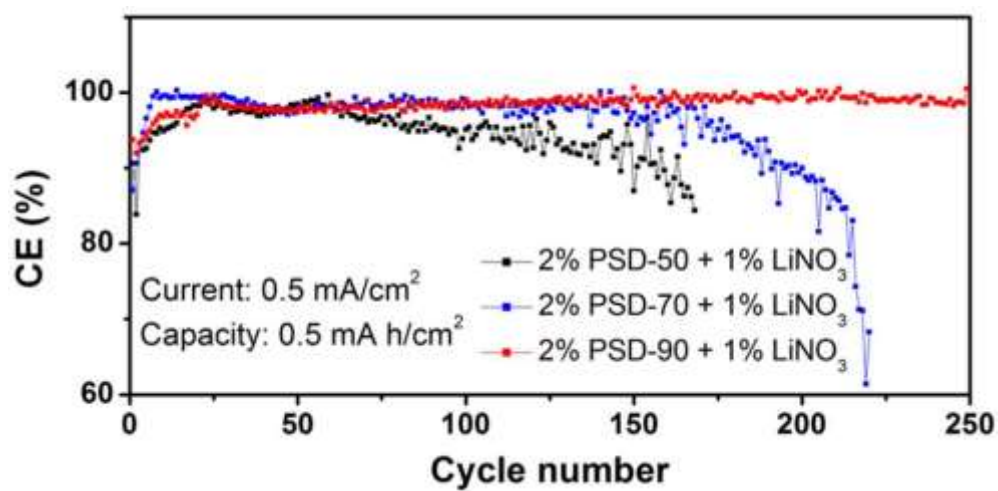


Figure 70. Cycling performance of 2 wt% PSDs containing different sulfur contents as additives.

TASK 6 – AIR ELECTRODES / ELECTROLYTES

Summary and Highlights

High-density energy storage systems are critical for EVs required by the EV Everywhere Grand Challenge. Conventional Li-ion batteries still cannot fully satisfy the ever-increasing needs because of their limited energy density, high cost, and safety concerns. As an alternative, the rechargeable lithium-oxygen (Li-O₂) battery has the potential to be used for long-range EVs. The practical energy density of a Li-O₂ battery is expected to be ~ 800 Wh kg⁻¹. The advantages of Li-O₂ batteries come from their open structure; that is, they can absorb the active cathode material (oxygen) from the surrounding environment instead of carrying it within the batteries. However, the open structure of Li-O₂ batteries also leads to several disadvantages. The energy density of Li-O₂ batteries will be much lower if oxygen must be provided by an onboard container. Although significant progress has been made in recent years on fundamental properties of Li-O₂ batteries, research in this field is still in an early stage, with many barriers to be overcome before practical applications. These barriers include:

- Instability of electrolytes—The superoxide species generated during discharge or O₂ reduction process is highly reactive with electrolyte and other components in the battery. Electrolyte decomposition during charge or O₂ evolution process is also significant due to high over-potentials.
- Instability of air electrode (dominated by carbonaceous materials) and other battery components (such as separators and binders) during charge/discharge processes in an O-rich environment.
- Limited cyclability of the battery associated with instability of the electrolyte and other battery components.
- Low energy efficiency associated with large over-potential and poor cyclability of Li-O₂ batteries.
- Low power rate capability due to electrode blocking by the reaction products.
- Absence of a low-cost, high-efficiency oxygen supply system (such as oxygen selective membrane).

The main goal of this Task is to provide a better understanding on the fundamental reaction mechanisms of Li-O₂ batteries and identify the required components (especially electrolytes and electrodes) for stable operation of Li-O₂ batteries. PNNL researchers will investigate stable electrolytes and oxygen evolution reaction (OER) catalysts to reduce the charging overvoltage of Li-O₂ batteries and improve their cycling stability. New electrolytes will be combined with stable air electrodes to ensure their stability during Li-O₂ reaction. Considering the difficulties in maintaining the stability of conventional liquid electrolyte, the Liox team will explore use of a nonvolatile, inorganic molten salt comprising nitrate anions and operating Li-O₂ cells at elevated temperature (> 80°C). It is expected that these Li-O₂ cells will have a long cycle life, low over potential, and improved robustness under ambient air compared to current Li-air batteries. At ANL, new cathode materials and electrolytes for Li-air batteries will be developed for Li-O₂ batteries with long cycle life, high capacity, and high efficiency. The state-of-the-art characterization techniques and computational methodologies will be used to understand the charge and discharge chemistries. The University of Massachusetts/BNL team will investigate the root causes of the major obstacles of the air cathode in the Li-air batteries. Special attention will be paid to optimization of high-surface carbon material used in the gas diffusion electrode, catalysts, electrolyte, and additives stable in Li-air system and with capability to dissolve lithium oxide and peroxide. Success of this project will establish a solid foundation for further development of Li-O₂ batteries toward their practical applications for long-range EVs. The fundamental understanding and breakthrough in Li-O₂ batteries may also provide insight on improving performance of Li-S batteries and other energy storage systems based on chemical conversion processes.

Task 6.1 – Rechargeable Lithium-Air Batteries (Ji-Guang Zhang and Wu Xu, Pacific Northwest National Laboratory)

Project Objective. The project objective is to develop rechargeable lithium-oxygen (Li-O₂) batteries with long-term cycling stability. The team has found that the corrosion of Li-metal anode is a critical degradation mechanism of Li-O₂ batteries. Realization of very high energy density of Li-O₂ batteries strongly depends on the stability of Li-metal anodes. In FY 2018, the focus will be on protection of Li-metal anodes for Li-O₂ batteries. Several approaches, including *in situ* and *ex situ* methods will be used to study the corrosion of Li-metal anode in Li-O₂ cells under different treatment/protection conditions.

Project Impact. Li-air batteries have a theoretical specific energy more than five times that of state-of-the-art Li-ion batteries and are potential candidates for use in next-generation, long-range EVs. Unfortunately, the poor cycling stability and low CE of Li-air batteries have prevented their practical application. This work will explore well-protected Li-metal anodes, new electrolytes, and high-loading air-electrodes that could lead to long cyclability and high CE in high-energy Li-air batteries that can be used in the next-generation EVs required by the EV Everywhere Grand Challenge.

Out-Year-Goals. The long-term goal is to enable rechargeable Li-air batteries with a specific energy of 800 Wh/kg at cell level, 1000 deep-discharge cycles, improved abuse tolerance, and less than 20% capacity fade over a 10-year period to accelerate commercialization of long-range EVs.

Collaborations. This project collaborates with Chongmin Wang of PNNL on characterization of cycled air electrodes by TEM/SEM.

Milestones

1. Investigate electrolyte additives to form stable SEI layer on Li-metal anode of Li-O₂ batteries. (Q1, December 31, 2017; Completed)
2. Develop inorganic/polymeric composite hybrid electrolyte membranes to protect Li-metal anode in Li-O₂ batteries. (Q2, March 31, 2018; Ongoing)
3. Develop thick air electrodes of at least 4 mg/cm² areal loading for Li-O₂ batteries. (Q3, June 30, 2018; Ongoing)
4. Evaluate cycling performance of Li-O₂ batteries with protected Li-metal anode and thick air electrode. (Q4, September 30, 2018; Ongoing)

Progress Report

In FY 2017, the project found that cycled Li-metal anodes recovered from Li-O₂ cells showed significant corrosion, while the cycled air-electrodes could still work well when paired with new Li-metal anode. These results reveal that Li-metal stability should be considered as an important factor to realize highly stable operation of high energy density Li-O₂ batteries. This quarter, through the screening of electrolyte additives for Li-metal protection, the team found that TTMSPi is a good alternative additive that enhances stability of lithium metal during cycling. Cycling stability of Li||Li cells containing electrolytes of 1 M LiTFSI-DME without and with 2% or 5% TTMSPi was measured at a current density of 0.2 mA cm⁻²; the results are shown in Figure 71a. It can be seen that Li||Li cell with the baseline electrolyte indicates significant voltage change in the early cycles. After that, the lithium plating/stripping voltage values gradually increase due to increase of cell polarization as cycling proceeds. In contrast, stable cycling beyond 280 h with very low hysteresis could be obtained in the Li||Li cells when 2% or 5% TTMSPi was added into the baseline electrolyte. To study evolution of the voltage profiles in detail, the selected cycles from 100 h to 280 h of Li||Li cells containing electrolytes of 1 M LiTFSI-DME with 2% and 5% TTMSPi are enlarged in Figure 71b. Addition of 2% TTMSPi results in slightly lower voltage polarization than that of 5% TTMSPi. It is well known that LiDFOB as electrolyte additive has been proven to build dense SEI films on electrode surfaces. Here, a clear cycling stability comparison of Li||Li cells using electrolytes of 1 M LiTFSI-DME with 2% TTMSPi and with 2% LiDFOB additives has been provided in Figure 71c. Although the hysteresis of the Li||Li cell using the electrolyte with 2% LiDFOB gradually deceased and then stabilized, the voltage profiles of the Li||Li cell containing the electrolyte with 2% TTMSPi showed much more stable and lower hysteresis. This interesting phenomenon can be attributed to the more stable and robust SEI protective films induced by addition of TTMSPi additive, which is beneficial for Li-metal stabilization. More characterizations are being conducted.

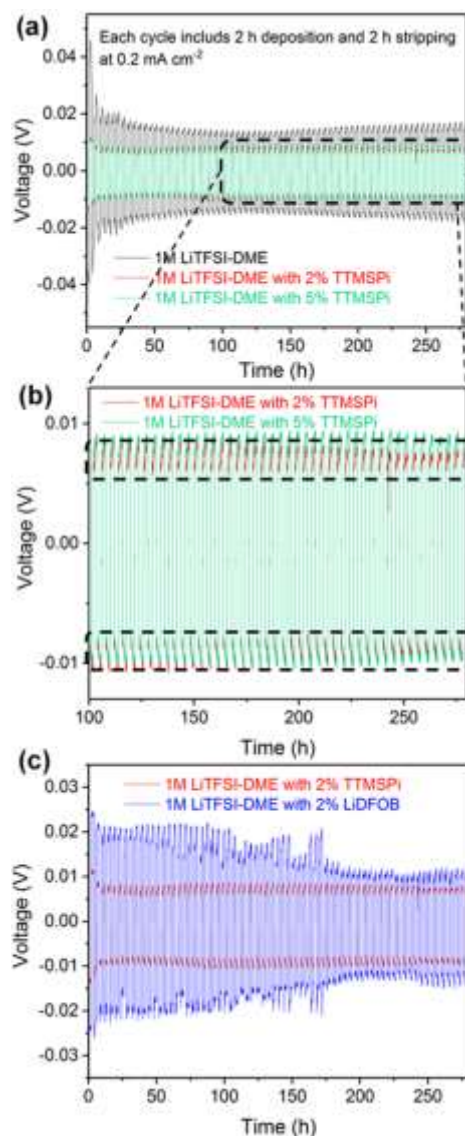


Figure 71. (a) Voltage profiles of Li||Li cells in 1 M LiTFSI-DME, 1 M LiTFSI-DME with 2% TTMSPi, or 1 M LiTFSI-DME with 5% TTMSPi electrolytes, respectively, cycled at 0.2 mA cm⁻². (b) Enlarged voltage profiles of (a). (c) Voltage profiles of Li||Li cells in 1 M LiTFSI-DME with 2% TTMSPi and 1 M LiTFSI-DME with 2% LiDFOB electrolytes, respectively, cycled at 0.2 mA cm⁻².

Patents/Publications/Presentations

Publications

- Xu, W., B. Liu, and J.-G. Zhang. “Preformation of Solid Electrolyte Interphase on Electrodes for Rechargeable Lithium Metal Batteries.” PNNL Invention Disclosure Report 31087-E.
- Liu, B., W. Xu, J. Zheng, P. Yan, E. D. Walter, N. Isern, M. E. Bowden, M. H. Engelhard, S. T. Kim, J. Read, B. D. Adams, X. Li, J. Cho, C. Wang, and J.-G. Zhang. “Temperature Dependence of Oxygen Reduction Mechanism in Nonaqueous Li-O₂ Batteries.” *ACS Energy Letters* 2017. In press. doi: 10.1021/acsenergylett.7b00845.

Presentation

- 254th American Chemical Society National Meeting & Exposition, Washington, D. C. (August 2017): “Development of Stable Rechargeable Lithium-Oxygen Batteries”; W. Xu, B. Liu, S. Song, and J.-G. Zhang. Invited.

Task 6.2 – Lithium–Air Batteries (Khalil Amine and Larry Curtiss, Argonne National Laboratory)

Project Objective. This project will develop new cathode materials and electrolytes for Li-air batteries for long cycle life, high capacity, and high efficiency. The goal is to obtain critical insight that will provide information on the charge and discharge processes in Li-air batteries to enable new advances to be made in their performance. This will be done using state-of-the-art characterization techniques combined with state-of-the-art computational methodologies to understand and design new materials and electrolytes for Li-air batteries.

Project Impact. The instability of current nonaqueous electrolytes and degradation of cathode materials limits the performance of Li-air batteries. The project impact will be to develop new electrolytes and cathode materials that are stable and can increase cycle life and improve efficiency of Li-air batteries.

Approach. The project is using a joint theoretical/experimental approach for design and discovery of new cathode and electrolyte materials that act synergistically to reduce charge overpotentials and increase cycle life. Synthesis methods, in combination with design principles developed from computations, are used to make new cathode architectures. Computational studies are used to help understand decomposition mechanisms of electrolytes and how to design electrolytes with improved stability. The new cathodes and electrolytes are tested in Li-O₂ cells. Characterization along with theory is used to understand the performance of the materials used in the cell and make improved materials.

Out-Year Goals. The out-year goals are to find catalysts that promote discharge product morphologies that reduce charge potentials and find electrolytes for long cycle life through testing and design.

Collaborations. This project engages in collaboration with Prof. Kah Chun Lau (University of California at Norridge), Prof. Yiying Wu (Ohio State University), Dr. Dengyun Zhai (China), and Reza Shahbazian-Yassar (University of Illinois at Chicago).

Milestones

1. Investigation of highly uniform Pt₃Co nanoparticles in biphasic nitrogen-doping cobalt@graphene heterostructures as cathode materials. (Q1, FY 2018; Completed)
2. Computational studies of dependence of stability and composition of discharge products in Li-O₂ batteries on ether-based electrolytes. (Q2, FY 2018; Ongoing)
3. Use of highly uniform small iridium clusters supported on reduced graphene oxide to study formation of Ir₃Li alloys for lithium superoxide based batteries. (Q3, FY 2018; Ongoing)
4. Investigation of dependence of discharge composition on type of ether used electrolytes from experimental studies. (Q4, FY 2018; Ongoing)

Progress Report

Metal-organic framework-derived catalysts have received increasing attention as promising cathode materials for Li-O₂ batteries because of their superior catalytic activity and high theoretical capacity. However, further optimization of their structural and electrochemical properties is necessary to promote practical applications. The project has used a bulk-doping approach to encapsulate platinum nanocomponents into the bulk of the catalyst. The fabricated cathode architecture features highly uniform platinum and Pt₃Co nanoparticles within biphasic nitrogen-doping (BND) cobalt@graphene heterostructures. Because of improvement in the materials for optimizing catalytic and electrical properties and maximizing active regions, such a cathode design has enabled promising electrochemical performance in the project's testing. This has included higher specific capacity and a dramatic reduction in charge overpotential to 0.4 V. DFT calculations have provided mechanistic insights into the promotional effect of the platinum and Pt₃Co nanoparticles in reducing the charge overpotential. In addition, it reveals a dramatically different structural evolution of lithium peroxides dependent on the platinum modification approach. This dependence contributes to the influence of platinum component and diffusion on the formation and decomposition mechanism of lithium peroxides.

The synthetic routes are illustrated in Figure 72. Firstly, the team synthesized a Co-based zeolitic imidazolate framework-derived, BND cobalt@graphene catalyst via a co-precipitation and calcination process. Then, it fabricated the electrodes by pasting the catalysts with PVDF onto carbon fibers, followed by sputtering platinum nanoparticles onto the electrode surface by employing a thin-film deposition system, forming a platinum surface-coated cathode. The other approach was to infuse the Pt²⁺ solution within the same base catalyst followed by H₂ reduction to form a well-defined platinum bulk-doped structure. This latter cathode architecture with highly uniform catalytic nanocomponents and abundant active regions in the material bulk gave improved catalytic efficiency. Catalyst properties were characterized by high-energy XRD, Raman spectroscopy, XPS, XAS, and small-angle X-ray scattering.

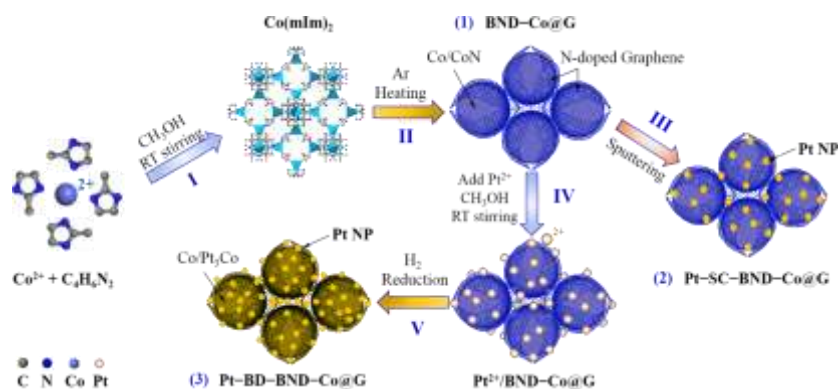


Figure 72. Schematic of platinum modified MOF-derived catalysts. BND-Co@G = biphasic N-doped cobalt@graphene, Pt-SC-BND-Co@G = Pt surface-coating BND-Co@G, and Pt-BD-BND-Co@G = Pt bulk-doping BND-Co@G.

Patents/Publications/Presentations

Publication

- Luo, X. Y., R. Amine, K. C. Lau, J. Lu, C. Zhan, L. A. Curtiss, S. Al Hallaj, B. P. Chaplin, and K. Amine. “Mass and Charge Transport Relevant to the Formation of Toroidal Lithium Peroxide Nanoparticles in an Aprotic Lithium-Oxygen Battery: An Experimental and Theoretical Modeling Study.” *Nano Research* 10 (2017): 4327–4336.